COMPARATIVE ANALYSIS OF CO_2 CAPTURE SYSTEMS: AN EXERGETIC FRAMEWORK

A DISSERTATION
SUBMITTED TO THE DEPARTMENT OF MECHANICAL ENGINEERING
AND THE COMMITTEE ON GRADUATE STUDIES
OF STANFORD UNIVERSITY
IN PARTIAL FULFILLMENT OF THE REQUIREMENTS
FOR THE DEGREE OF
DOCTOR OF PHILOSOPHY

Adelaide S. Calbry-Muzyka
December 2015

This dissertation is online at: http://purl.stanford.edu/kp828rc7449

I certify that I have read this dissertation and that, in my opinion, it is fully adequate in scope and quality as a dissertation for the degree of Doctor of Philosophy.

Chris Edwards, Primary Adviser

I certify that I have read this dissertation and that, in my opinion, it is fully adequate in scope and quality as a dissertation for the degree of Doctor of Philosophy.

Adam Brandt

I certify that I have read this dissertation and that, in my opinion, it is fully adequate in scope and quality as a dissertation for the degree of Doctor of Philosophy.

Reginald Mitchell

Approved for the Stanford University Committee on Graduate Studies.

Patricia J. Gumport, Vice Provost for Graduate Education

This signature page was generated electronically upon submission of this dissertation in electronic format. An original signed hard copy of the signature page is on file in University Archives.

Abstract

A portfolio of technology strategies will be needed to reach overall greenhouse gas emissions targets. Implementing systems to separate CO_2 from atmospheric emissions of fossil-fuel power plants is predicted to be a necessary part of this portfolio, especially in the near term. However, existing carbon capture systems are quite inefficient, using or otherwise reducing a significant portion of power plants' electricity output. In order to improve future systems and make them viable, it is important to understand which aspects of each system have the most potential to improve, and which systems overall are most promising for future research and development.

In this work, we examine three representative options for CO_2 capture systems. The first option, an amine absorption system for post-combustion capture, is studied due to its relative technological maturity. The second system uses vacuum-swing adsorption and is examined as a post-combustion alternative to the amine system. The third option is a novel system using oxyfuel combustion in supercritical water, which facilitates CO_2 separation while reducing the irreversibility inherent in fuel combustion.

For each of these options, the current state of the system is modeled and assessed, and the potential for improvement of the system's efficiency is identified and discussed. This assessment is done via an exergy analysis, for several reasons. First, an exergy analysis provides a direct way to compare each process or unit operation to its thermodynamically optimal limit. This gives an immediate sense of how much improvement is actually still possible, thermodynamically, in that process or unit operation. Second, exergy analysis is a useful tool to compare—on a common basis—systems that use different types of inputs (heat vs. work vs. matter transfers), such

as the three systems studied here.

The first goal of this work is to give targeted recommendations for each type of system—and to discuss potential limitations—based on the results of the exergy analyses. A second goal of this work is to provide the correct theoretical modeling framework to allow an exergy analysis of these types of systems. Because each of these systems deal with non-standard fluids, calculation of thermodynamic properties relevant to performing an exergy analysis of these systems is not trivial. The relevant thermodynamic theory is extended where necessary, in particular in the case of the adsorption system.

Acknowledgments

The acknowledgments section is always the first part I read in any thesis, and it's usually my favorite. It's a humbling experience to reflect on just how much of the work that goes into a thesis could never have happened without a huge team of academic and social support. It's also just a lovely experience to get a small glimpse at the personality of the author before digging into their parametric fits or thermodynamic derivations. I will do my best, then, to write an acknowledgments section that I would have enjoyed reading.

Chris Edwards was my advisor for this thesis, and he is indeed excellent at giving advice (the role of the *advisor*, as he would remind us). His scientific knowledge appears inexhaustible, his advice on teaching is always thoughtful, and his positivity is always a welcome boost. He is also, somehow, always available to meet. Thank you for all the conversations on technical and non-technical topics, both of which I'll miss dearly, and for having let me be part of this great team that you assembled.

I was fortunate to get to know all members of my thesis committee at various points in my graduate career. Adam Brandt in particular started meeting with me regularly, along with his students Stuart Sweeney Smith and Yuchi Sun, thanks to this shared carbon capture project. His advice was always on point, and he was always excited to jump into the obscure problems I was having. His genuine enthusiasm for learning and research is inspiring and infectious. Reggie Mitchell was the professor of the very first class I attended at Stanford, and continued giving me helpful thermodynamics advice over the years that followed. And Jennifer Wilcox taught me the fundamentals of carbon capture systems, both in her Stanford class and in her book. Finally, I am very thankful to John Weyant for accepting to be the chair of my

defense despite not having met me beforehand. Thank you to all for your insightful questions and comments.

Thank you very much to the Global Climate and Energy Project and the Edgar N. Meakin Fellowship Fund for funding me and my research, and to everyone at the ME Student Service office for making sure everything always worked smoothly. It goes without saying that this thesis couldn't have happened without your support.

For each of the systems studied in this thesis, there were people who were essential contributors or assistants to the work presented here. Paul Mobley was my research mentor in my first year in the lab, and he taught me almost everything I know about eastern North Carolina BBQ and maintaining a supercritical water combustion system. He also very patiently brainstormed with me the first designs of the system in Chapter 6. Reza Haghpanah was just as patient in teaching me about his area of expertise, adsorption-based CO_2 capture. The work in Chapter 4 would simply have been impossible without our discussions and collaboration. I'm very thankful that he took me seriously despite the fact that I knew nothing about adsorption processes when I first got in touch with him. Finally, I was lucky to have the indomitable Chris Cameron as my enthusiastic summer undergraduate researcher in 2014. His work building the base of the Aspen model for the system in Chapter 3 was invaluable.

Thanks to everyone else in the lab group for being my Stanford home base. To Julie Blumreiter—you were my very first friend at Stanford, and then somehow we also finished our theses from the same lab at the same time. Thanks for all of the Queen study breaks, ethical conversations, and thesis writing sessions. Thanks to BJ Johnson, Greg Roberts, and Ben Kessel for being part of this "wad" of people joining the lab in 2010; you were all great fun to be around for so many years. Sankaran Ramakrishnan, I'm glad I could always count on you for interesting philosophical discussions, and even more so that these continued after you graduated. Mark Donohue, Carol Regalbuto, John Fyffe, and Natt Oliver, the "younger" contingent of the lab, always kept life fun. J.R. Heberle, thanks for being my conference buddy after having been my labmate. Scott Sutton was always willing to lend his valuable experience to answer my many questions about the combustor system.

Thanks to the rest of the academic support group: everyone who helped me study

for quals, the group of Aspen users at Stanford, and Mairi Litherland for being my thesis writing buddy in that final push in the summer. On a related note, I'd like to acknowledge my new colleagues at the Paul Scherrer Institut for giving me a job that actually required me to finish this up. Thanks to all the students I taught during grad school, both at Stanford and at Castilleja—you were all easily my strongest motivation to continue in grad school, because teaching you was so rewarding. And finally, I think it's important to thank the people whose papers or theses I have read over the years, but whom I don't otherwise know. I sincerely appreciate your efforts in communicating your research to me.

I had fantastic housemates while at Stanford: Catie Chang, Agnes Zapata, Jessica Faruque, Lauren Pischel, Chao Long, and Aparna Bhaduri. Aparna in particular was my housemate (and bathroom-mate!) for four years, and it was very hard to adjust to not having her next door to discuss the latest Gail Collins column.

Rebecca Zarin Pass is the rock on which this thesis was built. If that sounds a little sensational, it's partly because I'm writing acknowledgments but mostly because it's true. I am not sure I could have ever imagined a friend who would be just as good at understanding my thermodynamic proofs as my views on the world and life—and really just about anything else—but it's a truly wonderful combination. Thank you for everything.

And finally, thank you to my family. My parents supported me through all the years before and during this thesis, and were equally patient with me when I wanted to talk about my thesis and when I didn't. My sister Amelia did the same, but she usually had to field slightly more frantic version of the stories, and did so with her usual reassuring insight. And Amy somehow, miraculously, stuck by me even though we met during quals and I then tried to cram an impossible number of life events into a single summer at the end. She dealt with far more thesis-related stress than anyone should have to when not actually doing a thesis. Thank you for keeping me grounded, for explaining analytical chemistry to me, for making me coffee, and for not letting me give up.

Contents

List of Tables

List of Figures

Chapter 1

Introduction

1.1 Motivation

Awareness of the global climatic impacts of large-scale anthropogenic carbon dioxide (CO_2) emissions has led to a wide range of research and industry efforts to curtail or mitigate these emissions. Notably, given that the electric grid still accounts for 42% of CO_2 emissions worldwide [7] and 38% in the United States [8], the electricity sector has been a particular focus of these decarbonization efforts. The grid has been an especially attractive target for decarbonization because it consists chiefly of large, stationary emission sources, rather than small and mobile sources like the transportation sector. This makes replacement or retrofitting of existing power plants more tractable than, for example, replacing an entire fleet of standard internal-combustion automobiles with low-carbon alternatives.

Some of the reduction in CO_2 emissions from the electricity sector can be achieved by increased use of low-carbon-intensity electricity generation technologies, such as those using renewable resources, nuclear fuels, and lower-carbon combustible fuels (biomass, and natural gas as a replacement for coal). Further reductions can be achieved by improved efficiency of electricity production, transmission, and end use. However, the most aggressive scenarios for CO_2 emissions reduction all involve a significant contribution from carbon capture and sequestration (CCS) technologies.

These technologies involve the separation of the CO_2 produced when burning a carbonaceous fuel to isolate it as a relatively high-purity stream (the process referred to as *carbon capture*), and its subsequent permanent storage away from the planet's atmosphere (known as *carbon sequestration* or *carbon storage*). In scenarios based on predictive technological, economic, and policy models, CCS technologies are a necessary supplement to emissions reductions from renewable technologies and improved efficiencies.

For example, the 2015 Energy Technology Perspectives report published by the International Energy Agency (IEA) defines several possible technology scenarios to stabilize average global temperature increases due to greenhouse gas emissions [4]. The business-as-usual scenario, in which current trends are extrapolated to 2050 and beyond, results in a global temperature stabilization at an average of 6°C above pre-industrial levels. It is therefore known as the six-degree scenario, or 6DS. By contrast, the 2DS, which predicts global temperatures stabilizing at an average of 2°C or less above pre-industrial levels, and is the most conservative scenario modeled by the IEA, requires significant implementation of CCS over the next 35 years. Figure 1.1 illustrates this point, indicating that in order to follow the 2DS, 13% of the reductions in global CO_2 emissions across all sectors, and approximately 18% of emissions from the electricity sector, will need to come from deployment of CCS technologies.

It is worth placing these scenarios in their proper context. Even a two-degree increase in average global temperatures will have a noticeable effect on our environment. Although it is the most conservative realistic scenario considered by the IEA, it is by no means an indicator of zero—or even low—risk. As seen in Figure 1.2, a two-degree temperature increase will result in high risk to "unique and threatened systems" including cultures and ecosystems, and high risk of extreme weather events such as floods and droughts, often affecting different portions of the globe much more strongly than others. An average global temperature increase greater than 2°C would then have greater adverse effects on the planet. In this context, the need for short-term implementation of carbon capture systems is even clearer.

This reality has led to a surge in research efforts, both in academia (e.g., as reviewed by Kenarsari et al. [9], or by D'Alessandro et al. [6]) and in industry (e.g.,

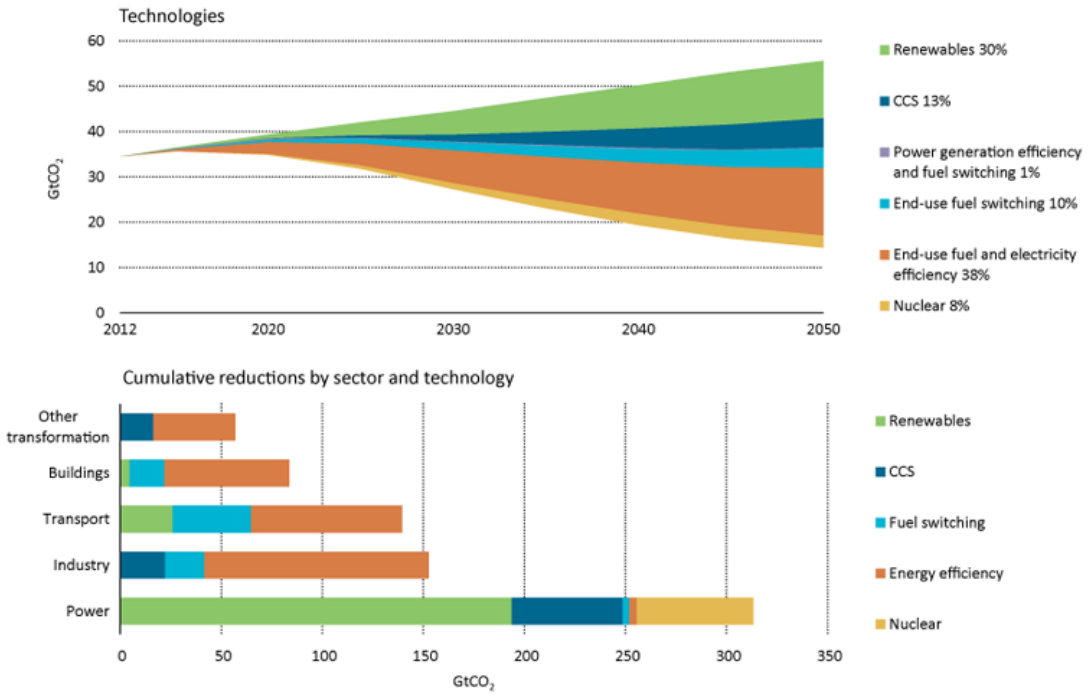

Figure 1.1: Contribution of various technologies in different sectors to reductions in CO_2 emissions necessary to move from the 6-degree scenario (6DS, the extrapolation of current trends) to the 2-degree scenario (2DS, the best-case scenario considered by the IEA). From [4].

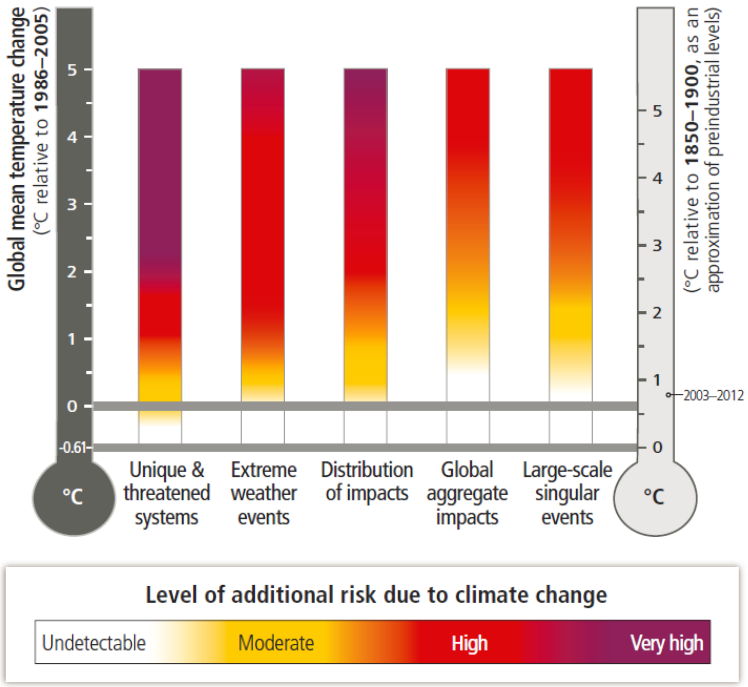

Figure 1.2: Level of risk for people, economies, and ecosystems due to average global temperature increases, as assessed by Working Group II of the Intergovernmental Panel on Climate Change (IPCC). From [5].

by Mitsubishi Heavy Industries [10], Shell Cansolv [11], Alstom [12]), to develop and implement carbon capture systems. Complementary but separate research efforts are studying the feasibility of permanent storage of CO_2 away from the Earth's atmosphere (e.g. [13], [14]), as well as the potential for the commercial use of CO_2 either directly or as a feedstock for making a useful product—a research area known as *carbon utilization* (e.g. [15], [16], [17]).

The focus of this dissertation is the thermodynamic evaluation of carbon capture systems. Given the need for technology development in this area, many systems are being proposed, researched, and developed. Some of these rely on well-established methods, while others rely on completely novel materials and process units in an attempt to improve upon existing technology. These systems therefore exist at vastly different levels of technological development: some are merely theoretical concepts, others rely on lab-scale or bench-scale experiments, while others still are complete pilot plants. Due to this vast range in degree of technological maturity, as well the variety in system type and operation, it can be difficult to compare and evaluate these systems quantitatively against a common baseline.

In this work, we use the laws of thermodynamics to inform this evaluation process. The method of exergy analysis, used here, consists of tracking the absolute thermodynamic potential—the exergy—of all energy and material flows through a process. The goal of this analysis is two-fold. First, completing an exergy analysis will result in the exergy efficiency of the system studied. When properly defined, this value can serve as a directly comparable, rigorous metric by which to assess different systems' performance. Second, conducting the exergy analysis of a system has the outcome of identifying the parts of the process that are the most ineffective at converting the useful energy supplied to them into a different useful form—they destroy exergy, the useful part of the energy. These parts of the system are thereby identified as the areas with the most potential for process improvement, and most in need of future research investment. This can lead to system improvement in two ways: by better (less irreversible) integration between devices, and by reducing the exergy destuction in individual devices through reducing existing internal gradients in chemical potential.

1.2 Carbon capture systems

The various kinds of carbon capture systems are generally organized into three broad categories: post-combustion capture, pre-combustion capture, and oxyfuel combustion. Post-combustion capture refers to separating CO_2 downstream of the combustion process that exists in fossil-fueled power plants. These are currently the most technologically mature of CO_2 capture systems. In these systems, the flue gas from a fossil-fuel power plant, consisting primarily of nitrogen, carbon dioxide, water, oxygen, and trace species, is passed through a system that separates the gas mixture to isolate a stream of CO_2 at relatively high purity (>90%, >95%, or even >99%, depending on the desired final use of the CO_2[1]). The remaining gases, having been cleaned of CO_2, are then vented to the atmosphere.

Pre-combustion capture refers to a process by which CO_2 is separated from a fuel prior to its complete combustion, but after its gasification or partial oxidation. In this process, combustible synthesis gas (or syngas), comprised mainly of carbon dioxide and hydrogen with some water vapor and carbon monoxide, is produced by gasification and reformation of a solid fuel (or simple reformation of a gaseous fuel), and subsequent use of the water-gas shift reaction. The CO_2 is then separated from the gas mixture, so that the hydrogen—the remaining fuel—can be used in an electricity-producing system. The separation process for removing CO_2 from syngas is generally easier than the separation in post-combustion capture. The CO_2 in syngas is at high pressures and at relatively high concentrations, which results in large driving forces for separation, and also delivers the CO_2 stream at higher pressures than post-combustion systems (this is helpful because CO_2 must be pressurized to ≈150 bar for pipeline transportation). However, pre-combustion capture units may be more difficult to add as retrofits to existing plants than post-combustion units.

In oxyfuel systems, the entire combustion strategy is changed to facilitate the isolation of CO_2. In electricity-generating systems associated with post-combustion or pre-combustion capture, the combustion itself is done in the presence of air. The air supplies both the oxidizing agent (oxygen) needed to burn the fuel, as well as an inert

[1]For example, the CO_2 injected at the Weyburn-Midale site in Saskatchewan, Canada must be at a purity of 95% [18].

moderator (nitrogen and other inert gases) needed to keep combustion temperatures below materials limits. For pre-combustion capture systems, the presence of nitrogen in combustion does not affect the separation, as this will have been completed prior to the fuel's combustion. However, one of the difficulties in achieving *post*-combustion capture is that the large amount of nitrogen in the flue gas dilutes the CO_2, making the separation challenging. Oxyfuel systems attempt to remedy this issue by combusting the fuel in high-purity oxygen instead of air, with some combination of CO_2 and/or water vapor supplied to moderate the reaction and keep the temperatures within acceptable limits. This combustion strategy has the effect of producing a flue gas stream that is primarily CO_2 and water. The separation of water from CO_2 by condensation is then much more easily achieved than the separation of CO_2 from N_2 in post-combustion capture. The penalty paid by oxyfuel systems, however, is that they must expend useful energy isolating a stream of oxygen in an air separation unit.

As of 2015, carbon capture and sequestration technologies are still in a relatively early stage of technological development. That said, significant progress has been achieved over the course of the past year. The first—and only, as of 2015—project to be built by industry, operated by an electric utility, and to successfully capture CO_2 at a commercial scale went online in late 2014 at the Boundary Dam coal-fired power station operated by SaskPower in the Canadian province of Saskatchewan. The capture system was added as a retrofit to a unit of the power plant that currently generates 120 MW (net) of electricity, according to a press release from SaskPower in February 2015 [19]. The Boundary Dam carbon capture system is expected to isolate CO_2 at the rate of 1 million tonnes per year over the course of 2015. The captured CO_2 will be used primarily for enhanced oil recovery in the adjacent Weyburn oil field, but approximately 10% of the CO_2 will be sequestered permanently underground in a deep saline aquifer at the nearby Aquistore Project. An April 2015 press release by Aquistore indicated that initial injection had begun at this site, at a depth of 3.4 km underground [20]. The system used at the Boundary Dam power plant is a post-combustion capture unit. At the moment, neither pre-combustion capture nor oxyfuel combustion have yet achieved the degree of technological maturity of post-combustion capture.

When discussing the three broad categories of carbon capture systems, it is important to note that no one single technology or process configuration exists for each one. Post-combustion capture can be achieved in a variety of ways, as can pre-combustion capture and oxyfuel combustion. Figure 1.3 gives a simple, though not exhaustive, description of the variety of possible mechanisms used in CO_2 capture. While we will not detail the operation of each of the separation techniques here, several points are worth appreciating from the diversity shown in this diagram.

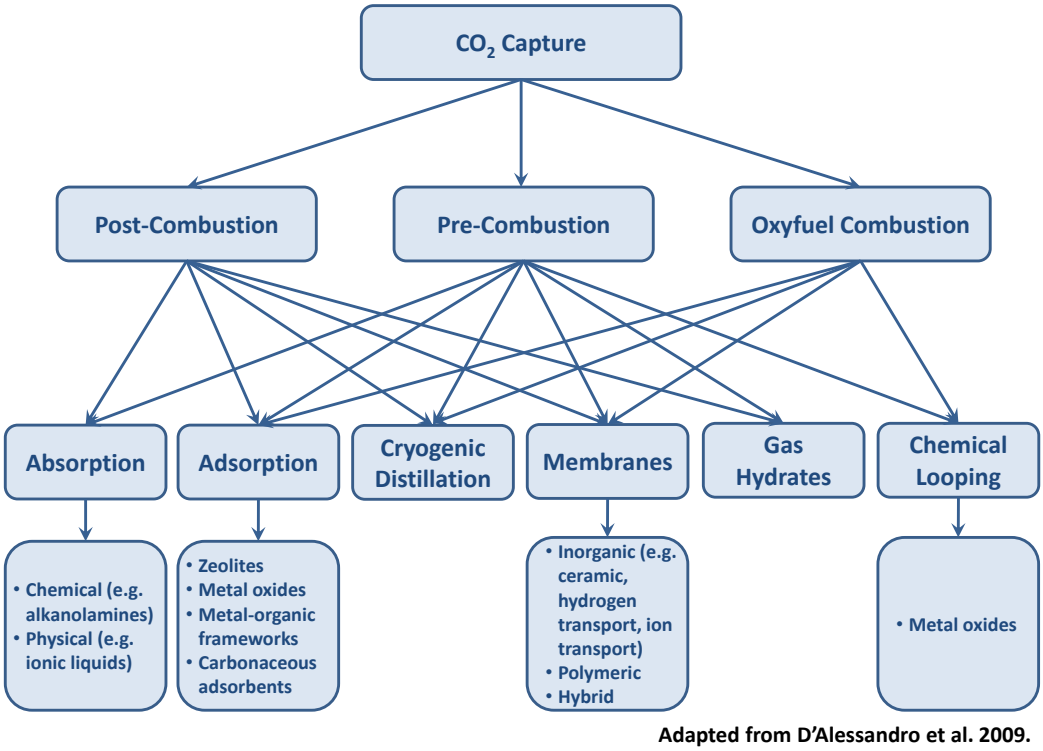

Figure 1.3: Diagram adapted from [6] illustrating the large variety in proposed and existing carbon capture types (second row), separation techniques (third row), and specialized materials needed to enable the separation (bottom row).

First, these technologies can be integrated with the power plant in different ways: for example, by steam extraction from the electricity-generating cycle, by using electricity generated on site, or by using waste heat from elsewhere in the plant. This integration with the plant may or may not have been optimized to minimize the

reduction in electricity generation depending on how well-studied the technology is. Second, the separation techniques listed in the third row span a range of technological maturity, from absorption systems at the best-developed, to the use of chemical looping and gas hydrates at the least. There is a concomitant range in our understanding of the system's actual operation, and whether its operating parameters have been chosen near-optimally or merely as placeholders awaiting future refinement. Finally, some of the materials listed in the bottom row are very well understood, and well-validated models exist to represent their physical and/or chemical behavior. This is the case of some alkanolamines and some zeolites, for example. At the other end of the spectrum are materials that have been merely theorized in computer simulation—for example, some metal-organic frameworks and some ionic liquids—and for which no comprehensive, experimentally-based property models exist yet.

This discussion is intended to show the considerations that must be taken into account when making comparisons of different systems—our current level of understanding of that system must be acknowledged. We will revisit this issue when justifying the system modeling choices made over the course of this dissertation.

1.3 Bases for evaluating carbon capture systems

Evaluating and comparing carbon capture systems is a common goal of many academic researchers, research funding groups, and researchers in industry. Therefore, there currently exist numerous published studies intended to deepen the scientific community's understanding of the current state of this technology. These studies range in scope from detailed studies of a subset of systems, to review papers surveying the progress of current research efforts in a specific subfield, to multi-year analyses and exhaustive descriptions of large numbers of existing and proposed systems. Depending on the intent of the study, they also vary in their analysis techniques.

Detailed technological assessments (such as those produced for the IPCC [21], or for the Clean Air Task Force [22]) can identify existing gaps in the scientific or engineering understanding of carbon capture systems, in order to help set future research direction. They can also be used to compare different systems, for example,

by tabulating the reduction in plants' electricity output for different combinations of fuels and capture techniques. An analysis performed for the IEA in 2007 indicated a reduction of output in the range of 17-21% for coal plants, and 11-20% for natural gas plants [23]. Here, post-combustion capture by absorption had nearly the same impact on coal plants' output as oxyfuel combustion or pre-combustion capture, whereas for natural gas plants post-combustion capture by absorption was significantly better from an output standpoint. The U.S. Department of Energy (DOE) and National Energy Technology Laboratory (NETL) published an extensive study of several fossil-fuel power plants with and without CO_2 capture [1] [2]. They observed that the addition of CO_2 capture units resulted in a 28% reduction in output (per unit fuel input) for pulverized coal (PC) plants with post-combustion capture, and a 16-27% reduction for coal plants with pre-combustion capture (using integrated gasification combined-cycle plants, IGCC). For natural gas combined cycle (NGCC) plants, a 15% output reduction occurred due to post-combustion capture. Another detailed study in 2012 [24] indicated a reduction in net plant output of 18-30% for coal plants, and 14% for natural gas plants, and as in the NETL report, the oxyfuel technologies were somewhat better than post-combustion capture for coal plants—indicating either an improvement since 2007, or slightly different base configurations considered in each study.

Carbon capture systems can also be evaluated by quantifying their economic impact on the power plant. Various methods can be used to evaluate this impact, as laid out by Rubin et al. in a 2013 white paper [25]. Here, we will only give an indication of the effect of carbon capture processes on the resulting cost of electricity (COE). In the 2007 IEA study, capturing CO_2 from a coal plant was seen to increase the COE by around 40% for post-combustion capture, by 45% for oxyfuel combustion and by 24-32% for pre-combustion capture [23]. However, it must be noted that the base plant used for pre-combustion capture (IGCC) already had a significantly higher COE than the other plants, such that the final COE for plants with pre-combustion capture was not significantly different than the COE for the other coal plants with capture.

[2] Note that the version of the DOE/NETL study used in this work is the 2013 version. During the writing of this thesis, DOE/NETL released an updated version [**?**] that uses the Shell Cansolv amine used at the Boundary Dam site instead of the Fluor Econamine system.

For natural gas plants, post-combustion capture incurred a 25-29% increase in the COE, while oxyfuel systems resulted in a 60% increase. By the 2013 DOE/NETL report, the COE penalties were found to be even greater for all systems: around 80% COE increase for post-combustion capture from coal plants, 38-50% increase in COE for pre-combustion capture from coal plants, and 46% increase in COE for post-combustion capture from natural gas plants [1].

Some of the difficulty in comparing capture technologies can be due to disparate degrees of development. The *Technology Readiness Level* (TRL) scale is often used to systematically organize this information. Originally developed by NASA as a gauge of space-readiness and now adapted to other fields including carbon capture and storage, the TRL classification ranges from 1 at the least developed to 9 at the most. This scale is often used in comprehensive reports on the state of carbon capture, such as those by the U.S. DOE [26], the Global CCS Institute in Australia [27], or the Electric Power Research Institute (EPRI) [28]. At the moment, the majority of carbon capture systems are at a TRL of 3-4, indicating a lab-scale or bench-scale level, with solvent-based post-combustion capture systems the only ones to have achieved the pilot-plant level (TRL 7 and up). The value in organizing systems in this way is both to quantify the risk still remaining before investing in building a new systems (less-developed systems being riskier), and to give a sense of how much uncertainty still exists in economic or other metrics (less-developed systems being more uncertain).

Regardless of the metric—whether evaluating economics, technological maturity, or technical performance—several questions often arise: How much better can these systems become? How much potential for improvement is there in newer technologies relative to established ones? And how much potential still remains in the more established systems? Finally, how do we fairly compare different technologies, which could be integrated with different plants powered by different fuels and in different configurations?

Using exergy analysis can help answer these questions from a technical standpoint, by identifying the thermodynamic potential of the system, and the places where this potential is not realized. By identifying the locations where exergy is destroyed in the system—the locations of greatest inefficiencies—we can begin to understand the

limitations of each system, whether they due to issues inherent in the capture process or merely due to poor integration with the rest of the plant. This is the approach taken in this dissertation.

1.4 Organization of the dissertation

A key part of this thesis is the analysis technique, which is motivated in a more detailed manner in Chapter 2, along with a survey of previous exergy or other 2nd-Law analyses of carbon capture systems. As is seen in Chapter 2, carbon capture systems do not currently separate CO_2 in a thermodynamically efficient way, with exergy efficiencies around 20% for the separation alone in post-combustion capture systems (indicating that five times more exergy must be supplied than is theoretically required).

The reasons for these inefficiencies is explored over the four subsequent chapters through the use of three carefully chosen canonical examples for systems with CO_2 separation. First, a post-combustion capture system using amine absorption is analyzed in Chapter 3. This system, which is modeled after the post-combustion capture unit from the 2013 DOE/NETL report [1], is representative of a highly advanced, technologically mature process. Analyzing it will enable us to discern whether there are significant remaining areas for improvement in this system. Due to its relative level of development, this system also serves as a baseline against which to evaluate other carbon capture systems, particularly other post-combustion capture options.

Chapter 4 introduces and examines such a system: a post-combustion capture process by vacuum-swing adsorption (VSA). Pressure-swing adsorption systems (of which VSA systems are a subset) have been used industrially to separate CO_2 from mixtures of other gases, but have not yet been built to capture CO_2 from the flue gas of a power plant at scale. As such, this system is representative of a technology at an intermediate level of maturity, where some aspects of the system operation are known, well-validated, and even optimized, but others are not. In Chapter 4, it becomes clear that a clear understanding of the thermodynamics of adsorption and of adsorbed phases are necessary to enable a detailed exergy analysis of the adsorption

column. This is explored in detail in Chapter 5. Therefore, Chapters 4 and 5 should be considered to exist together as a complementary but distinct sections of the overall VSA system analysis.

The third chosen process, in Chapter 6, is a novel system based on oxyfuel combustion in a moderating medium of supercritical water. This is a system that is in an early stage of technological development: while some segments of the system have been studied experimentally, the majority of the process has been explored through building appropriate models. Moreover, because this is a system in which CO_2 is separated differently than in a post-combustion system, the inclusion of this system provides an opportunity to discuss proper choices of system boundary and reference systems for comparison.

Chapter 7 then closes with discussion and concluding statements. First, the potential for improvement of carbon capture systems as identified by exergy analysis is discussed. A secondary theme runs through this dissertation, however. For each of the three systems considered, careful modeling decisions are necessary to enable exergy analysis. Each of these systems include fluids, substances, or mixtures that behave very non-ideally, and for which well-defined property models are needed. In some cases, it was found that the property models in common use were either not sufficient for exergy analysis, or needed significant adjustment. Therefore, while each chapter (including the concluding Chapter 7) will certainly have the primary goal of providing an assessment of the exergy destruction in the system, its secondary goal will be to build a framework for the property modeling decisions that are necessary to enable this analysis.

Chapter 2

Exergy Fundamentals for CO_2 Capture

In this chapter, we introduce the framework to be used in the analysis of the systems modeled in this dissertation. The use of exergy analysis to evaluate carbon capture systems will first be explained, in particular relating to the careful identification of system boundaries, and of the requirements that must be fulfilled for properties models for fluids to enable this analysis. The use of thermodynamic metrics, including exergy, to evaluate carbon capture systems is not new. Therefore, it is worth reviewing some of the ways in which previous studies have used thermodynamic analyses for carbon capture in order to position the framework presented here in their context. This is done in the latter portion of the chapter.

2.1 Exergy analysis as a method for process evaluation

Exergy is a thermodynamic property that quantifies the maximum possible work that could be extracted from a resource if that resource were to be fully equilibrated—thermally, mechanically, and chemically—with the environment. Given this description, it can also be thought of as the *environmental free energy* [29]. By comparison,

the Gibbs free energy is the maximum possible work that can be extracted from a resource undergoing an isothermal and isobaric process, and the Helmholtz free energy is the maximum possible work that can be extracted from a resource undergoing an isothermal and isochoric process.

Unlike energy, exergy is not a conserved quantity. In any real process, exergy is destroyed. In this quality as a non-conserved property, it is more akin to entropy, although it does have the same units as energy. A process that is more thermodynamically efficient—less irreversible—will destroy less exergy, and a process that destroys large amounts of exergy should be examined for possible improvement. Mentioning *irreversibility* suggests a direct relationship between entropy generation and exergy destruction. This relationship is given by the Gouy-Stodola equality [30]

$$X_{dest} = T_o S_{gen} \tag{2.1}$$

which is valid for any process, and where T_o refers to the environmental temperature. In any process, the exergy destruction can be found from the balance equation

$$X_{dest} = X_{in} - X_{out} - \Delta X \tag{2.2}$$

Tracking and quantifying the exergy destroyed in a system is useful for two primary reasons. The first is the identification of a performance metric, the exergy efficiency η_x, for a system. Depending on the desired output of the system (e.g., shaft work, or high-purity product), the exergy efficiency may be defined differently. However, all definitions amount to comparing the exergy supplied to the system to the exergy of the desired output of the system. Because exergy can be precisely defined for any substance or energy transfer, systems that may otherwise take very different inputs (e.g. work, steam, heat transfer) can be compared on an even basis: on the basis of how well they use the exergy supplied to them, as quantified in an exergy efficiency. The definition of exergy efficiency for different types of carbon capture processes is discussed in Section 2.1.1.

The second reason for tracking exergy destruction is to analyze the internal operation of a system. This consists of finding not just the exergy efficiency of the system,

but also identifying the locations in the system where the exergy destruction occurs. This is calculated by applying the balance equation in Eq. 2.2 to individual devices or processes. In order to perform these calculations on individual devices, the operation of the system must be understood well enough to be able to calculate the exergy and entropy of any transfers to the device as well as any exergy or entropy accumulated inside the system. This is discussed in Section 2.2.

2.1.1 Exergy efficiency of a system

Post-combustion capture systems

Post-combustion CO_2 capture systems are separation processes. As shown in Figure 2.1, they take in a flue gas that contains 4-15% CO_2 by mole (for fossil-fuel power plants), and deliver high-purity CO_2 as well as a waste stream largely scrubbed of CO_2. Afterwards, the CO_2 is often compressed to high pressures (around 150 bar) for transport or storage.

The laws of thermodynamics indicate that a minimum amount of exergy must be supplied to any system to achieve such a separation, even when operating ideally (reversibly). This minimum exergy of separation $\dot{X}_{min,sep}$ is then the bar against which real separation systems can be evaluated. This quantity is sometimes referred to as the minimum work of separation [31], [32], but we prefer the term exergy here to indicate that any kind of useful energy could be supplied, not only work (for example, the exergy supplied to amine-based post-combustion capture systems is typically from heat exchange with steam, not from work). Similarly, a minimum amount of exergy $\dot{X}_{min,comp}$ is necessary to compress the CO_2 product stream to high pressures.

The minimum exergy of separation for a steady-flow system can be found from a balance equation,

$$\dot{X}_{min,sep} = \dot{N}_{LPCO2}\hat{\psi}_{LPCO2} + \dot{N}_{waste}\hat{\psi}_{waste} - \dot{N}_{flue}\hat{\psi}_{flue}, \tag{2.3}$$

where $\dot{N}$ is the molar flow rate, and $\hat{\psi}$ is the mole-specific flow exergy of the fluid, and is given by differences in the thermodynamic properties of the fluid stream at its

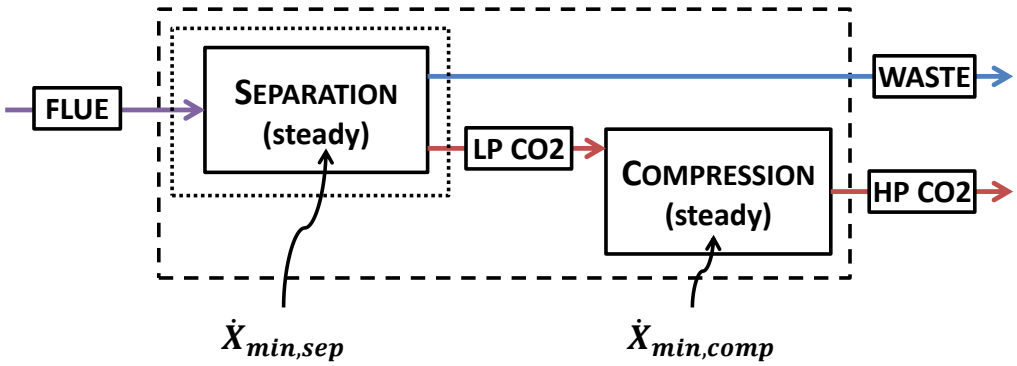

Figure 2.1: Definition of the minimum exergy of separation.

state in the system and at the environmental state

$$\hat{\psi} = \hat{h} - \hat{h}_o - T_o(\hat{s} - \hat{s}_o) - \sum \mu_{i,o}(y_i - y_{i,o}) \tag{2.4}$$

Here, the subscript o refers to properties at the environmental state, μ_i is the chemical potential of chemical species i, and y_i is the mole fraction of species i. The properties without subscript o are evaluated at the state of fluid. For example, the minimum exergy needed to isolate a stream of CO_2 at 95% purity from a model of flue gas as a binary mixture of 85% N_2 and 15% CO_2, while capturing 90% of the CO_2, is 0.13 MJ/kg-product if all fluids are taken to be at 25°C and 1 atm.

We can then define the exergy efficiency of a real separation process η_x by comparing the actual exergy supplied $\dot{X}_{sep,actual}$ to the minimum exergy of separation,

$$\eta_x = \frac{\dot{X}_{min,sep}}{\dot{X}_{sep,actual}}. \tag{2.5}$$

Because we have so far not imposed anything about the operation of the system, nor the path through the separation process, we could refer to this as a "black-box" exergy efficiency—a valid metric that can be identified from the transfers alone.

This metric provides a direct way to compare different post-combustion capture systems to each other. Systems with lower exergy efficiency are further from their

thermodynamically ideal operation, and therefore could still have room for improvement. In fact, the "room for improvement" can be defined directly from the difference between the known values of $\dot{X}_{actual}$ and $\dot{X}_{min}$ as the exergy destroyed in the system

$$\dot{X}_{destroyed} = \dot{X}_{actual} - \dot{X}_{min}. \tag{2.6}$$

This is simply a statement that any exergy that is supplied that is not strictly required by the laws of thermodynamics is instead destroyed in the system. When we then perform a detailed exergy analysis of each of the devices in the system (as described in Section 2.2), the sum of all the exergy destruction identified in each of the devices in the separation must equal the total exergy destroyed in the system as identified in Eq. 2.6. This provides a way to check that the same system boundary is used for both the black-box exergy efficiency calculation and the detailed exergy analysis.

We used an example of separating flue gas that was modeled as a binary mixture of nitrogen and carbon dioxide, and a separation process for which the inlet and outlet flows were imposed to be at constant temperature and pressure. Often however, published information about the actual operation of carbon capture units includes flue gas that enters the separation system as a mixture including several more gases (including water vapor), and at temperatures that are higher than the temperature of the waste gas and CO_2 product. A minimum exergy input can still be defined for such a system, following Eq. 2.3. Arguably, this is then not just a minimum exergy *of separation*, and instead a combined minimum exergy of separation and of some other state change. When defining a performance metric like an exergy efficiency in Eq. 2.5 then, it is important to define the minimum exergy requirement a system with the same boundaries and the same transfers—with the same flows of flue gas, stack gas, and CO_2 product at the sames states—as the system for which the actual exergy transfer is defined.

Quantifying the actual exergy transfer may require some thought as well, depending on the type of system. If the exergy supplied to the system is in the form of work, the situation is relatively simple, because the entirety of energy transferred as work has the potential to be useful (so $\dot{X}_W = \dot{W}$). However, if exergy is supplied to the

system as heat transfer or with matter, it is important to pay careful attention to defining the system boundary. The exergy transferred with heat is

$$\dot{X}_Q = \dot{Q}\left(1 - \frac{T_o}{T_b}\right) \tag{2.7}$$

where T_b is the temperature of the boundary at which the heat transfer enters the system.

Placing the boundary in the "correct" position depends on what one considers the carbon capture system to be, and for which analysis purpose. For example, if heat is transferred to the capture system from a hot process stream from elsewhere in the plant, it would be valid to define the boundary to be at the point where the hot process stream enters and leaves the heat exchanger (as shown in Figure 2.2b). With the system boundary drawn this way, the entirety of the exergy destruction that happens as a result of the carbon capture process is accounted for—and therefore, the entire effect on the rest of the plant is counted. It would also be valid to define the boundary right at the temperature of the carbon capture system (as shown in Figure 2.2a). However, in this case, one would only evaluate how well the capture process performs with the exergy that is directly supplied to it (i.e., how far from thermodynamically optimal the capture process itself is, rather than how well it is integrated into the rest of the plant). This issue will be revisited in Chapter 3.

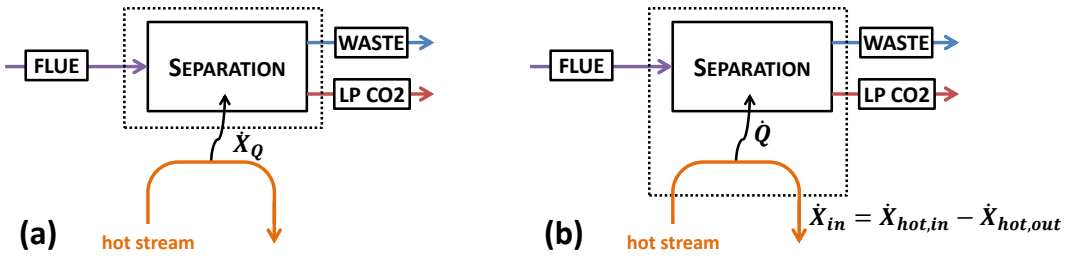

Figure 2.2: The system boundary is not necessarily clearly defined when exergy is transferred to the separation system via heat transfer from another process stream.

Integrated capture systems

Some types of CO_2 capture processes do not occur as separate modules independent from the electricity-producing system, but are instead an intrinsic part of it. This is the case for oxyfuel systems, for example. In oxyfuel systems, the CO_2 separation occurs because the fuel is first combusted in an environment of oxygen, CO_2, and water. Separating CO_2 from the resulting combustion products, which are only CO_2 and water, is much easier than separating CO_2 from nitrogen and other non-condensable gases as is needed in post-combustion capture.

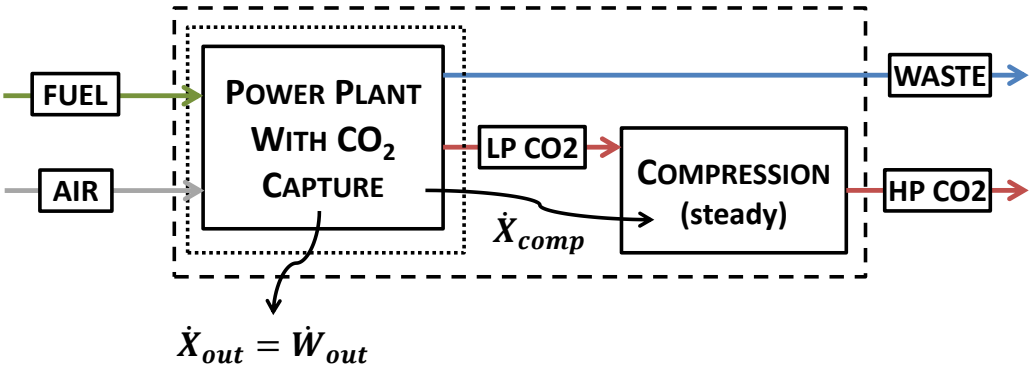

Figure 2.3: Power plant with completely integrated CO_2 separation system (e.g., oxyfuel system).

In these systems, the process of separating CO_2 does not happen in a specific part of the system, so it is not possible to define a minimum exergy of separation in the same way as for post-combustion CO_2 systems. However, we can still define a thermodynamic metric for the operation of the system. The exergy efficiency η_x is once again a ratio between the actual operation of the system and the exergy supplied to it. The exergy supplied to this system is in the fuel for the power plant, which transfers exergy to the system at the rate of $\dot{X}_{fuel}$. If there were no exergy destruction in the system, all of the fuel exergy would be converted to electrical work output, $\dot{W}_{out}$. In reality, some of the fuel exergy is destroyed in the system, and the exergy

efficiency for this type of process is defined as

$$\eta_x = \frac{\dot{W}_{out}}{\dot{X}_{fuel}} \tag{2.8}$$

However, the exergy efficiency of this system (which is mainly an electricity-generating system, not mainly a separation system) cannot be directly compared to the exergy efficiency of a post-combustion capture system alone[1]. Instead, the exergy efficiency of the plant in Figure 2.3 could be compared to a power plant operated using the same fuel, but without a carbon separation process, in order to isolate the effect of having incorporated such a process. This issue will be revisited in Chapter 6.

2.1.2 Exergy analysis to identify losses and drive system improvement

After a black-box exergy efficiency is defined, the potential for improvement in the system can be explored by the calculation of the exergy destruction in each of the devices in the system. For each device, Eq. 2.6 is used to calculate $\dot{X}_{dest}$. The first necessary step is to build a computer model of the system in order to identify the state at which streams enter and leave each device, based on the known overall transfers to and from the system, and based on other known information about the particular system's operation. The second necessary step is to use a set of fluid property models that allow for an exergy analysis to be performed.

2.2 Fluid property methods to enable exergy analysis

In order to model and analyze a chemical system, the thermodynamic properties of the working fluid(s) must be accurately represented. First, there must exist accurately

[1]Except to say which is farther from its own thermodynamically-ideal operation.

measured experimental data for the fluid in the thermodynamic region of interest (or, barring this, a well-known and well-understood representation should apply in a certain limit—for example, the ideal gas law at large specific volumes, or Henry's law at low solute concentrations). Then, a mathematical model is fit to a certain range of these experimental data, generally representing some parts of that range more closely than others. Uncertainty or inaccuracy in either the original data measurement, or in the local behavior of the mathematical fit, will lead to uncertainty or inaccuracy in the results of the system operation.

However, stricter constraints than simply accuracy are imposed on the forms of mathematical property models by the laws of thermodynamics. All bulk[2] fluids—whether pure substances or mixtures—have thermodynamic properties that are interrelated by way of a single equation [33], the *fundamental relation*

$$S = S(U, V, \{N_i\}) \tag{2.9}$$

the differential form of which is the Gibbs equation

$$TdS = dU + PdV - \sum_i \mu_i dN_i \tag{2.10}$$

and the integral form of which is the Euler relation.

$$TS = U + PV - \sum_i \mu_i N_i \tag{2.11}$$

From the combination of Eqs. 2.10 and 2.11 comes the Gibbs-Duhem equation, which must hold as a relationship between thermodynamic properties of the same bulk fluid at all times in order to ensure thermodynamic consistency.

$$\sum_{i=1} N_i d\mu_i = -SdT + VdP \tag{2.12}$$

Equations of state, and property methods that result from the implementation of

[2]Bulk fluids as separate from a two-dimensional surface phase, which will be treated in Chapter 5.

these equations of state in computer code or software, should exist in a way that is thermodynamically consistent in order to correctly calculate properties, such as entropy, at a given thermodynamic state.

In theory, stating that property models must agree with Eq. 2.12 mainly has implications for identifying correct and incorrect mixing rules for chemical species. For example, the issue of identifying thermodynamically consistent activity coefficients for real mixtures can be resolved by testing for adherence to Eq. 2.12, as explained by Van Ness [34]. For mixtures of bulk gases, thermodynamically correct mixing rules are often taken for granted. However, for non-ideal liquids (such as solutions of electrolytes) or for unusual phases such as the adsorbed surface phase considered in Chapter 5, mixing rules may exist that are correlation-based or which use simple addition of properties with weighting factors (for ease of calculation). Following a thermodynamically consistent rule that obeys Eq. 2.12 may not necessarily be important for systems where the analysis goal is related to the first law of thermodynamics (e.g., calculating heat transfer from an absorber column), but it is essential for calculating entropy values. The idea that any chemical equilibria that are modeled in the system must be modeled consistently with the rest of the thermodynamic framework (rather than by an independent correlation, as is sometimes done for equilibrium constants) is also an important issue for these calculations.

In practice, even if Eq. 2.12 is correctly built into the theory of the equation of state or mixing rule, the implementation of complex mixtures in commercial or custom-written code is not always correct due to inadvertent error. Testing the computer modeled system for adherence to Eq. 2.12 can then serve as a useful way to identify any problems in implementation. In this dissertation, we revisit the issue of thermodynamically consistent equations of state, mixing rules, and computer implementation in several systems in which the correct calculation of entropy values is not trivial.

2.3 Previous thermodynamic analyses of carbon capture systems

Several previous studies have attempted to structure, explore, and resolve the issue of exergy destruction in carbon capture systems. These studies can be classified into three general categories: (1) discussion and prescription of the correct choice of framework to analyze these systems in a useful way; (2) black-box comparisons of several different systems; and (3) detailed exergy analyses of specific system to enable process improvement.

2.3.1 Thermodynamic frameworks

In a 2011 publication, House et al. discussed the thermodynamic limits relevant to carbon capture systems using the minimum work (exergy) of separation discussed earlier [35]. Although their study is primarily concerned with the feasibility of CO_2 capture from ambient air rather than from point sources like power plants, a noteworthy comment about point-source capture is made. In their Figure 3, the exergy efficiencies of several separation processes relevant to carbon capture—post-combustion from coal and natural gas with amine absorption, air separation, pre-combustion separation of CO_2 from syngas—are plotted. All of these efficiencies are between 15 and 25%; moreover, the efficiencies generally decrease as the mole fraction of CO_2 in the inlet stream decreases. These values are very low. By comparison, the exergy efficiency of electricity-producing cycles (e.g. natural gas combined cycles) can reach nearly 60%. This leads us to ask *why* these values are so low, and whether they can be raised.

Luis [36] made an appeal to the chemical process industry to use exergy analysis as tool for improving the operation of separation processes in general, and of CO_2 capture processes in particular. She drew upon the work of Leites et al. [37] to give specific recommendations, including the reduction of driving forces in contacting columns and other process units.

Jordal [38] additionally pointed out the importance of carefully selecting appropriate system boundaries and reference systems when analyzing and comparing carbon

capture systems. Although her recommendations are for technical analyses in general (using LHV efficiencies as a metric), they are very relevant to exergy analyses. Jordal's discussion of sensitivity to chosen fuel, of the inclusion of auxiliary systems (e.g. air separation units) within the system boundary of the plant, and of other considerations, is important when comparing any dissimilar systems on an even basis.

Finally, we mention the University of Texas metric for measuring reduced work output from power plants due to CO_2 capture units (as implemented in Rochelle et al. 2011 [39], among others). In these calculations, an efficiency metric is defined by a fraction that places the minimum work (or exergy) of separation in the numerator. The denominator is the sum of the work actually supplied to the system, and a "work-equivalent" value of the heat transferred to the system from steam. While this initially appears to be similar to an exergy efficiency, it is not an exergy efficiency due to way in which the heat transfer is valued. The work-equivalent value in these systems is the heat transfer to the system, multiplied by a Carnot fraction with the stripper reboiler temperature as T_{hot} and the steam cycle condenser temperature as T_{cold}, multiplied by the isentropic efficiency of the steam turbine. This quantity is therefore not the steam's exergy, but instead a measure of the steam's ability to do work in the power plant—which is a smaller quantity than its exergy, since power plants are not 100% exergy efficient. An efficiency defined in this way thus results in higher percentage values than the corresponding exergy efficiency in most cases. While this efficiency metric does account for the fact that electrical work is more valuable to the steam power plant than steam exergy, it cannot be directly compared with exergy efficiencies of other systems.

2.3.2 Black-box comparisons

Treating separation units as black boxes can be useful to compare different systems quickly without making detailed process models.

Simpson and Simon [40] compared an oxyfuel combustion process to a system with post-combustion capture by amine absorption, in order to identify the exergy efficiency improvements in separation processes that would be necessary to make one

viable relative to the other. They used exergy efficiencies from the literature, finding that amine absorption systems had exergy efficiencies of 10-14% and air separation units (for the oxyfuel system) had exergy efficiencies of 15-25%. These efficiencies were defined on the basis of comparing the actual exergy supplied to these systems to the minimum exergy of separation.

Lara et al. [41] compared the exergy efficiency of six options of processes for CO_2 separation from coal-fired power plants. Two were post-combustion capture systems: one by amine absorption, and one using a calcium oxide/calcium carbonate looping cycle. Three were pre-combustion capture systems: one using adsorption, one using a zeolite membrane, and one using absorption in the solvent Selexol. The sixth system was an oxyfuel process. The importance of clearly defining the system boundary and the desired product for an exergy analysis can be seen in this study. For the pre-combustion capture systems, the exergy efficiency was defined by dividing the exergy of the hydrogen produced by the exergy of the coal supplied, and the resulting values were in the range of 68-79%. By contrast, the exergy efficiencies for the post-combustion and oxyfuel systems were found to be in the range of 32-39%, because the exergy efficiency for these systems was defined as the exergy of the steam sent to the power cycle, divided by the exergy of the coal supplied to the system. Therefore, while each of these values can be used to compare systems defined within the same system boundary, a direct comparison of these pre-combustion exergy efficiency values to those of post-combustion systems is not possible.

Kvamsdal et al. [42] studied nine different concepts, including many novel systems, for electricity generation from natural gas including CO_2 capture. Although these systems are analyzed on the basis of LHV efficiency and not on the basis of either exergy efficiency or of identifying exergy destruction in devices, this study is useful due to having implemented the well-defined boundaries and consistent assumptions outlined by Jordal [38]. In this study, several systems were found to perform much better than the standard NGCC with post-combustion amine absorption capture. However, these were mostly new concepts where the combustion strategy was altered significantly from the base case. For example, the two best-performing systems included one based on a solid-oxide fuel-cell, gas-turbine hybrid system; the second concept

replaced the combustor with a mixed combusting membrane. Therefore, this study's results can be interpreted more as a statement on alternative combustion strategies than on varying carbon capture methods.

Treating separation systems as black boxes can also be useful for combining several different post-combustion capture options in a hybrid system. For example, Fong et al. [43] combined a vacuum-swing adsorption system with a membrane system and a cryogenic separation system to achieve higher CO_2 purity and recovery, while maximizing the exergy efficiency of the overall separation system.

2.3.3 Detailed exergy analyses

Exergy analyses of detailed process models have been performed, sometimes in order to improve a particular system, and other times to provide a comparison of two systems in a more detailed way than could be done by merely defining a black-box exergy efficiency.

Pre-combustion capture and oxyfuel systems

Guedea et al. [44] compared two novel ways to use coal as a fuel for electricity generation. The first system they modeled used oxyfuel combustion in a pressurized fluidized bed combustor. The second system they examined used chemical looping combustion, which is an oxyfuel strategy that uses oxygen from a metal oxide instead of from an air separation unit. Therefore, they were comparing two different implementations of oxyfuel systems with coal. In both cases, the majority of the exergy destruction was found to be in the combustion section (as expected), but the chemical looping cycle was found to have an overall higher exergy efficiency.

Erlach et al. [45] also compared two novel coal-based systems, but both using an integrated gasification combined cycle (IGCC) system rather than a simple cycle. One of the systems captured CO_2 by using the solvent Selexol in a pre-combustion capture process, while the other used chemical looping combustion. They calculated the exergy destruction in individual devices in each of the two base systems. Then, they used these results to vary targeted operating parameters and achieved small

efficiency gains, with overall plant exergy efficiencies reaching 36-38% for the chemical looping combustion case and 34-35% for the pre-combustion capture case. In a similar study, Kunze et al. [46] also modeled an IGCC system with pre-combustion capture by solvent absorption, and found a 40% exergy efficiency in their base case. However, by altering the process parameters (and the process units, to some extent) to include hot gas clean up, they improved the integration of system components and raised the overall plant exergy efficiency to 54%.

The effect of pre-combustion capture on natural gas power plants has also been studied, by Ertesvåg et al. [47]. As with the coal studies, they first found the exergy efficiency of their base plant with CO_2 capture, which was 47%, and adjusted process parameters until achieving an improvement in the overall efficiency (in their case, by 3 percentage points).

Post-combustion capture

Exergy analyses of post-combustion capture systems have been performed for systems using coal as a fuel as well as natural gas. Romeo et al. [48] modeled a type of post-combustion capture process that reacts calcium oxide with CO_2 to form calcium carbonate. They used flue gas from a coal plant. By using the results of a detailed exergy analysis to direct process improvement, they were able to reduce the consumption of additional coal in their system (relative to the plant with no CO_2 capture) by a factor of 2.5. Meanwhile, Zhang et al. [49] also studied post-combustion capture from coal plants, but used a two-stage membrane process to achieve the separation. They found the combined capture and compression process to have an exergy efficiency of 53%, with the greatest exergy destruction occurring in the first membrane stage.

Three key studies have performed exergy analyses of post-combustion capture by amine absorption, and all three used systems that captured CO_2 from the flue gas of a natural gas combined cycle plant. In 2004, Geuzebroek et al. [50] identified the absorber, stripper, and flash condenser (at the top of the stripper) as the areas of greatest exergy destruction in these systems. In 2011, Amrollahi et al. [51] confirmed that these areas were still the locations of greatest irreversibility, even with the improvements in amine absorption systems during the intervening decade. They found

that these systems had an exergy efficiency of 32% for the separation and compression of CO_2. Having identified the two columns as the sources of the greatest exergy destruction, they then attempted to improve upon the base case in a separate study [52]. Their approach was to reduce the driving forces in the columns, by intercooling the absorber, and in the stripper by compression of the reboiler vapor for injection into a higher point in the column. This allowed them to improve the efficiency of the separation and compression system to 36%.

We note here that, to our knowledge, no exergy analysis has been performed of any of the systems modeled in this dissertation. The system modeled in Chapter 3, which uses amine absorption to capture CO_2 from the flue gas of a coal plant, is very similar to the systems studied by Geuzebroek et al. [50] and by Amrollahi et al. [51], except for the different flue gas used. Therefore, we expect similar results, and this system can serve as a baseline to compare back to existing literature. At this time, the exergy destruction in post-combustion systems using pressure-swing adsorptions is not well understood, and this is covered in Chapters 4 and 5. Chapter 6 will introduce a new system entirely, based on a type of oxyfuel combustion of natural gas.

Chapter 3

Post-Combustion Capture by Amine Absorption

In this chapter we introduce and analyze what is easily the best-studied CO_2 capture system in order to serve as a baseline against which to compare newer systems. This system uses chemical absorption in an amine solution to drive a post-combustion CO_2 separation process. The background of this type of system and the reasons for studying it in this work are presented first. Then the process modeling environment and design decisions are explained with particular emphasis on the choice of property methods necessary to enable an exergy analysis. Finally, the exergy analysis is completed, and its results are shown and discussed. The importance of choosing thermodynamically correct models when analyzing exergy destruction in these systems is illustrated in this final section, by showing the apparent results of a similar analysis done with incorrect property models.

3.1 System description

3.1.1 General system: post-combustion capture by absorption

The use of amines to absorb CO_2 from a stream of other gases has been known since at least 1930, although its greatest industrial use so far has been to isolate CO_2 from natural gas or hydrogen rather than flue gas [53]. Because of its long history at large scale for these other applications, the adaptation of amine absorption for carbon capture from flue gas is considered to be less risky (and thus less costly to implement when building a first-of-kind pilot operation) than many other proposed carbon capture systems. As a result, this type of capture system is the only one to have yet been built and operated at a major electricity producing plant, such as at the SaskPower coal plant at Boundary Dam in Canada [19].

The basic operation and general nomenclature of the system components in a post-combustion, solvent-absorption capture process are illustrated in Figure 3.1. Cleaned and cooled flue gas is introduced into the bottom of a contacter column, the absorber. In the absorber, the flue gas bubbles up through a down-flowing stream of liquid solvent, into which CO_2 from the flue gas will dissolve as the two streams are kept in contact over the length of the column. The flue gas, having been scrubbed of its CO_2, then exits the top of the absorber to be released to the atmosphere as stack gas. This is the *capture* part of the process: The CO_2 from the flue gas has been trapped into liquid solution by the solvent.

The rest of the process is necessary to regenerate the solvent, and by doing so, to isolate high-purity CO_2 for eventual sequestration or utilization. The solvent flowing out of the bottom of the absorber column is enriched in CO_2 relative to that entering the top of the absorber. These streams are referred to as the *rich* and *lean* solvent streams, respectively. The rich solvent has CO_2 removed from it in a second column: the stripper, or desorber. The separation in the desorber is achieved primarily by the heat transferred to the reboiler at the bottom of the column. This is where CO_2 is boiled out of the liquid solution. The liquid that remains at the outlet of the

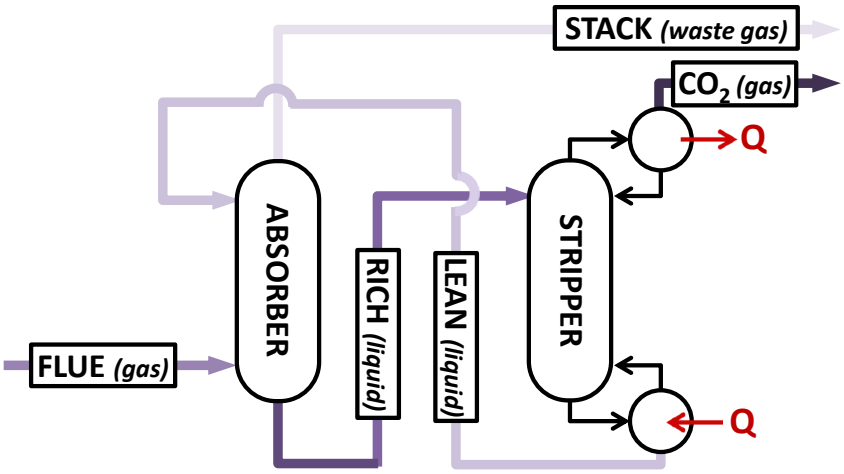

Figure 3.1: Basic representation and nomenclature of solvent-based post-combustion carbon capture systems. Darker stream colors are used to indicate higher amounts of CO_2 in that stream.

reboiler is the lean solvent, which is recirculated. Meanwhile, the vapor (primarily CO_2) bubbles up to the top of the column. The temperature in this column is highest at the reboiler. The rest of the column is colder, with the coldest section existing at the top of the column in the condenser, which is actively cooled. This has the effect of condensing nearly all other species (e.g., water or other solvents) out of the gas phase, leaving a high-purity stream of CO_2 to exit the column. After this point, the separation process is complete, and the CO_2 goes through a series of intercooled compression stages to deliver it at pressures appropriate for pipeline or other transport (around 130-150 bar).

While the solvents used in these processes are often amine aqueous solutions due to these solvents' long history of industrial use, they do not have to be—many solvents have been and are continuing to be considered for post-combustion capture. Other aqueous solutions can be used, such as aqueous solutions of potassium carbonate (see Smith et al. 2014 [54], among others) or of ammonia (e.g., by Alstom [12]). Even within the aqueous amine solution family of solvents, there is a fair amount of variation. Primary amines—organic molecules with an -NH_2 group appended to the end of a hydrocarbon chain or aromatic ring—such as monoethanolamine (MEA)

have been used in industrially developed carbon capture units (e.g., by Fluor [55]). Secondary amines, which are organic molecules with an -NH group inserted into a hydrocarbon chain or aromatic ring; and tertiary amines, which are organic molecules in which an N atom joins three separate hydrocarbon chains or aromatic rings, have also been used. These include the secondary amine KS-1 by Mitsubishi Heavy Industries [10], the secondary amine piperazine (PZ) at the University of Texas and others (e.g., [39], [56]), and the tertiary amine MDEA, which is often used in mixtures with other amines (e.g., with MEA [57] or with PZ [58]). Non-aqueous solvents can also be used, notably the class of substances known as ionic liquids. These are salts that exist in the liquid phase at room temperature and pressure (and at absorption process conditions), see Gurkan et al. 2010 as an example [59]. These substances have been the subject of recent research due to the tunability of their properties. The anion and cation ends of these large molecules can be varied nearly independently, allowing for a large number of potential configurations whose properties can be optimized for efficient post-combustion capture.

3.1.2 Specific system: DOE/NETL baseline

The specific system analyzed here uses the primary amine monoethanolamine (MEA, C_2H_7NO) in aqueous solution as the solvent for post-combustion capture of CO_2. It is based on the system used by the DOE/NETL in their extensive detailed study of fossil-fuel power plants with and without CO_2 capture (most recently updated in 2013 as *Cost and Performance Baseline for Fossil Energy Plants Volume 1: Bituminous Coal and Natural Gas to Electricity, Revision 2a* [1]). The DOE/NETL baseline system is itself based on the Econamine FG Plus^{SM} technology developed by Fluor [60], [61].

This system is chosen for study here not because it is necessarily the best post-combustion absorption system in terms of technical performance—in fact, several systems have been predicted to cause less reduction in the power plant's output, notably systems using piperazine [39] [56]. However, it is a very well-understood system that has been studied extensively and is often used as the baseline against

which newer carbon capture systems are evaluated (in terms of technical performance as well as cost and operability). It is therefore a useful system to study in an exergy-based evaluation of several classes of carbon capture systems.

The model developed here was intended to match key DOE/NETL baseline performance values. These values, which are taken directly from the DOE/NETL baseline report, are listed in Table 3.1, where the location of the streams are illustrated in Figure 3.2. This post-combustion capture system takes flue gas from a subcritical, pulverized coal power plant with a net power output of 550 MW. Before entering the carbon capture unit, the flue gas first undergoes two stages of sulfur removal. Because SO_2 reacts with MEA to form solid salt precipitates which foul the absorption system, it is important to remove sulfur from the flue gas to a greater degree than is required for emissions to the atmosphere directly. The flue gas is therefore passed through a flue gas desulfurization (FGD) unit, and then through an additional SO_2 polishing unit. This results in such low levels of sulfur that the SO_2 mole fraction at the inlet of the carbon capture unit was modeled to be zero in the DOE/NETL report as listed in Table 3.1.

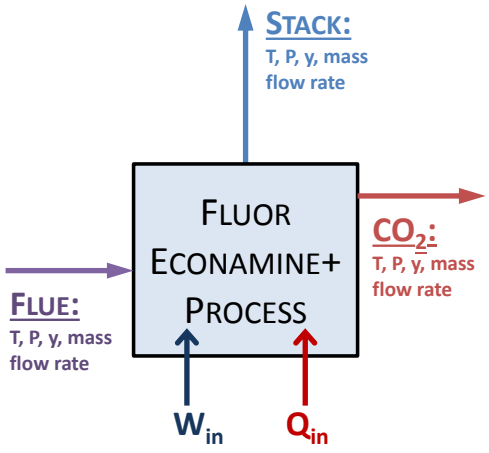

Figure 3.2: Basic information given by the DOE/NETL report.

The transfers listed on Figure 3.2 and in Table 3.1 constitute the majority of the information that is directly given about the operation of the absorption system in the

Table 3.1: Values and state information of all transfers to and from the MEA absorption capture unit, given by the DOE/NETL baseline report. [1]

Streams	Flue	Stack	CO_2
Mole Fractions			
Ar	0.0081	0.0108	0.0000
CO_2	0.1350	0.0179	0.9961
H_2O	0.1537	0.0383	0.0039
N_2	0.6793	0.9013	0.0000
O_2	0.0238	0.0316	0.0000
SO_2	0.0000	0.0000	0.0000
Flowrate (kmol/s)	30.959	23.332	3.7772
Flowrate (kg/s)	892.57	657.31	165.86
Temperature (°C)	58	32	21
Pressure (MPa)	0.10	0.10	0.16
Enthalpy (kJ/kg)	301.43	93.86	19.49
Heat Transfer (MW)	588.572		
Work (MW)	22.400		

DOE/NETL baseline report. Detailed, device-by-device state information is not given for the internal operation of the absorption system. However, we can build a model based on the known operation of these systems from studies of similar systems, and based on making informed decisions from the data given by DOE/NETL. Moreover, we do know that the heat transfer listed comes from steam extracted from the steam power cycle, and that it is used exclusively in the reboiler at the bottom of the stripper column.

As a first pass towards understanding this system, we will note that the system described in Figure 3.2 and Table 3.1 is neither in mass nor energy balance as listed. Tracking the balance of chemical species reveals that the missing mass flow is water alone, and that this water should be exiting the system boundary at a rate of 69.4 kg/s. Although we do not yet know at which temperature this water will leave the system, we do know that our model must account for this water leaving. Similarly, tracking the energy balance of this system as described in the DOE/NETL report reveals that energy should flow out of the system at a rate of 815.1 MW. This is

assumed to leave the system as heat transfer directly or in the enthalpy of cooling water (and of the waste water flow identified). We can then draw an updated version of the black-box MEA system, as shown in Figure 3.3. At the moment, it is not yet clear from which devices in the system these transfers are assumed to occur. However, in order to match the general behavior of this system, our model should match these transfers closely—both the ones explicitly given in the DOE/NETL report, and the ones implied by them.

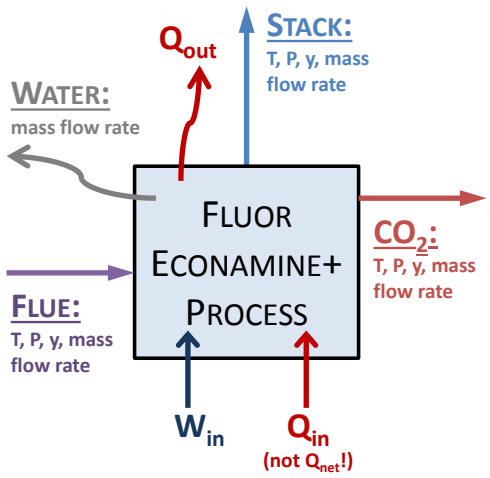

Figure 3.3: Basic information given by the DOE/NETL report, updated to account for mass and energy closure.

3.2 Modeling decisions

3.2.1 Modeling environment

This model was built in Aspen Plus V8.0. The Aspen Plus environment is particularly useful for systems in which state information must be determined in many different devices simultaneously, some of which are relatively complex. In particular, modeling thermodynamic and chemical properties of electrolytes is not trivial, and the Aspen Plus environment includes many built-in property methods (including extensive databases for various chemical species) to enable the modeling of these types

of fluids.

3.2.2 Modeling thermodynamic properties

The thermodynamic model used in this work is taken directly from the Ph.D. thesis of Marcus Hilliard at the University of Texas [3]. Hilliard's work was chosen as the basis for this work because of his attention to thermodynamic consistency in the representation of chemical equilibria, his extensive experimental work to inform the activity coefficient models, and the clarity in the communication of his Aspen Plus modeling framework. In particular, the parameters given in the Fortran source code in Hilliard's Appendix J were entered directly into the Aspen property model used in the current work, supplemented by additional property parameters from Hilliard's Chapters VII, VIII, and XIII.

In Aspen Plus, there are several sets of property methods that use the electrolyte-NRTL model to represent activity coefficients. Here, the ELECNRTL property method set is used, both because this was the one used by Hilliard, and for reasons that will be elaborated in Section 3.3.3.

Chemical reactions

The chemical equilibria between various species in the gaseous and aqueous phases are the true drivers of absorption-based separation processes. Specifically, the following five aqueous-phase chemical reactions are the relevant ones to consider in this system:

$$CO_2 + 2H_2O \longleftrightarrow HCO_3^- + H_3O^+ \tag{3.1}$$

$$HCO_3^- + H_2O \longleftrightarrow CO_3^{2-} + H_3O^+ \tag{3.2}$$

$$MEA + HCO_3^- \longleftrightarrow MEACOO^- + H_2O \tag{3.3}$$

$$MEA + H_3O^+ \longleftrightarrow MEAH^+ + H_2O \tag{3.4}$$

$$2H_2O \longleftrightarrow H_3O^+ + OH^- \tag{3.5}$$

The mechanism for CO_2 absorption in MEA systems can be understood by reading through these five equations in order. Before Eq. 3.1, which is an aqueous-phase reaction, CO_2 in the gas phase dissolves into the aqueous phase until its chemical potential μ_{CO2} is the same in both phases. In practice, at the temperatures and pressures relevant in typical amine absorption systems, very little CO_2 exists in the aqueous phase. The aqueous CO_2 is then described as being in its dilute limit, where the CO_2 mole fraction in solution can be approximated as varying linearly with its fugacity (this is Henry's Law). Equations 3.1 and 3.2 then indicate the formation of bicarbonate and carbonate ions as the aqueous CO_2 reacts with water. This causes additional CO_2 to enter the aqueous phase from the gas phase in order to preserve the equilibrium in Eq. 3.1, which in turn causes the CO_2 removed from the gas phase to increase slightly.

This effect—that of increasing the amount of CO_2 that leaves the gas phase by forming ionic species from the aqueous CO_2—is what we are trying to amplify when we add an additional solvent (beyond water) to the system. Therefore, the key to MEA's ability to be a solvent for CO_2 capture is seen in Eqs. 3.3 and 3.4, both of which consume species that are on the right-hand side of Eq. 3.1 and therefore increase the amount of CO_2 removed from the gas phase. Equation 3.3 shows the formation of carbamate ($MEACOO^-$) from MEA and bicarbonate, while Eq. 3.4 shows the protonation of MEA. Finally in this system, the final relevant dynamic equilibrium to consider is that of water's autoionization (Eq. 3.5).

Chemical equilibria

The five reactions in Eqs. 3.1- 3.5 determine the ionic and molecular composition, at equilibrium, of a liquid mixture composed of a combination of MEA, water, and CO_2. The thermodynamic condition for equilibrium at a given T and P for each reaction

k is given by

$$0 = \sum_{i=1}^{NS} \nu_{i,k}\mu_i \tag{3.6}$$

where $\nu_{i,k}$ is the stoichiometric coefficient of species i in reaction k, which takes the convention that $\nu_{i,k} > 0$ for reaction products and $\nu_{i,k} < 0$ for reactants. The summation limit NS is the total number of chemical species, which includes molecular species like CO_2 and H_2O as well as ionic species. Note that the chemical potential μ_i of species i does not have a k reaction subscript, because it is a property of the overall mixture and not of a particular reaction. Equation 3.6 is the basis of thermodynamically-consistent representations of chemical equilibria at a given temperature and pressure, and is therefore the equation that must be satisfied in any model of these equilibria.

The chemical potential μ_i can be written as the sum of a standard- or reference-state contribution μ_i^* (where the relevant reference state will be defined below for the different species involved) and a term that accounts for the species' activity a_i in the mixture.

$$\mu_i = \mu_i^* + RT\ln(a_i) \tag{3.7}$$

Substituting Eq. 3.7 into Eq. 3.6 and isolating the reference-state terms from the activity term,

$$\prod_{i=1}^{NS} a_i^{\nu_{i,k}} = \exp\left(\frac{-\sum_i \nu_{i,k}\mu_i^*}{RT}\right) \tag{3.8}$$

results in the isolation of the definition equilibrium constant K_{eq} for the mixture

$$K_{eq,k} \equiv \prod_{i=1}^{NS} a_i^{\nu_{i,k}}. \tag{3.9}$$

Therefore, the equilibrium constant $K_{eq,k}$ can also be found from known properties

of the chemical species at their standard state

$$K_{eq,k} = \exp\left(\frac{-\sum_i \nu_{i,k}\mu_i^*}{RT}\right). \tag{3.10}$$

where the reference-state summation term is known as the reference-state Gibbs free energy of reaction, ΔG_k^*.

$$\Delta G_k^* \equiv \sum_i \nu_{i,k}\mu_i^* \tag{3.11}$$

Equation 3.9 is used to solve for the activity a_i of the species, given K_{eq} calculated from Eq. 3.10 (and the set $\{\nu_i\}$ from the reaction stoichiometry). This is as opposed to using an experimentally-derived correlation, such as a linear temperature fit, for K_{eq} instead of Eq. 3.10. The Aspen Plus 8.0 interface allows the calculation of K_{eq} in either of these two ways, as chosen by the user. However, given these two options K_{eq} must be found using the reference-state calculation in Eq. 3.10 for a thermodynamically-consistent formulation that follows the equilibrium condition given by Eq. 3.6. This is done in this work, and it was also done in building Hilliard's original model [3].

The reference state used for calculating properties of electrolytes is typically different from that used for calculating properties of non-electrolytes [62]. In gas phases for example, it is common to use the state of the pure species at 1 atm and a stated temperature as the reference state. In electrolyte solutions however, the reference state for solutes—whether molecular solutes like CO_2, or ionic solutes like HCO_3^-—is often taken to be the dilute limit, at *infinite dilution* of the solute in the solvent. In other words, the activity coefficient of the solute γ_i goes to 1 as the mole fraction of that solute goes to zero. The reference state for the solvent—H_2O in this case—is taken to be at the dilute limit as well. However, for the solvent this means that its activity coefficient will go to 1 as its mole fraction goes to 1, the opposite trend to that of the solutes. This is known as the *asymmetric* convention because of the asymmetric treatment of solvents and solutes. It is commonly used for treatment of electrolyte systems, including in Hilliard's work and in Aspen Plus' ELECNRTL property model as used here. It is worth noting that using a symmetric reference

state convention instead would be perfectly valid. It is only that the values of the activity coefficients and reference-state equilibrium constants calculated using a symmetric reference state could not be directly compared to those using the asymmetric convention.

After Eq. 3.9 is used to solve for the activity a_i of the species in the solution, the final step to determine the solution's composition is to extract mole fraction or molality information from the activity. Activity as a quantity is not always defined in the same way.

First, it can be the product of a mole fraction x_i and a mole-fraction based activity coefficient $\gamma_{x,i}$

$$a_i = \gamma_{x,i} x_i \tag{3.12}$$

or the product of a molality M_i and a (different) molality-based activity coefficient $\gamma_{M,i}$.

$$a_i = \gamma_{M,i} M_i \tag{3.13}$$

The activity coefficients in Aspen Plus are generally given on a molality basis [63].

Second, the activities and activity coefficients will be different if using a symmetric reference state convention or an asymmetric reference state convention (as stated earlier, we used the latter here).

The composition of the solution can therefore be found from the activities, using either Eq. 3.12 or Eq. 3.13, a known reference state convention, and an appropriate model for calculating the activity coefficients.

Activity coefficients using electrolyte-NRTL

The model used to represent the activity coefficients is the electrolyte, non-random two-liquid (electrolyte-NRTL or e-NRTL) model. This model was originally developed by Chen et al. [64], [65] to represent the non-ideal mixing of aqueous electrolytes. At the basis of the e-NRTL model is the *local composition* concept used by Renon and

Prausnitz in their original NRTL model [66], to which e-NRTL reduces in the limit where the electrolyte concentration goes to zero. The local composition concept is based on the idea that mixing non-idealities (which give rise to the need for activity coefficients) can be found from representations of the interactions of individual molecules with their neighbors.

Chen et al.'s expression is based on two key local-composition assumptions. First, the like-ion repulsion assumption is the statement that the local composition around an anion will contain no anions (only cations and uncharged molecules), and vice versa. Second, the local electroneutrality assumption states that any uncharged molecule in the mixture (e.g. H_2O) will have equally distributed charges of cations and anions as its immediate neighbors. These assumptions are used to calculate the contribution of short-range interactions to the non-ideal mixing.

Additionally, Chen et al.'s expression considers the long-range interaction of ions' electrical charge by incorporating a Pitzer-Debye-Hückel term. This term accounts for the fact that in electrolyte solutions, non-ideal mixing is due not only to local interactions between immediate neighbors—the local composition concept—but also to the effect of the charge distribution in the solution (beyond the "immediate" neighborhood) on ions' behavior.

Non-ideal mixing in the e-NRTL model is therefore represented by the sum of these two contributions to the excess Gibbs free energy:

$$G_i^e = G_{i,LC}^e + G_{i,PDH}^e \tag{3.14}$$

where the subscript LC refers to the short-range local composition contribution, the subscript PDH refers to the long-range Pitzer-Debye-Hückel contribution, and G^e refers to the excess Gibbs free energy, representing non-ideal mixing. Equation 3.14 is sometimes written with a third term $G_{i,Born}^e$ for the Born correction term [3], [67]. This term is an adjustment to the Pitzer-Debye-Hückel term to account for mixed solvents (i.e., including more than just water), if the PDH term is written assuming water as the only solvent. The PDH term included here has assumed that the correct representation is used for the relevant solvent, not just for water.

The Pitzer-Debye-Hückel term, including the Born correction, is calculated purely analytically. However, the local composition term is calculated based on binary interaction parameters which are fit to experimental results. The e-NRTL model is therefore a semi-empirical formulation. The experimentally-fit binary interaction parameters relevant to the H_2O-MEA-CO_2 system are taken directly from Hilliard [3].

From Eq. 3.14, the activity coefficients are then found by the thermodynamic relationship

$$\ln \gamma_i = \frac{1}{RT} \left[\frac{\partial G_i^e}{\partial N_i} \right]_{T,P,N_{j \neq i}} \tag{3.15}$$

thus completing the list of parameters required to find the equilibrium composition of the mixture.

3.2.3 Modeling devices

Description of device operation

The basic structure of amine absorption systems was shown in Figure 3.1. In this section, we give a more detailed, device-by-device operation of the MEA absorption system as modeled in this work and illustrated in Figure 3.4. State information for each of the streams is tabulated in Appendix A.

The flue gas enters the system at the state described in Table 3.1. Before entering the absorber, it is cooled to condense the majority of the water out of the flue gas. In this model, the flue gas was cooled to 34.5°C, which results in water leaving the system at the rate of 58.4 kg/s (note that this is therefore the majority of the extra water flow leaving the system, identified in Figure 3.3). After this, the flue gas is pressurized slightly by a blower with an isentropic efficiency of 0.61, which was the blower efficiency used in a 2002 DOE/NETL report for an MEA absorption system, and was based on matching observed experimental values [68]. Raising the pressure of the gas to 1.18 atm in the blower is necessary to overcome the pressure drop in the absorber.

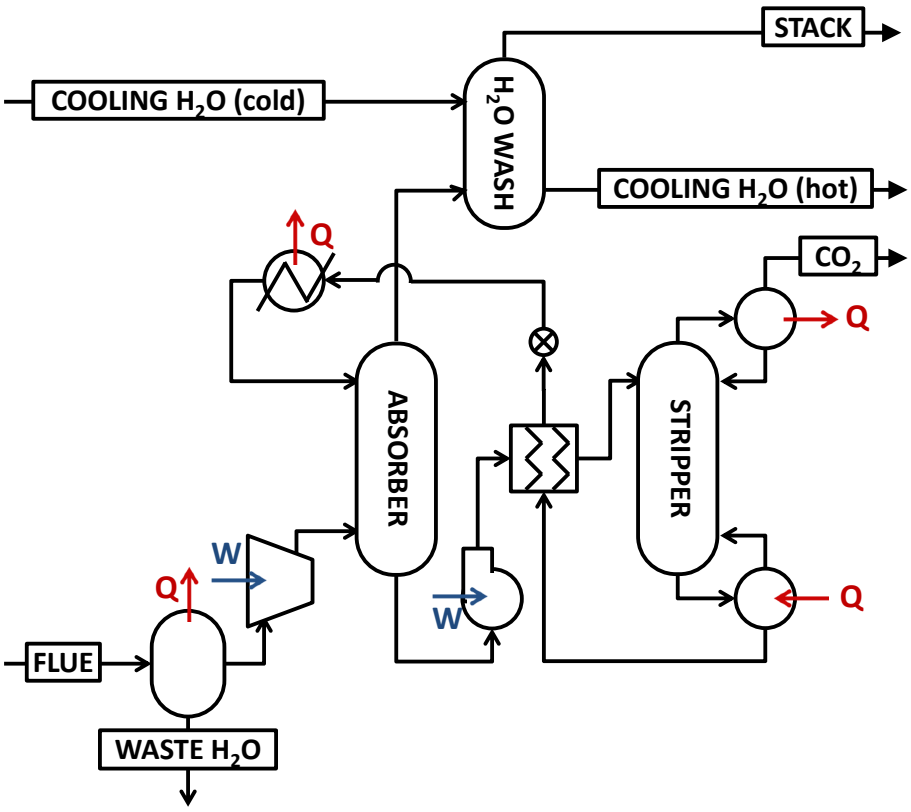

Figure 3.4: Diagram of the MEA absorption carbon capture system modeled.

Next, the gas enters the bottom of the absorber column, while lean solvent enters the top. The absorber is modeled in Aspen using the RadFrac block, which uses equilibrium-based stages—and stage efficiencies if necessary—to model separation columns, and is to be distinguished from the RateFrac block, which allows the calculation of internal rate-based processes (kinetics, transport) in each stage. For the purposes of completing a device-by-device exergy analysis, only the states and extensive size of the *transfers* to the column are needed. The internal column profiles, or the physical height of the column (which would result from a stage efficiency calculation), are not needed. Therefore, the use of the RadFrac block is sufficient for this analysis, as long as the transfers are correct.

The transfers to and from the absorber column are the flue gas from the blower (at a known state), the stack gas leaving the top of the column (with a known CO_2 flow rate), and the two solvent streams. The lean and rich solvent streams are typically characterized by their *effective loading* α which is the molar ratio of all CO_2-derived species in the aqueous mixture to the sum of all MEA-derived species in the mixture.

$$\alpha = \frac{\dot{N}_{CO2} + \dot{N}_{HCO3^-} + \dot{N}_{CO3^{2-}} + \dot{N}_{MEACOO^-}}{\dot{N}_{MEA} + \dot{N}_{MEAH^+} + \dot{N}_{MEACOO^-}} \tag{3.16}$$

In general, the lean solvent loading for these systems should be between 0.2-0.3, while the rich solvent loading should be near 0.5 [69]. In this model, the lean solvent loading is 0.285, and the rich solvent loading is 0.522. The mass fraction of MEA in the completely clean solvent (i.e., mass of MEA poured into solution divided by the sum of the MEA and water mass) is 30%. The number of equilibrium stages used in the model—which do not represent true stages in an actual column, but are simply mathematical constructs in this case—of the absorber column was varied until the gas outlet stream converged at the desired CO_2 outlet of 10% of the CO_2 in the flue gas (see Table 3.1). A pressure drop of 0.1 bar was included in the absorber column.

The absorber column modeled here is not intercooled, and is therefore modeled as adiabatic. However, the stack gas should leave the system at a temperature of 32°C (from Table 3.1), which means that it should be cooled. Absorber columns typically include a water wash section at the top of the column in order to capture

any vaporized solvent and prevent it from being released into the atmosphere. Here this is modeled as a separate column through which water flows, cools the stack gas, and dissolves any remaining solvent. The flow rate of water was increased until the stack gas reached the desired 32°C outlet temperature, which means that the water wash section and intercooling were effectively combined into a single section.

The rich solvent leaves the bottom of the absorber and is pumped to 2 bar to enter the stripper. The purpose of the stripper is to remove CO_2 from the rich solvent by boiling it out of solution, so preheating the rich solvent stream is advantageous for reducing the stripper reboiler steam needed. The rich solvent is preheated in a heat exchanger by the hot, lean solvent stream leaving the bottom of the stripper. An 8°C minimum approach temperature difference is maintained in the heat exchanger, and a 5% pressure drop is imposed on both the hot and cold sides.

The stripper operation is specified by imposing the reboiler duty of 588.572 MW and the condenser temperature of 21°C at a pressure of 1.6 bar, based on the known values from the DOE/NETL baseline. The stripper pressure is set to be 1.7 bar at the bottom of the column (at the reboiler) and 1.6 at the top. The stripper, for the same reason listed for the absorber, is modeled using the RadFrac block with the number of equilibrium stages that resulted in the regeneration of the lean solvent to a loading of $\alpha = 0.285$. The resulting reboiler temperature was 114°C, and the resulting condenser cooling required was 199.1 MW. The reboiler temperature is generally limited by the fact that MEA degrades thermally above a temperature of around 120-125°C, and the reboiler temperature is generally kept as high as possible as limited by this thermal degradation limit. A reboiler temperature of 114°C is therefore slightly on the low side, although still within the range of considered temperatures [69]. The effect of raising the reboiler temperature by a few degrees on the exergy analysis results will be discussed in Section 3.3.2.

Finally, to complete the cycle, the lean solvent exiting the reboiler is used to preheat the rich solvent and is then throttled from 1.6 bar to 1 bar. The lean solvent is further cooled until it reached 40°C, which is typical for a lean solvent temperature (e.g., [69], [70]), at which point it re-enters the absorption column.

Comparison to DOE/NETL values

Detailed state information for the streams in the model are given in Appendix A, but a side-by-side comparison of the values given by the DOE/NETL report in Table 3.1 to the resulting values from the model is given in Table 3.2. Additionally, the work and heat transfer to the system as modeled here are compared to the values given by DOE/NETL in Table 3.3.

Table 3.2: Stack and CO_2 product gas streams, comparing DOE/NETL baseline report values [1] and values in this model.

Streams	Stack			CO_2		
	DOE/NETL	Model	% err.	DOE/NETL	Model	% err.
$\dot{N}_i$ (kmol/s)						
Ar	2.520E-1	2.538E-1	7.143E-1	0.0000	4.713E-6	—
CO_2	4.176E-1	4.145E-1	7.423E-1	3.762E0	3.798E0	9.569E-1
H_2O	8.936E-1	1.119E0	25.22E0	1.473E-2	6.140E-2	3.168E2
N_2	2.103E1	2.103E1	6.490E-3	0.0000	1.978E-4	—
O_2	7.373E-1	7.368E-1	6.782E-2	0.0000	1.272E-5	—
SO_2	0.0000	0.0000	0.0000	0.0000	0.0000	0.0000
$\dot{m}$ (kg/s)	6.573E2	6.612E2	5.933E-1	1.659E2	1.683E2	1.447E0
T (°C)	32	32	0.0000	21	21	0.0000
P (MPa)	0.10	0.10	0.0000	0.16	0.16	0.0000

In Table 3.2, the streams are specified in terms of molar flow rates of each chemical species in the fluid, instead of by mole fractions. The reason for this is to allow a species-by-species comparison—when comparing mole fractions, a discrepancy in the flowrate of a single chemical species would affect the mole *fractions* of all other species, obscuring the real difference. More specifically, in Table 3.2, we see that the CO_2 is captured at the same effectiveness (90%) as in the NETL report, and that non-condensable gases are correctly eliminated from the CO_2 product stream.

The water remaining in both the stack gas and the CO_2 product gas, however, is higher than in the DOE/NETL baseline report. In the Aspen model, both streams were assumed to be at a relative humidity of 1, which assumes that no additional dehumidification of the streams (by silica gel or other extra drying technique, for

example) occurred. Therefore, either the DOE/NETL report *did* assume additional dehumidification after leaving the water wash section (for the stack gas) or the stripper condenser (for the CO_2 stream), or slightly different property methods for the vapor-liquid equilibrium (VLE) calculations of water were used in both models, resulting in slightly different vapor phase mole fractions at saturation at a given temperature and pressure. This will not significantly affect the overall exergy analysis results.

Table 3.3: Heat transfer and work to the system, comparing DOE/NETL baseline report values [1] and values in this model.

	DOE/NETL	Model	% err.
Reboiler $\dot{Q}$ (MW)	588.572	588.572	0.00000
Reboiler T (°C)[1]	Unspecified	114	—
Condenser $\dot{Q}$ (MW)	Unspecified	199.051	—
Condenser T (°C)	21	21	0
Lean solvent $\dot{Q}$ (MW)	Unspecified	218.043	—
Work input (MW)	22.40	20.87	6.830

In Table 3.3, we list the work, heat transfers, and relevant heat transfer temperatures in this model and in the NETL/DOE baseline report. Because the system model was specified using the reboiler heat transfer and the condenser temperature, these agree exactly with the DOE/NETL values. The necessary work to operate the rich solvent pump and the flue gas blower is approximately 7% less in our model than in the DOE/NETL baseline report. This could be attributed to the fact that we neglected to model several smaller auxiliary systems—for example, pumps for make-up water and MEA, pumps to overcome pressure drops through solid salt filtering processes, and other clean-up and maintenance systems—that were included in the DOE/NETL report.

3.3 Exergy analysis

3.3.1 Results and discussion: exergy efficiency

We begin the exergy analysis of the MEA absorption system with a discussion of the exergy efficiency of this system, and in particular how the position of the chosen system boundary affects this value.

The separation process that occurs in this system is not just a separation of nitrogen from CO_2 at 25°C and 1 atm, but instead a separation of flue gas containing CO_2, N_2, O_2, H_2O, and Ar and delivered at 58°C, into a stream of nearly-pure CO_2 at 1.6 bar, a stream of waste water separated from the process, and a stream of stack gases at 32°C. For calculating the minimum exergy of separation and the exergy efficiency of this system, we impose that the waste liquid water must depart the system at 25°C, the reference environmental temperature T_o. Even if it were to depart at a higher temperature, the ensuing additional exergy would be destroyed in the environment. Therefore imposing an outlet temperature of 25°C ensures that we account for all of the exergy destruction caused by this system. Similarly, we adjust the outlet temperature of the stack gas from 32°C to $T_o = 25$°C, effectively imposing that a cooling process—with associated exergy destruction—occurs for this stack gas to return to environmental conditions. The flue gas entering the system boundary, however, is kept at 58°C, since this is a stream that is delivered directly from the power plant.

Under these conditions, the minimum exergy of separation for this process is 105.5 kJ per kg of CO_2 product. In order to calculate the exergy efficiency of this system, we must understand how to quantify the exergy supplied to the system. Accounting for the electric work is simple: The DOE/NETL baseline report indicates that 22.4 MW of work is supplied to this system, and this is equivalent to 22.4 MW of exergy supplied, or 135.1 kJ per kg of CO_2 product.

Reboiler heat transfer discussion

The reboiler heat transfer is more complicated. We know from the DOE/NETL baseline report that 588.572 MW of thermal energy is supplied to this system in the form of heat transfer from steam extracted from the power cycle of the plant. The steam is condensed as a result of this process, and is returned to the power cycle as liquid water. In order to account for all of the exergy destruction caused by the carbon capture process, the system boundary should be drawn so that the high-temperature, high-exergy stream enters, and the low-temperature, low-exergy stream exits. In this way, the exergy supplied to the system by the steam is given by the difference in flow exergy of the hot steam and colder water (where the chemical portion of the exergy is neglected because it does not change in this process—both the inlet and outlet streams are only comprised of water):

$$\dot{X}_{in,steam} = \dot{m}_{steam}[\psi_{in} - \psi_{out}] = \dot{m}_{steam}[(h_{in} - h_{out}) - T_o(s_{in} - s_{out})] \tag{3.17}$$

This is as opposed to counting the exergy of this transfer as heat transfer occurring at the reboiler temperature, which neglects the significant exergy destruction in the heat transfer from the much hotter steam, and its subsequent condensation. These two options for the system boundary can be seen in Figure 3.5.

As given in the DOE/NETL baseline report, the steam supplied to this system has a mass flow rate of 243.4 kg/s. Moreover, it arrives as a superheated vapor at 296°C and 0.51 MPa, and is returned to the power cycle as a subcooled liquid at 151°C and 0.9 MPa. The exergy supplied to the system by the steam, as calculated by Eq. 3.17, is therefore 183.3 MW, or 1105.1 kJ/kg-CO_2. By contrast, the exergy of the heat transfer from the steam, if assumed to be crossing the system boundary at the reboiler temperature[2], is 135.3 MW, or 815.7 kJ/kg-CO_2 (as calculated by $X_Q = Q * (1 - T_o/T_{boundary})$). The difference of 52.0 MW is the exergy destruction that occurs in the steam condensation process and in the heat transfer across a

[2]This is 114°C in our model. Even if it were increased, for example to 120°C (as 114°C is on the low end of reboiler temperatures for these systems), the effect on this analysis is small, and the main point—that the majority of the exergy destruction occurs in the steam extraction—still holds.

non-zero temperature difference between the steam and the reboiler. This issue and options for improvement are discussed in detail in Section 3.3.2.

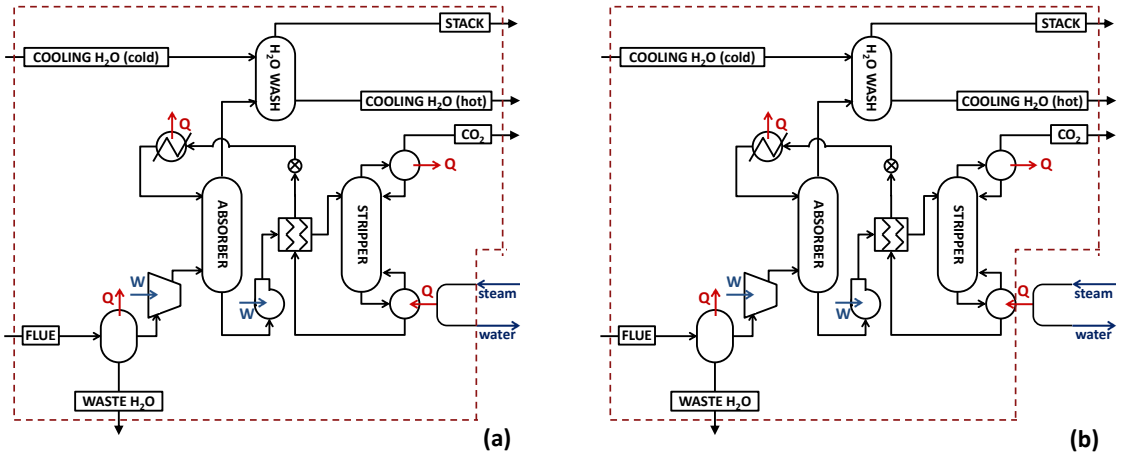

Figure 3.5: Diagram of the MEA absorption carbon capture system modeled, showing the system boundary as drawn at the steam inlet and return (a), or alternately at the reboiler surface (b). The difference in exergy efficiency between these two choices of boundary locations is significant.

The exergy efficiency of this separation system is 8.51%, which is quite low. By comparison, the exergy efficiency of the separation if the exergy destruction in the steam is not included in the system boundary is 11.1%. Finally, if the minimum exergy of separation were calculated assuming an inlet flue gas at 25°C (which is commonly seen), *and* the exergy destruction in the steam were neglected from the system, the exergy efficiency of this system would be 12.1% (this gives "free" exergy to the system in the form of a flue gas that actually arrives at 58°C instead of 25°C, which is why the correct calculation of the minimum exergy of separation is important).

3.3.2 Results and discussion: detailed exergy analysis

The detailed exergy analysis of this system is performed, by first extracting the entropy values reported by Aspen Plus for each of the matter streams in the system,

and using them to find the entropy generated in each device by an entropy balance.

$$\dot{S}_{gen} = \sum \dot{m}_{out} s_{out} + \frac{\dot{Q}_{out}}{T_o} - \sum \dot{m}_{in} s_{in} - \frac{\dot{Q}_{in}}{T_b} \tag{3.18}$$

Then, the entropy generation value is used to find the exergy destruction in each device using the Gouy-Stodola relationship

$$\dot{X}_{dest} = T_o \dot{S}_{gen}. \tag{3.19}$$

Each device has been assumed to be operated at steady state, hence the lack of an accumulation term in Eq. 3.18. Whenever heat is transferred out of a device in the system, it is assumed that the heat transfer occurs at the environmental temperature T_o, in order to account for all irreversibility created by the system.

The results of the detailed exergy analysis are shown in Figure 3.6. The overwhelming majority of the exergy destruction in this system occurs in the two columns, the absorber and stripper. The exergy destruction in the water wash section at the top of the absorber, included in Figure 3.6 as a separate section from the absorber, could arguably be counted as part of the absorber as well, increasing the fraction of the overall irreversibility that occurs in the columns. The fact that a relatively small fraction of the overall exergy destruction occurs in the rest of the system indicates that the other devices are relatively well integrated into the process, and that the initial focus for process improvement should be on the two columns.

The next step is to ask how we can reduce the exergy destruction in the absorber and stripper column. For the stripper, part of the answer lies in reducing the exergy destruction that occurs in and around the reboiler. In fact, the destruction in the mixing and condensing of the steam extracted is very significant, separate from what happens on the solvent side of the reboiler. If we were to plot the exergy destruction distribution for this system while drawing the system boundary at the reboiler temperature (as discussed in Section 3.3.1), we would arrive at Figure 3.7. Comparing the relative sizes of the stripper column destruction in Figure 3.6 and Figure 3.7 shows how much of the exergy destruction assigned to the stripper is actually happening

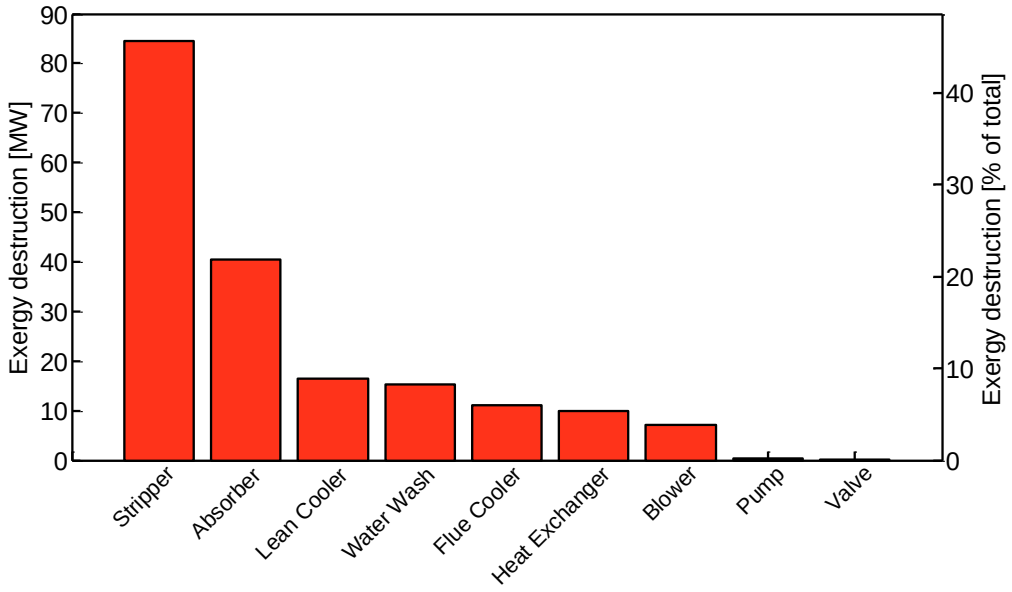

Figure 3.6: Exergy destruction in the MEA absorption capture system modeled, based on stream entropy values reported by Aspen Plus using the ELECNRTL property method with Hilliard's property information [3]. Note that the water wash has been included as separate from the absorber because they were modeled as separate units, but the exergy destruction in these two units could be summed to compare to absorber models that include the water wash.

in the heat transfer process from the hot steam to the reboiler. Recent research in improving absorption-based carbon capture systems has indeed focused on reducing the amount of steam that is necessary to operate the reboiler (for example, the reduction in necessary reboiler steam is one of the primary advantages of the piperazine systems relative to this MEA system [39], [56]).

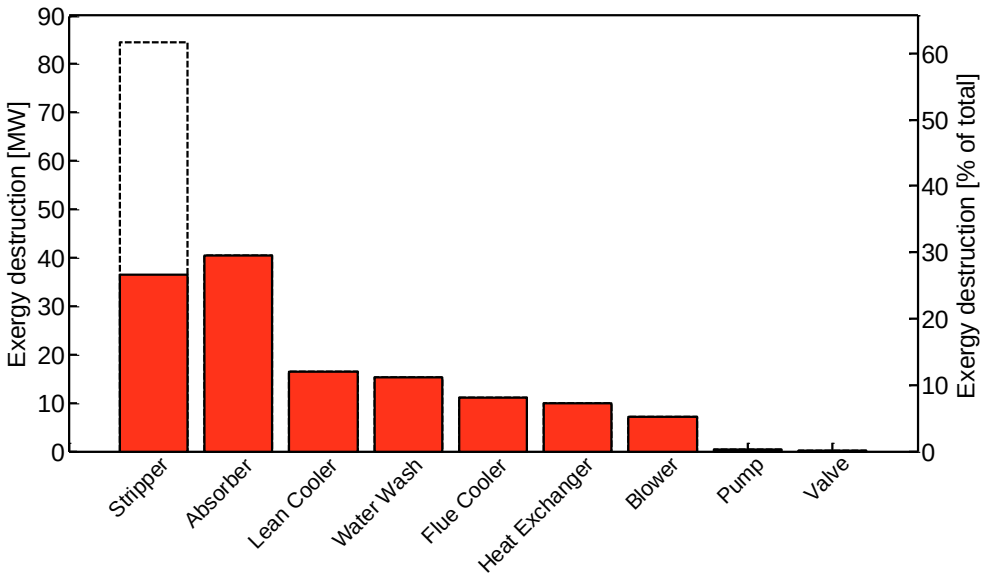

Figure 3.7: Exergy destruction in the MEA absorption capture system modeled, using the same thermodynamic property environment as in Figure 3.6, but drawing the boundary at the reboiler heat transfer surface instead of at the steam transfer point.

As explained in Section 3.3.1, the steam that is extracted from the power cycle for the reboiler leaves the power cycle with a temperature of 296°C at a pressure of 0.51 MPa (these are values from the DOE/NETL report, not results of the model in this work). This results in a significantly more exergetic stream (or "higher-grade heat") than is needed for the 114-120°C reboiler, and is the reason for the very high exergy destruction on the steam side of the reboiler. The first obvious step for improving the exergy efficiency of this system and reduce the parasitic load on the power plant is to better integrate the reboiler with the power cycle. This means extracting steam that

is about 10-30 K hotter than the solvent side of the reboiler. This could be done with no significant increase of heat exchanger area, given that the DOE/NETL system already reduces the temperature of the hot incoming steam to 152°C by mixing it with a slipstream of the cold return condensed water [1].

For both the stripper and the absorber, however, the answer to the question of reducing exergy destruction also lies in reducing the driving forces operating inside these columns. Exergy destruction (or entropy generation) occurs when transfers—of heat, or of chemical species—are driven by large gradients (in temperature or chemical potential, respectively). The idea of trying to *decrease* the driving force inside an absorber or stripper column can run counter to the common engineering goal of increasing throughput and reducing column size by *increasing* driving forces inside columns. However, this is the way to reduce exergy destruction and improve system efficiency. The issue of reconciling a need for smaller driving forces to reduce exergy destruction with the desire for faster rates of transfer inside chemical process columns is discussed in detail by Leites, Sama, and Lior [37].

In order to identify the locations where the driving forces in the columns are greatest and then reduce them, a detailed model of the column profiles (composition, temperature) is needed. This cannot be directly extracted from our model as it exists, because we treated the columns as black-boxes with known inputs and outputs. This was the level of detail necessary to identify the magnitude of the exergy destruction in each of the system components. To find the internal profiles and improve on them, the column must be modeled with knowledge of the type of packing, transport mechanisms, and column size, which is left to a future study. This could be done by starting from this existing model, for example by exchanging the column models for the RateFrac block and collecting expected packing information. However, the existing model can be used to study the effect of changing the integration between system components. This includes the effect of changing the reboiler steam temperature so that it better matches the reboiler solvent temperature (as already discussed with Figure 3.7), or of varying the temperature difference in the lean-rich heat exchanger.

3.3.3 A note on 2nd law analyses of electrolyte systems, or dependence on modeling environments

Over the course of modeling and analyzing this system, it became clear that extracting useful information from commercial flowsheeting software for an exergy or other second-law analysis is not always straightforward. In order to facilitate future users' research in related applications, the key difficulty we encountered is explained here.

In Aspen Plus, there are several options of property methods for electrolyte solutions. For systems with amine solvents, this includes the method AMINES, which AspenTech documentation describes as a "correlation-based property method" as opposed to one based on activity coefficients, and was therefore dismissed for this work because of the need for strictly thermodynamically consistent methods, using activity coefficients [63]. Several activity-coefficient methods exist for electrolytes: ELECNRTL, ENRTL-RK, ENRTL-SR, ENRTL-HF, and ENRTL-HG. All are originally based on the electrolyte non-random, two-liquid (E-NRTL) model for liquid activity coefficients first developed by Chen et al. [64], [65].

We will focus here on the first two—ELECNRTL and ENRTL-RK—because these are overwhelmingly the ones most often used for modeling carbon capture systems with MEA absorption. The method ELECNRTL is an older version of the electrolyte non-random, two-liquid activity coefficient model implemented in Aspen. At the release of Aspen Plus V7.2, the method ENRTL-RK was introduced as an upgraded version of ELECNRTL with more consistent thermodynamics (see, for example, the industry white paper released by Tremblay et al. from Aspen Tech in 2012 [71]). The user manual "Aspen Physical Property System: Physical Property Methods" [63] describes the main difference between the two methods:

> The ENRTL-RK method is identical to ELECNRTL for systems containing a single electrolyte. However, [...] the ENRTL-RK uses a single thermodynamics framework to calculate the activity coefficients, Gibbs free energy and enthalpy, instead of using separate models as in ELECNRTL.

This stated attention to thermodynamic consistency lead us to first consider the ENRTL-RK method for the work presented here.

In Figure 3.8, we show the results of the exergy analysis of the same system presented in Figure 3.6, but using ENRTL-RK instead of ELECNRTL. The ENRTL-RK method was implemented exactly as in the *RateBasedMEAModel.bkp* example file provided by Aspen Tech with Aspen Plus as a sample file for MEA-based CO_2 capture systems. It should be noted here that the two models are the same on the basis of the first law of thermodynamics: They capture the same amount of CO_2 from the same stream, with the same work input, same heat transfer to the reboiler, and same heat transfer out of the system. However, the exergy destruction calculated using the entropy values from ENRTL-RK and Eq. 3.19 are different—and they are incorrect.

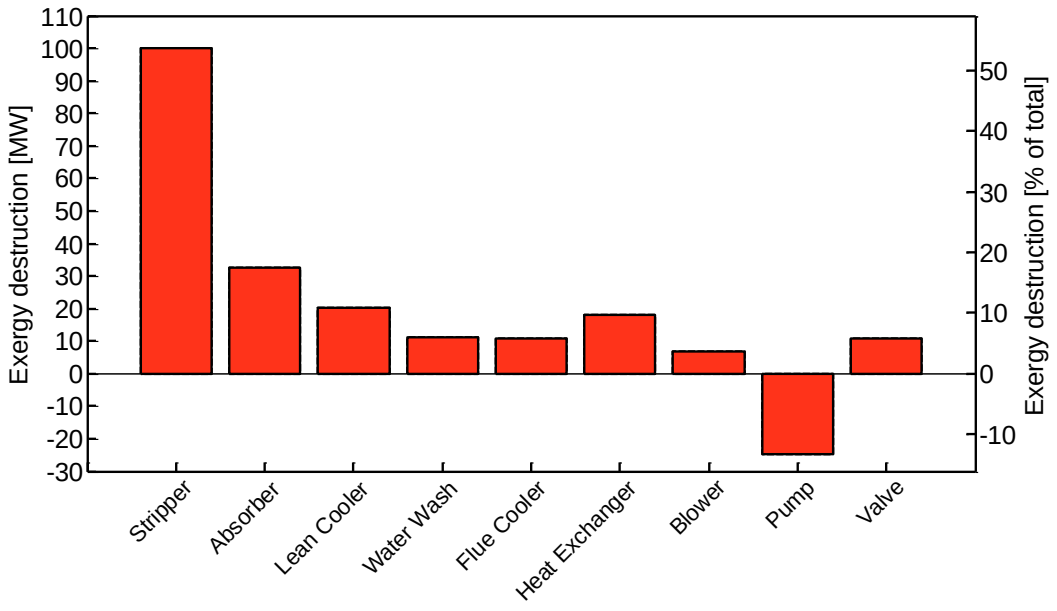

Figure 3.8: Exergy destruction in the MEA absorption capture system modeled, based on stream entropy values reported by Aspen Plus using the ENRTL-RK property method as implemented in the *RateBasedMEAModel.bkp* example file provided with Aspen Plus. Note that the existence of a negative valued column on this plot indicates an impossible result (and thus an incorrect calculation of entropy), as it violates the 2nd law of thermodynamics.

The most obvious incorrect result is the negative exergy destruction in the rich

solvent pump; this would indicate negative entropy generation, disobeying the second law of thermodynamics. The calculation of entropy changes through this device are therefore wrong. However, the exergy destruction value in the valve is also incorrect, though less obviously so. This valve is a simple throttle, though which a subcooled liquid mixture (the lean solvent) is brought to a pressure of 1 bar from 1.6 bar. No phase change occurs—both inlet and outlet are subcooled liquids. Although this is certainly an irreversible process, it is completely unlikely that an incompressible substance undergoing a small isenthalpic pressure drop would destroy more exergy than the blower, which compresses a large flow rate of a hot ideal gas mixture at a relatively low isentropic efficiency. The ratio of exergy destruction between these two devices shown in Figure 3.6 is much more realistic. Therefore, the underlying issue does appear to be based in the property method, and not just in a spurious incompatibility between ENRTL-RK and pumps.

AspenTech has been made aware of this issue (Incident Number 1486298), and is working to resolve it. Therefore, this note is intended as a temporary warning to approach the ENRTL-RK method with some caution for the purposes of entropy calculations, until the issue is resolved.

3.4 Summary

In this chapter, we modeled and analyzed a well-known post-combustion CO_2 capture system, which operates by selective absorption of CO_2 in an aqueous solution of 30wt% monoethanolamine. The modeling decisions and comparison with the DOE/NETL baseline report equivalent system are presented and discussed.

The goal of this modeling exercise was to develop a detailed exergy analysis of this system. The system was modeled using Aspen Plus due to this software's extensive database of property methods for fluid and chemistry properties as well as its ability to quickly model different devices in the system. It was identified that the overwhelming majority of the exergy destruction in the system occurs in the stripper and absorber columns. Paths towards improving these was discussed. Existing limitations of Aspen Plus for modeling this system for the purposes of exergy analysis were discussed.

Chapter 4

Post-Combustion Capture by Vacuum-Swing Adsorption

In this chapter, we model and analyze a process that separates CO_2 from flue gas of a coal plant by vacuum-swing adsorption in a packed bed of zeolite 13X. This type of system is less well understood than the amine absorption system described in the previous chapter. While several system components have been tested and small pilot systems have been studied, detailed information about the operation of these systems at power-plant scale is not known. Therefore, when explaining the model and the results of the exergy analysis, we discuss the types of exergy destruction that may differ between the system modeled here and a scaled-up system.

4.1 System description

4.1.1 General system: post-combustion capture by adsorption

Adsorption refers to the mechanism by which molecules from a bulk fluid adhere onto the surface or into the pores of a solid (the adsorbent or sorbent). This is as opposed to the process of *absorption*, treated in the previous chapter, which describes the mechanism by which bulk fluid molecules dissolve into the *bulk* of another substance

(the solvent). When certain species adsorb preferentially over others, this mechanism can be used to drive separation processes. Adsorption processes are in use industrially in applications as varied as air separation ([72], [73], [74]), purification of hydrogen ([75], [76], [77]), and the dehumidification of gases ([78], [79]), among others.

In practice, adsorption systems are often batch-cyclic processes. Some operate by letting the more strongly-adsorbed species adsorb onto a solid at high pressures for a period of time, then regenerating or cleaning the sorbent by dropping the pressure. This is known as a *pressure-swing adsorption*, or PSA, process. These PSA systems can be sub-classified further based on the sign of the gauge pressures used in the cycle. If all pressures in the cycle are at or below atmospheric, the process is known as *vacuum-swing adsorption* (VSA). The term *PSA*, as independent from *VSA*, would then indicate that all pressures reached in the cycle are at or above atmospheric. Finally, systems that swing between pressures above and below atmospheric are known as *pressure-vacuum swing adsorption* (PVSA) systems. Another class of adsorption systems operate by allowing the more strongly-adsorbed species to adsorb onto the sorbent at a low temperature, after which the sorbent is regenerated by raising its temperature—for example, by passing hot steam over it. This is known as a *temperature-swing adsorption*, or TSA, process.

Webley [80] outlined the history and existing technical challenges of using adsorption-based systems to capture CO_2 from flue gas, an application that was first considered in the 1990s [81]. One of the key differences between CO_2 capture from flue gas and the other adsorption-based gas separation systems mentioned previously relates to how CO_2 adsorbs relative to N_2. In many adsorption systems, the desired high-purity product (which is CO_2 in capture processes, but would be O_2 in air separation processes, or H_2 in hydrogen purification processes) is the more *weakly* adsorbing species. However, because CO_2 has a larger quadrupole moment than N_2 does, it generally adsorbs more *strongly* than the nitrogen waste gas. In practice, this means that adsorption cycle configurations that would work in other settings—for example, in air separation—would not achieve the desired purification of CO_2 from flue gas. New cycle configurations need to be developed.

In addition to developing new cycle configurations for post-combustion capture

by adsorption processes, an active research area has been the development of better adsorbents to use in these cycles. Some of the more traditional options for CO_2 capture from flue gas include zeolites, in particular zeolite 13X and zeolite 5A. For example, these have been studied by Merel et al. in a TSA process [82], by Wang et al. in a hybrid VTSA process [83], and by many researchers in VSA and PSA processes, (e.g., by Ko et al. [84], Xiao et al. [85], Haghpanah et al. [86]).

Much of the research on new adsorbents for post-combustion capture has also focused on a class of materials known as *metal-organic frameworks*, or MOFs (see reviews by Sumida et al. [87] or Bae and Snurr [88]). Somewhat like the ionic liquids discussed in the absorption chapter, these materials are promising due to the tunability of their properties. By altering the metal sites in the crystal structure and the organic linkers between them, the sorbent will behave differently. Many MOF configurations are possible, and the properties of theorized MOFs can be estimated computationally without synthesizing them.

As a result of this wide variety of possible sorbents and development of new cycles, there has been interest in computationally screening MOF- and zeolite-based sorbents in conjunction with adsorption cycle optimization, for example by Lin et al. [89] or by Faruque Hasan et al. [90].

4.1.2 Specific system: optimized vacuum-swing adsorption

The post-combustion adsorption process studied here is a VSA system using zeolite 13X that has been optimized to minimize the electrical work input to achieve the separation. The separation in this system was designed to capture 90% of the CO_2 in the flue gas supplied, at a CO_2 product purity of 90%. It is worth noting that while the capture percentage (90%) is the same as in the MEA absorption system, the CO_2 purity is significantly lower than the >99% purity achieved in the MEA system. In general, vacuum-swing adsorption systems have lower CO_2 purities due to limits on the vacuum pressures reached. This means that the CO_2 from these systems may be better suited to a different end use than the CO_2 from amine absorption systems (for example, carbon capture and storage is known to have less stringent CO_2 purity

requirements than enhanced oil recovery [21]). Once again, the compression of CO_2 to pipeline pressures is not included in the system boundary, since we are focusing on the exergy efficiency of the separation alone.

The purity and capture percentages, the steps in this system, and the column modeling assumptions and process optimization, are taken directly from Haghpanah et al. 2013 [86] and were not altered here. This system was chosen for analysis here because it is representative of the current state of process development of adsorption systems for post-combustion capture. In these systems, the behavior in the adsorption column—the key unit for the separation—is well validated and even (as in Haghpanah et al.'s work) optimized, but other auxiliary parts of the system are less well established. Here, we summarize the key modeling assumptions of the adsorption column from the work of Haghpanah et al. [86]. A more detailed description can be found in the original reference. We also describe the modifications made to their column model to enable an exergy analysis of the system, and detail the assumptions about the other system devices (beyond the column) that are necessarily implied by their column model. The exergy analysis of the system is then presented.

In this process, a packed bed of zeolite 13X pellets undergoes a sequence of transient pressurization and depressurization steps, as shown in Figure 4.1. The first step in the cycle is a pressurization of the column with flue gas, raising the column pressure from vacuum levels to atmospheric. In this step, which is referred to as the *pressurization* step, the column inlet is open, but its outlet is closed. Next, in the *adsorption* step, the column outlet is also opened, and flue gas flows through the column. The inlet flue gas enters at a pressure slightly above atmospheric in order to overcome the pressure drop in the packed bed and ensure that the column outlet remains at atmospheric pressure. During this step, CO_2 will selectively adsorb onto the surface of the zeolite pellets, such that the outflow from the column is a waste gas that has been largely cleaned of its CO_2 content. After the adsorption step, the column inlet is closed. The next step, called *blowdown*, consists of drawing a vacuum at the column outlet until the column has reached an intermediate pressure, below atmospheric but above the lowest pressure in the cycle. The purpose of this step is to remove most of the nitrogen remaining in the column (largely in the gas phase), so

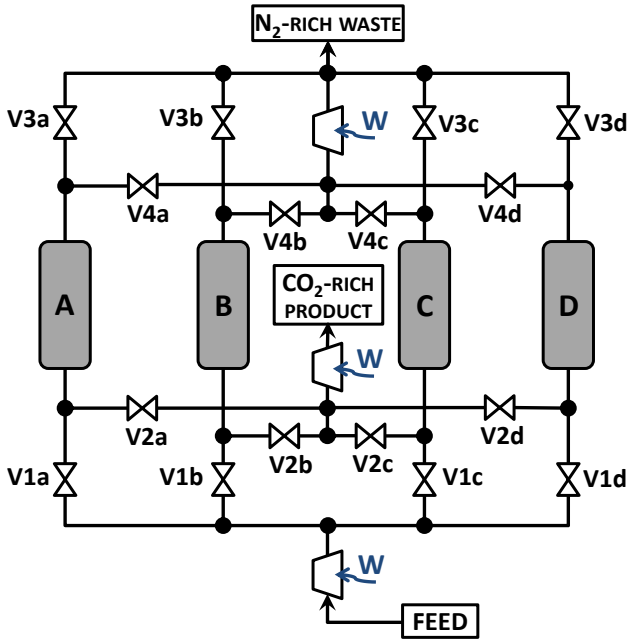

Stage (A)	V1a	V2a	V3a	V4a
Pressurization	1	0	0	0
Adsorption	1	0	1	0
Blowdown	0	0	0	1
Evacuation	0	1	0	0

Figure 4.1: Cyclic operation of the four-step, four-column VSA system studied here, where "1" indicates an open valve and "0" indicates a closed valve (the table indicates the valve state for column A).

that higher-purity CO_2 remains. The CO_2 is recovered in the final step, the *evacuation* step. In this step, a deeper vacuum is drawn on the column, although this time it is drawn from the front end of the column—the area of the column that had been the inlet in the pressurization and adsorption steps, and which therefore contains the most CO_2.

The parameters for this cycle (intermediate and low pressures, time elapsed for each step in the cycle, etc.) are taken directly from Haghpanah et al. 2013 [86] and are detailed in Appendix B. The electrical work necessary for this cycle is used for the blower in the adsorption step and the vacuum pumps in the blowdown and evacuation steps. For this optimized cycle at 90% capture and 90% purity, Haghpanah et al. reported a necessary work input of 149.0 kWh per tonne of CO_2 in the product stream, or 536.4 kJ per kg of CO_2 in the product stream.

4.2 Exergy analysis at cyclic steady state

We can begin the exergy analysis of this process by noting the exergy efficiency of this system. For a separation process that takes an input of flue gas at 25°C and 1 atm with a molar composition of 15% CO_2 and 85% N_2, then captures 90% of the CO_2 at a purity of 90%, the minimum exergy of separation can be calculated to be 124.6 kJ per kg of CO_2 in the product. With a work input of 536.4 kJ/kg-CO_2 required and no other exergetic inputs, the exergy efficiency of this system is **23.2%**.

The composition of the flue gas in this system model is worth discussing here. As in many adsorption column models, the flue gas in this system is a binary mixture of CO_2 and N_2 at mole fractions of 15% and 85%, respectively. If this flue gas were to come from a coal plant, it would contain at least water and oxygen, and perhaps remaining SO_x and NO_x depending on the type of coal and existing clean-up process. The flue gas modeled in the DOE/NETL amine absorption system in Chapter 3, for example, does include non-negligible oxygen and water, and small amounts of argon—though no SO_x or NO_x. The lack of oxygen in a model of flue gas for a zeolite 13X system is not very concerning, given that oxygen adsorbs even more weakly than nitrogen on this sorbent (see adsorption isotherms for several relevant gases on zeolite 13X in Appendix C). The same is true for argon.

The water question is a more involved one. Zeolites tend to be very sensitive to water, because the highly polar water molecules will tend to adsorb very strongly. Sending wet flue gas directly into a zeolite column would severely affect the primary CO_2-N_2 separation process because the zeolite would quickly become saturated with water and be unusable. Some of the options for removing water prior to PSA systems using zeolites include cooling the flue gas to 25°C to condense a large fraction of the water vapor (note that the flue gas in Haghpanah et al.'s system is indeed assumed to arrive at the PSA system at 25°C, which implies prior cooling). Then, the remaining water can be removed by an additional dehumidification system, for example by passing the gas over silica gel, either as a separate first layer in the adsorption column, or as a completely independent column. Interested readers can see Krishnamurthy et al. 2014 [91] for an extension of the VSA system presented here to include a water

separation process as well. There has been at least one study of exergy destruction of drying air with silica gel [102], but no exergy analysis yet of CO_2 capture from flue gas including dehumidification. This could be foreseen as an extension of the work in this chapter.

For the purposes of the results here then, the separation process is of dry flue gas containing only CO_2 and N_2. The *minimum* exergy of separation calculation reflects this separation, which makes it the valid metric to use in the calculation of the 23.2% exergy efficiency value stated earlier.[1] The remainder of this chapter will explain how to interpret this efficiency value by showing a detailed exergy analysis of the system.

4.2.1 Modeling environment

The VSA system is modeled in Matlab, partly because the existing adsorption column model had been built in Matlab, and partly because building custom code in Matlab allows more direct control and fewer black boxes than pre-built packages for modeling adsorption columns. Aspen Adsorption (formerly Aspen Adsim) was also considered and evaluated for modeling this system. However, this environment was found to be difficult to use for the purposes of a detailed exergy analysis because returning entropy values in this environment was not straightforward, neither for gases, nor more importantly for adsorbed phases.

4.2.2 Analytical modeling of the column

The basic assumptions governing the transport and conservation equations in this system are presented here. More detail is given in Haghpanah et al. [86] for the calculation of coefficients and dimensionless parameters, and for the experimental validation of this model; however, the general behavior is explained here. The values of relevant parameters are listed in Appendix B.

[1] In a system that included dehumidification, the required exergy input would be higher, but the *minimum* exergy of this different separation would be higher as well. Therefore, while the exergy efficiency of a system with dehumidification would likely be different, no statement can be made about its value relative to the exergy efficiency of this system without choosing a specific dehumidification technology to model.

Species balance

The conservation of species i in this system is represented by a balance of the amount of species per gas-phase volume, as shown in Eq. 4.1. The transport of species i in the gas phase along the axis of the column is driven both by advective and dispersive effects, with negligible effect of radial gradients. Species i will also leave or enter the gas phase from the adsorbed phase, as represented by the final term in Eq. 4.1.

$$0 = -\varepsilon D_L \frac{\partial^2 C_i}{\partial z^2} + \varepsilon \frac{\partial \left(\mathbf{v} C_i\right)}{\partial z} + \varepsilon \frac{\partial C_i}{\partial t} + \left(1 - \varepsilon\right) \rho_s \frac{\partial q_i}{\partial t} \tag{4.1}$$

where $\mathbf{v}$ is the interstitial velocity, ε is the void fraction of the column (available to the gas phase), ρ_s is the density of the sorbent, and D_L is the axial dispersion coefficient. The quantity C_i is the amount of species i in the gas phase per unit volume, and is given by

$$C_i = y_i \hat{\rho}_g = \frac{y_i P}{RT} \tag{4.2}$$

assuming ideal gas behavior.

The quantity q_i is the amount of species i existing in the adsorbed phase per unit mass of sorbent (thus requiring the sorbent density ρ_s in that term). Its rate of accumulation is equal to the transfer rate of species i from the gas phase to the adsorbed phase. This transfer rate is driven by a difference in chemical potentials between the gas and surface phases, and is represented by a linear driving force (LDF) model with a lumped species transfer parameter ω_i.

$$\frac{\partial q_i}{\partial t} = \omega_i \left(q_{eq,i} - q_i\right). \tag{4.3}$$

In Eq. 4.3, $q_{eq,i}$ is the amount of species i that would exist on the sorbent at chemical equilibrium between the gas and the adsorbed phases. By contrast, q_i is the amount of species i currently existing in the adsorbed phase. The equilibrium value $q_{eq,i}$ depends on the adsorptive behavior of species i, but also of any other species that will compete with species i for adsorption sites. Therefore, $q_{eq,i}$ must be

found by assuming a mixing rule for competitive adsorption on the surface (the Ideal Adsorbed Solution model in this case). For example for a given $q_i < q_{eq,i}$, the transfer rate $\partial q_i/\partial t$ will be smaller if multiple species are adsorbed than if only one species is present, because the value of $q_{eq,i}$ would be smaller in the mixture case.

In this model, CO_2 and N_2 are the only two species modeled. The adsorption of each of these pure species, in equilibrium with a gas phase at $C = P/RT$, is represented by the dual-site (α and β) Langmuir isotherm

$$q_{eq,i} = \frac{q_{s\alpha,i} K_{\alpha,i} C}{1 + K_{\alpha,i} C} + \frac{q_{s\beta,i} K_{\beta,i} C}{1 + K_{\beta,i} C}. \tag{4.4}$$

The adsorption constant K_i is given by

$$K_i = K_{i,0} \exp(\frac{-\Delta U_i}{RT}) \tag{4.5}$$

with different parameters for each species on each site (these parameters' values are listed in Appendix B).

Thus far we have been describing the equilibrium adsorption of pure species. The adsorption of a *mixture* of the two species N_2 and CO_2 must be represented by the choice of a mixing rule. In the work of Haghpanah et al., the mixing rule used was the competitive- or extended-Langmuir, where adsorption of species i on any site is represented by a summation in the denominator,

$$q_{eq,i} = \frac{q_{s,i} K_i C_i}{1 + \sum_i K_i C_i}. \tag{4.6}$$

However, for reasons of thermodynamic consistency that will be elaborated in Chapter 5, the mixing rule was modified for the present work. Instead of Eq. 4.6, the Ideal Adsorbed Solution (IAS) framework of Myers and Prausnitz [92] was used due to its rigorous thermodynamic basis. There is no concise way to represent this mixing rule analytically here, but it will be discussed at much greater length in Chapter 5, and algorithms for its solution are given by O'Brien and Myers for example [93], [94].

Energy balance

The energy balance in the column rests on several key assumptions, notably that the column can be considered to be adiabatic, and that the gas, solid, and adsorbed phase are locally at the same temperature. Equation 4.7 gives the energy balance while explicitly tracking energetic quantities, while Eq. 4.8 gives the "temperature form" of the energy balance which is used to model the column numerically.

$$0 = -K_z \frac{\partial^2 T}{\partial z^2} + \varepsilon \frac{\partial(\mathbf{v}\hat{\rho}_g \hat{h}_g)}{\partial z} + \varepsilon \frac{\partial(\hat{\rho}_g \hat{u}_g)}{\partial t} + (1-\varepsilon)\,\rho_s \frac{\partial(u_s)}{\partial t} + (1-\varepsilon) \sum_{i=1}^{NS} \rho_s \frac{\partial(q_i \hat{u}_{i,a})}{\partial t} \tag{4.7}$$

The first term represents axial conduction with coefficient K_z in the column, the second term is advection of energy through the enthalpy of the flowing gas phase, and the final three terms represent internal energy accumulation in the gas, sorbent, and adsorbed phase respectively.

By incorporating the ideal gas law where relevant, we can write the temperature form of Eq. 4.7.

$$\begin{aligned} 0 = -K_z \frac{\partial^2 T}{\partial z^2} + \varepsilon \frac{\hat{c}_{p,g}}{R} \frac{\partial(\mathbf{v}P)}{\partial z} + \varepsilon \frac{\hat{c}_{v,g}}{R} \frac{\partial P}{\partial t} + (1-\varepsilon)\,\rho_s c_s \frac{\partial T}{\partial t} + (1-\varepsilon)\,\rho_s \sum_{i=1}^{NS} \hat{c}_{v,a} q_i \frac{\partial T}{\partial t} \\ + (1-\varepsilon)\,\rho_s \sum_{i=1}^{NS} \left(\hat{c}_{v,a} T + \Delta \hat{H}_i \right) \frac{\partial q_i}{\partial t} \end{aligned} \tag{4.8}$$

where $\Delta \hat{H}_i$ is the enthalpy of adsorption for species i, and c's are specific heat capacities. This has assumed that the reference states for energy terms (enthalpy, internal energy) are at 0 K with constant specific heats, as implemented in the final term.

Momentum correlation

The momentum balance is handled in this model by using Darcy's Law to correlate pressure drops with the advective velocity in the column

$$-\frac{\partial P}{\partial z} = \frac{150}{4r_p^2}\frac{(1-\varepsilon)^2}{\varepsilon^2}\mu_g \mathbf{v} \tag{4.9}$$

where r_p is the particle size and μ_g is the gas dynamic viscosity.

Summary

To summarize, the key assumptions in this model are given below.

- All gases behave as ideal gases at the states considered.
- The adsorption of pure CO_2 on the sorbent can be represented by a dual-site Langmuir expression, as can the adsorption of pure N_2.
- The competitive adsorption of CO_2 and N_2 can be represented by the IAS model of Myers & Prausnitz.
- The linear driving force (LDF) approximation is used for the transfer of species from the gas to the adsorbed phase, and is controlled by molecular diffusion in the macropores.
- The column can be modeled as adiabatic.
- Species' specific heats are constant with changes in temperature.
- Any radial inhomogeneities in temperature, gas phase composition, or adsorbed phase composition are negligible.
- At any axial position z in the column, temperature differences between the gas, sorbent, and adsorbed phases are negligible for the solution of the energy equation.

- Darcy's Law gives the correlation between velocity and pressure drop in the column.

- The sorbent properties are uniform everywhere in the column.

4.2.3 Numerical modeling of the column

The system is modeled using a finite-volume numerical scheme in space, the weighted essentially non-oscillatory (WENO) scheme. This non-oscillatory scheme is preferred for these systems to reduce non-physical oscillation around the fronts that form due to the strong source/sink term in the species balances. This is the term that accounts for adsorption and desorption in Eqs 4.1 and 4.7.

The details of this scheme and its application in this system are given by Haghpanah et al. No changes to the numerical scheme have been implemented here. As described in their work, the WENO scheme is applied to the advective terms, while the combination of a forward-difference term and finite-volume term is used for the second-derivative terms. The application of the numerical schemes for the space derivatives results in an algebraic expression in space, with remaining analytical derivatives in time. The time derivatives are isolated. Finally, the Matlab ODE stiff solver ode23s is used to solve the resulting system of ODEs in time.

4.2.4 Reaching cyclic steady state

When the adsorption column goes through the first four-step adsorption cycle, it is modeled as being filled only with nitrogen at the lowest pressure reached in the cycle and at 25°C. This is the initial condition given to the analytical and numerical problems described in the previous sub-sections. During the first pressurization step of the first four-step cycle, flue gas is used to pressurize this nitrogen-filled column to 1 atm, and the cycle continues. After several cycles, the nitrogen that initially filled the column is displaced, and the column is now filled with a mixture of nitrogen and CO_2 at the beginning of each new pressurization step. After many cycles, the composition, pressure, and temperature profiles in the column become the same from

one complete cycle to the next (although they will clearly vary from one cycle *step* to the next). At that point, we say that cyclic steady state (CSS) has been reached.

For optimization studies or other research areas that require fast solution of the column model, it may be important not to solve more cycles than are necessary to establish cyclic steady state. Often for carbon capture systems, it is most relevant to know whether cyclic steady state has been reached only relative to the purity and capture percentages of the CO_2 product stream. For example, cyclic steady state could be said to be reached when the CO_2 purity and capture does not change significantly over the course of several sequential cycles.

Exergy and entropy values tend to be more sensitive to small changes in the temperature or composition of a state than an overall CO_2 capture percentage. Therefore, it is not necessarily true that cyclic steady state criteria that are relevant for establishing CO_2 capture and purity levels are sufficient to ensure that cyclic steady state has been reached from an exergy point of view, too. In Figure 4.2, the net accumulation of mass, species, and energy in the column *for an entire cycle* is plotted over the course of 1000 cycles. Clearly, after approximately 150 cycles, the net, full-cycle accumulation of mass and energy in the column approaches zero. At this point, no net change is happening in the column over the course of a complete cycle—cyclic steady state has been reached.

In Figure 4.3, a similar plot is shown, this time tracking entropy and exergy values. Unlike mass, species, and energy, these two quantities are not conserved. The entropy-based quantity plotted is the difference between the extensive entropy exiting the column (integrated over the entire cycle) and the extensive entropy entering the column (also integrated over the entire cycle), multiplied by T_o. The plotted quantity is therefore the entropy generated over the entire cycle, minus the entropy accumulated in the column over the entire cycle (both multiplied by T_o).

$$T_o(S_{out} - S_{in}) = T_o S_{gen} - T_o \Delta S_{column} \tag{4.10}$$

Similarly, the plotted exergy quantity ($X_{in} - X_{out}$) is the sum of the exergy destruction and the exergy accumulated in the column. Around the 150th cycle, we observe that

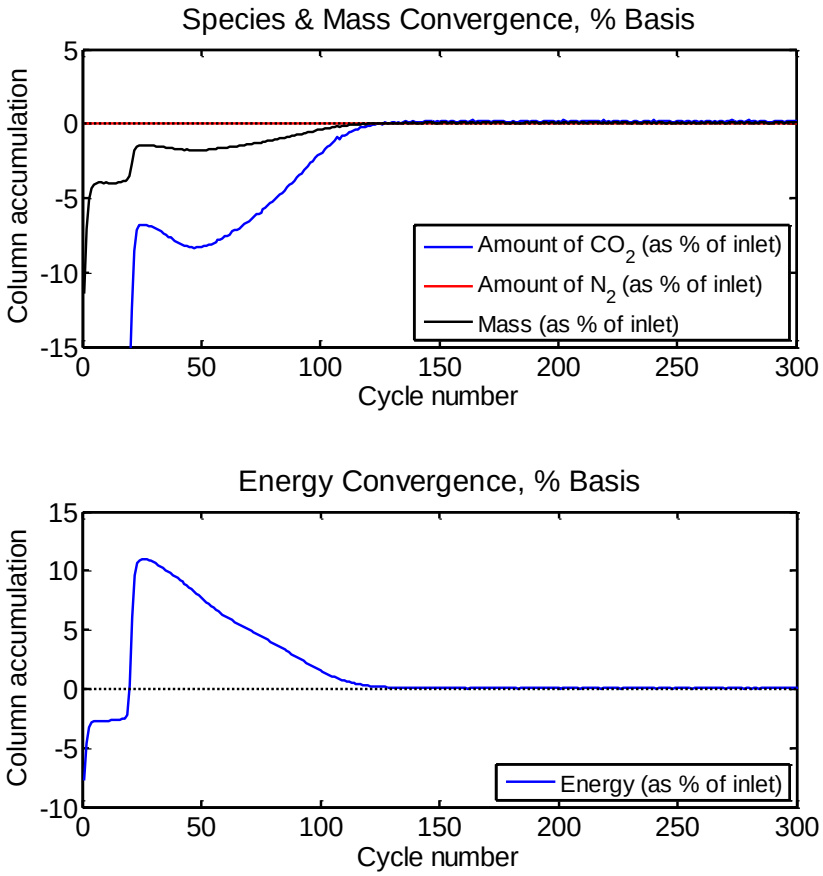

Figure 4.2: Establishing cyclic steady state, tracking mass, species and energy. Results are shown for a column modeled with 30 WENO volume elements.

the entropy quantity and the exergy quantity have converged and reached a steady-state value. At this point, the accumulation of entropy and exergy (and mass and energy) in the column is zero, and what remains is the Gouy-Stodola relationship between entropy generation and exergy destruction:

$$T_o S_{gen} = X_{dest}. \tag{4.11}$$

The steady-state value of X_{dest} shown in Figure 4.3 is the exergy destruction in the column alone, at steady state. Having established that cyclic steady state has been reached, we can also analyze the exergy destruction in the other devices in the system,

and thus achieve an exergy destruction breakdown for the entire separation process at cyclic steady state. We have also seen that in this case, cyclic steady state for the purposes of exergy calculations—as identified by the two quantities in Eq. 4.11 converging to the same value—is reached at the same time (around 150 cycles) as cyclic steady state for species and energy.

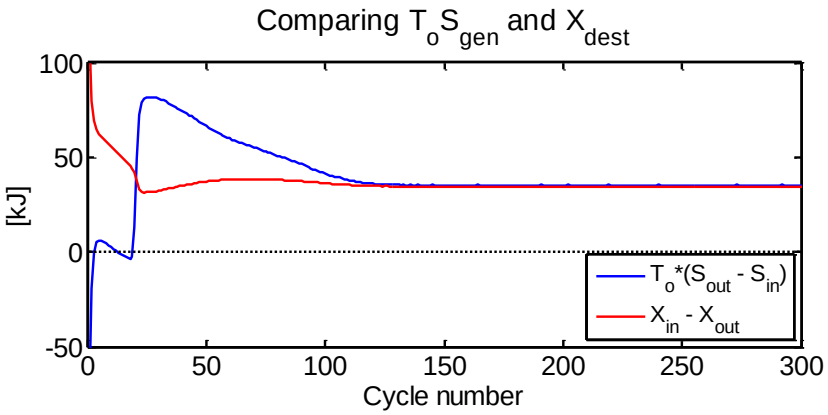

Figure 4.3: Establishing cyclic steady state, tracking exergy and entropy (entropy is multiplied by $T_o = 298.15$ K to compare to exergy directly). Results are shown for a column modeled with 30 WENO volume elements.

4.2.5 Assumptions about other system components

In the previous sub-section, it was established that at cyclic steady state, we could quantify the exergy destruction in the system's adsorption columns by subtracting the inlet exergy from the outlet exergy, because the exergy accumulation in the columns is zero at cyclic steady state.

$$X_{dest,column} = X_{in,column} - X_{out,column} \tag{4.12}$$

These two quantities are integrated over the course of the entire cycle,

$$X_{in,column} = \int_{t_{cycle}} \dot{N}_{in}(t)\hat{\psi}_{in}(t)dt \tag{4.13}$$

$$X_{out,column} = \int_{t_{cycle}} \dot{N}_{out}(t)\hat{\psi}_{out}(t)dt \tag{4.14}$$

with $\hat{\psi}$ indicating molar flow exergy.

Given the conditions Haghpanah et al. [86] have established about the operation of the adsorption column (which is the only system component modeled in their work), it is possible to draw some conclusions about which other devices or implied processes must exist elsewhere in the VSA system. These conclusions are illustrated in Figure 4.4, are explained below.

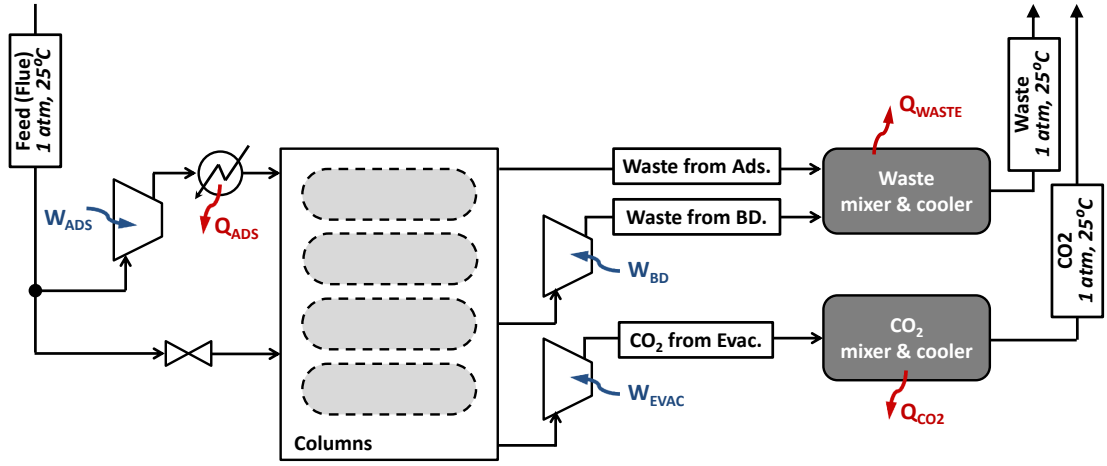

Figure 4.4: Other system components required given known operation of the column.

During the pressurization step, the column is supplied with flue gas at 1 atm and pressurized from a low pressure to 1 atm. Clearly, there must exist a throttle through which the flue gas passes as it pressurizes the adsorption column. Noting the existence of this throttle is not important for calculating the necessary electrical work for this system (a first-law analysis of the process), because throttles neither perform nor receive work. In fact, if the throttle is modeled as adiabatic, which is a common assumption for these devices, the device is isenthalpic: No energy change happens at all, nor a temperature change if the gas flowing through can be modeled as an ideal gas (as the enthalpy of an ideal gas is only a function of temperature). However, from a second-law point of view, recognizing that a throttle exists is not negligible.

Flow through a throttle is irreversible, and the entropy generation—and the exergy destruction—through this device can and should be quantified for an exergy analysis.

Assuming an adiabatic, isenthalpic throttle with ideal gases flowing through it, we can find the exergy destruction in the throttle,

$$X_{dest,throttle} = T_o \int_{t_{press}} \dot{N}_{in}(t)\hat{R} \ln \frac{P_{feed}}{P_{in,column}(t)} dt. \tag{4.15}$$

Substituting for the molar flow rate based on known properties at the column inlet,

$$X_{dest,throttle} = T_o \int_{t_{press}} \frac{P_{in,column}(t)}{T_{in,column}} \mathbf{v}\varepsilon A \ln \frac{P_{feed}}{P_{in,column}(t)} dt \tag{4.16}$$

where $\mathbf{v}$ is the interstitial velocity of the gas flowing into the column cross-section, A is the column cross-sectional area, and ε is the column void fraction.

Note that this assumes that the molar flow rate at the column inlet is the same as the molar flow rate through the throttle, which is an assumption of zero accumulation between the valve and the beginning of the packed bed. This includes an assumption of zero accumulation in any header space in the column, or more precisely of zero header volume, as well as zero accumulation in all valves and piping between the throttle and the column. Neither of these assumptions would be valid in reality. The header volume in particular should be better understood and modeled in future work, given that concentration, temperature, and possibly pressure gradients could exist in this space, which would all result in exergy destruction. However, as a first pass, neglecting the header volume is appropriate given that the rest of the column—with adsorption, desorption, and large composition and temperature gradients—will likely exhibit greater exergy destruction. The assumption of zero accumulation (and therefore zero mixing and zero irreversibility) in the pipes in the system could only be removed once an understanding of the actual system's operation were attained.

The throttle is the only system component that is implied by the column's operation during the pressurization step. During the adsorption step, flue gas is pressurized slightly above 1 atm, in order to ensure a continuous, steady flow of gas into the column (in the mathematical modeling of this step, the inlet *velocity* is specified rather

than the inlet pressure) and to maintain the column outlet at a constant pressure of 1 atm. The expression for the calculation of blower work given in Haghpanah et al. [86] has implicitly assumed an adiabatic compression with a constant isentropic efficiency η_s of 72%,

$$W_{blower} = \frac{1}{\eta_s} \int_{t_{ads}} \dot{N}_{in}(t) \cdot \hat{c}_p(t) \cdot T_{feed} \left[\left(\frac{P_{in,column}(t)}{P_{feed}} \right)^{\frac{\gamma-1}{\gamma}} - 1 \right] dt \tag{4.17}$$

where assuming that $\dot{N}$ through the blower equals $\dot{N}$ into the column (assumption of zero accumulation in other system components) results in

$$W_{blower} = \frac{1}{\eta_s} \int_{t_{ads}} \frac{\gamma}{\gamma - 1} P_{in,column} \cdot \mathbf{v} \varepsilon A \frac{T_{feed}}{T_{in,column}} \left[\left(\frac{P_{in,column}(t)}{P_{feed}} \right)^{\frac{\gamma-1}{\gamma}} - 1 \right] dt. \tag{4.18}$$

These assumptions allow us to define the exergy destruction in the blower as follows:

$$X_{dest,blower} = T_o \int_{t_{ads}} \frac{P_{in,column}(t)}{\hat{R} T_{in,column}} \cdot \mathbf{v} \varepsilon A \left[\hat{c}_p \ln \frac{T_{out,blower}(t)}{T_{feed}} - \hat{R} \ln \frac{P_{in,column}(t)}{P_{feed}} \right] dt. \tag{4.19}$$

where the temperature exiting the blower is given by

$$T_{out,blower}(t) = T_{feed} \left\{ 1 + \frac{1}{\eta_s} \left[\left(\frac{P_{in,column}(t)}{P_{feed}} \right)^{\frac{\gamma-1}{\gamma}} - 1 \right] \right\}. \tag{4.20}$$

At this point, we explicitly notice that the temperature of the gas exiting the blower will be higher than the feed gas, due to the adiabatic compression process. We also notice that the model of the adsorption column specifies that the temperature of the gas at the column inlet is constant at 25°C. This implies that the gas will be cooled after compression, which will also incur some exergy destruction. The heat transfer required to restore the gas stream to the required column inlet temperature

is given by

$$\dot{Q}_{ads} = \frac{\gamma}{\gamma - 1} P_{in,column}(t) \cdot \mathbf{v} \varepsilon A \left[\frac{T_{out,blower}}{T_{in,column}} - 1 \right] \tag{4.21}$$

The exergy destruction associated with this heat transfer depends on the temperature of the system boundary at which the heat transfer is defined to occur. In order to capture the entirety of the exergy destruction due to this process within the boundaries of the carbon capture process, the heat transfer must be rejected to the environment at T_o. If it were rejected at a higher (or lower) temperature, it would still have exergy which would then be destroyed by equilibration in the environment. Drawing the boundary at T_o ensures that the entire exergy destruction is counted.

$$X_{dest,cooler,ads} = T_o \int_{t_{ads}} \left[\frac{\dot{Q}_{ads}}{T_o} + \frac{\gamma}{\gamma - 1} P_{in,column}(t) \cdot \mathbf{v} \varepsilon A \cdot \frac{1}{T_{in,column}} \ln \frac{T_{in,column}}{T_{feed}} \right] dt \tag{4.22}$$

During the blowdown step, nothing enters the column, but gas is withdrawn from the column using a vacuum pump and delivered at 1 atm. Once again, the assumption made in the work calculation by Haghpanah et al. was that of a single-stage adiabatic compression with an isentropic efficiency of 72%, where there is zero accumulation between the column outlet and the vacuum pump outlet.

$$W_{pump,BD} = \frac{1}{\eta_s} \int_{t_B D} \dot{N}_{out}(t) \cdot \hat{c}_p(t) \cdot T_{out,column} \left[\left(\frac{P_{out,pump}}{P_{out,column}(t)} \right)^{\frac{\gamma-1}{\gamma}} - 1 \right] dt \tag{4.23}$$

Assuming that $\dot{N}$ through the vacuum pump equals $\dot{N}$ out of the column (assumption of zero accumulation in other system components) results in

$$W_{pump,BD} = \frac{1}{\eta_s} \int_{t_{BD}} \frac{\gamma}{\gamma - 1} P_{out,column}(t) \cdot \mathbf{v} \varepsilon A \left[\left(\frac{P_{out,pump}}{P_{out,column}(t)} \right)^{\frac{\gamma-1}{\gamma}} - 1 \right] dt \tag{4.24}$$

Here $\mathbf{v}$ is now the interstitial velocity at the column outlet. This results in the

following exergy destruction in the vacuum pump

$$X_{dest,pump} = T_o \int_{t_{BD}} \frac{P_{out,column}(t)}{\hat{R}T_{out,column}} \cdot \mathbf{v}\varepsilon A \left[\hat{c}_p \ln \frac{T_{out,pump}(t)}{T_{out,column}} - \hat{R} \ln \frac{P_{out,pump}(t)}{P_{out,column}} \right] dt \tag{4.25}$$

where the temperature exiting the vacuum pump is given by

$$T_{out,pump} = T_{out,column} \left\{ 1 + \frac{1}{\eta_s} \left[\left(\frac{P_{out,pump}}{P_{out,column}} \right)^{\frac{\gamma-1}{\gamma}} - 1 \right] \right\} \tag{4.26}$$

During the evacuation step, a vacuum pump is used to draw an even deeper vacuum on the column. The relevant equations for work done and exergy destruction in the vacuum pump follow those just described for the blowdown step. However, what happens to the waste stream and the CO_2 product stream after the vacuum pumps is also worth discussing.

The CO_2 product stream is considered to be delivered at 1 atm and 25°C, and at a constant composition. However, while the CO_2 stream leaving the vacuum pump during the evacuation step is at 1 atm, it is neither at 25°C (due to having gone through an adiabatic compression over a large pressure ratio), nor is it at constant composition (because the mole fraction of the gas leaving the column changes in time). Therefore, a cooling and mixing process are both necessary to bring the product gas to exit the cycle at the required conditions. In the absence of more detailed information about these two processes, they have been combined for analysis into a single, black-boxed step as a cooled mixer, see Figure 4.4. This cooled mixer will have significant accumulation of species over the course of a single cycle, but from one cycle to the next (at cyclic steady state) the net accumulation of species and energy in the cooled mixer will be zero.

Similarly, the waste streams from the adsorption step and from the blowdown step are both considered to be waste, and are considered to be delivered at 1 atm and 25°C at a constant mole fraction. This implies that there is also a mixing and cooling process undergone by both streams together, as shown in Figure 4.4.

The heat transfer out of each of the cooled mixers is given by

$$Q_{mix\&cool} = \int_{t_{cycle}} \dot{N}_{out}\hat{c}_{p,out}(T_{out} - T_{ref})dt - \int_{t_{cycle}} \dot{N}_{in}(t)\hat{c}_{p,in}(t)(T_{in}(t) - T_{ref})dt \tag{4.27}$$

where T_{ref} is an arbitrary reference temperature and can be chosen to be anything, since it will cancel out of this equation. The exergy destruction can be found for this process, again assuming that the heat transfer occurs at the temperature of the environment T_o to correctly account for all irreversibility.[2]

$$X_{dest,mix\&cool} = T_o \cdot \left[\frac{Q_{mix\&cool}}{T_o} + \int_{t_{cycle}} \dot{N}_{out}\hat{s}_{out}dt - \int_{t_{cycle}} \dot{N}_{in}(t)\hat{s}_{in}dt \right] \tag{4.28}$$

The irreversibility in this process will therefore come from both the heat transfer out of the system and also the entropy of mixing, as reflected in the $\hat{s}$ values.

4.2.6 Results and discussion

Earlier we stated that the exergy efficiency of this VSA carbon capture system was 23.2%, based on the purity of the CO_2 product, the capture fraction, and the necessary electrical work given by Haghpanah et al. [86]. This means that 76.8% of the exergy supplied to the system is destroyed. This section will discuss the potential to improve the exergy efficiency of this system. It is important to note that the system modeled by Haghpanah et al. has already been optimized for minimizing the required electrical work—under certain modeling assumptions—for separating CO_2 at a set purity and recovery. However, one of the conclusions of this section is that this work may still not have been minimized, due to assumptions about how the vacuum pumping is done. In Figure 4.5, we show the distribution of this exergy destruction in each system

[2]As a reminder, note that this is a different statement than saying that the gas, or the heat exchanger, or the cooling fluid are at T_o. If the heat transfer occurs at a different temperature than T_o, the heat transfer still has exergy. Eventually, that exergy must either be used or be dissipated in the environment. If it were used, the exergy efficiency of the system would be higher. By clearly defining the system boundary for calculating the minimum exergy of separation, we are imposing that any "extra" heat transfer out must no longer have exergy—i.e. it leaves the system at T_o.

component, modeled with the assumptions from Haghpanah et al. as described above.

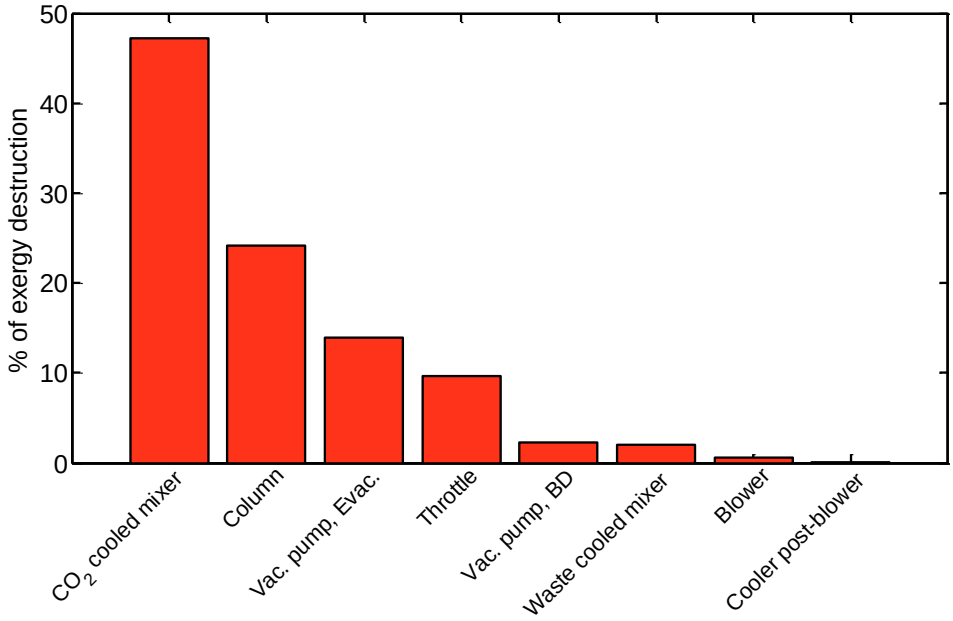

Figure 4.5: Exergy destruction in each section of the VSA system.

The greatest destruction by far is in the "cooled mixer" we introduced by logical deduction of the transformations necessary to restore the CO_2 stream to its intended final state after exiting the vacuum pump. In order to understand this somewhat surprising result, we can examine the state of the CO_2 product stream at the outlet of the vacuum pump. This stream has a constant pressure at 1 atm. However, its temperature will change over the course of the evacuation step as a deeper vacuum is drawn on the column, thus increasing the pressure ratio the gas will undergo in the adiabatic vacuum pump. Similarly, the mole fraction of this stream will change over the course of the evacuation step as more CO_2 is pulled from the adsorbed phase into the gas phase and out of the column. The purpose of the cooled mixer is to accumulate and cool the CO_2 product to release it as a homogeneous mixture at 25°C.

The temperature and mole fraction of the CO_2 stream exiting the vacuum pump during the evacuation step are shown in Figure 4.6. Clearly, this stream's temperature

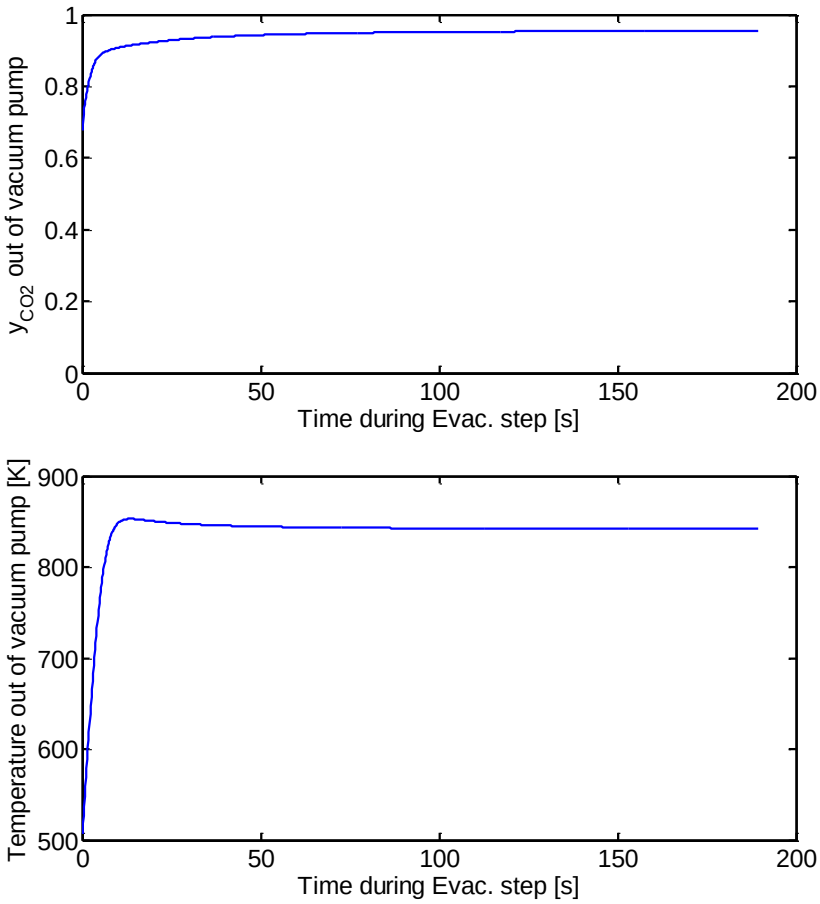

Figure 4.6: Mole fraction and temperature of the gas at the outlet of the vacuum pump in the evacuation step.

has increased very significantly as a result of being compressed adiabatically from the low pressure of 0.02 bar to atmospheric pressure in the vacuum pump. Cooling this high-temperature stream to 25°C results in a large amount of heat transfer, and if none of that heat transfer is used (which is the assumption taken here), a large amount of exergy is destroyed.

The question now is whether this is representative of what would actually occur in a real system. The concept of having a vacuum pump operated between 0.02 bar and 1 atm as a single adiabatic compression stage is unlikely. However, it is indeed what is often modeled when predicting the work necessary for operating these systems (see, for example, Riboldi and Bolland 2015 [95], Faruque Hasan et al. [90], Lin et al. [89]). In the literature, Xu and Webley mention this in a similar study of a vacuum swing adsorption system for post-combustion capture [96]. They note: "We expect commercial scale multiple stage vacuum units with efficiencies which depend on vacuum pressure. Therefore, it is important not to take the absolute power numbers as reliable predictors rather, our goal here is to compare the power between [several different cases]." A multi-stage, intercooled system would have the effect of reducing the exergy destruction observed in our simplified cooled mixer pseudo-device, and then have the effect of reducing the work necessary for the vaccum pump, raising the exergy efficiency for this separation system.

As a first-pass exercise to estimate the possible gains in system efficiency achievable by intercooling vacuum pump stages, we cool the stream to 35°C at evenly-divided pressure ratios between the two end points. In Figure 4.7 the effect of using even one intercooling stage is clear, with a 4.5 point exergy efficiency gain. The results for 5 and 10 stages are shown not as a realistic suggestion, but to give a sense of the limits of the efficiency gain that can be made by intercooling this vacuum pumping process, and to give context to the 4.5-point gain with a single stage. As the number of intercooling stages increase, the exergy destruction in the CO_2 cooled accumulator is nearly eliminated. What remain are the exergy destruction in the vacuum pump (due to the isentropic efficiency of the machinery)[3], in the intercooling itself, and

[3]Note that the exergy destruction in this device from 0 to 10 intercooling stages increases not due to changes in the isentropic efficiency—which is held constant—but instead because of the

finally—and most importantly—in the adsorption column.

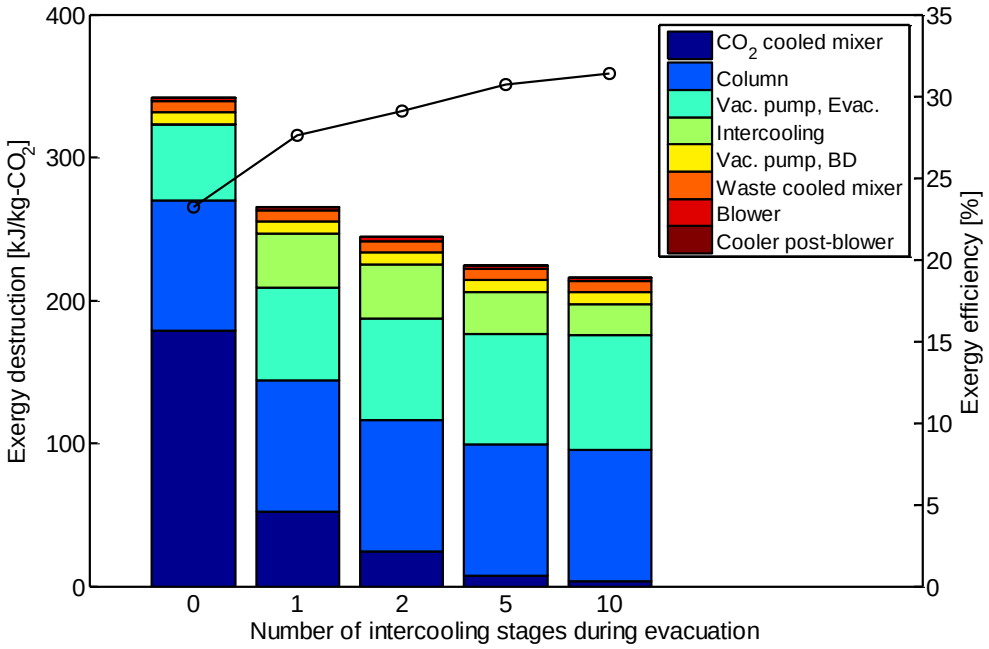

Figure 4.7: Distribution of the exergy destruction in the VSA system, with and without intercooling stages in the vacuum pumping process during the evacuation step. The black line shows the system exergy efficiency.

The proportion of the exergy destruction that occurs in the adsorption column is a more realistic value. Many adsorption column models are well-validated against lab-scale or even pilot-scale experiments, including the model used in this work [97]. Reducing the exergy destruction in the column requires a more detailed awareness of what is happening in each individual step in the cycle, in order to modify the path taken to reach the desired end states. In fact, a significant amount of adsorption research is concerned with increasing the system efficiency by changing the nature of the steps in the batch cycle. For example, the electrical work needed to operate the adsorption cycle can be reduced by adding extra pressure-equalization steps [85] or by including reflux steps [98]. In order to calculate the exergy destruction in the column during an individual cycle step, we must be able to quantify the exergy accumulated

dependence of compression irreversibility on pressure ratio.

in the adsorbed species on the surface of the sorbent. Understanding and exploring the thermodynamic relationships that are relevant to adsorbed phases, in order to enable the exergy analysis of a step in a batch adsorption cycle, is the focus of the next chapter.

4.3 Summary

In this chapter, we model and analyze a post-combustion CO_2 capture system that operates by selective adsorption of CO_2 on a porous sorbent, zeolite 13X, undergoing a vacuum-swing adsorption cycle. The modeling assumptions are discussed, and the exergy analysis of the system at cyclic steady state is presented, treating the adsorption columns as a black-box. It was found that the greatest exergy destruction in the system was in the mixing, and especially the cooling, of the CO_2 product stream, but the realism of this finding is uncertain and is discussed. Incorporating stages of intercooling in the vacuum pumping process would increase the system efficiency by several points.

The second largest exergy destruction in the system is found to be in the adsorption column. Therefore, Chapter 5 presents the derivation, from basic principles, of the exergy of an adsorbed phase, in order to enable the exergy analysis of unsteady adsorption steps in the column.

Chapter 5

Thermodynamic Properties for Exergy Analyses of Adsorption Columns

This chapter explains and develops the thermodynamic relations that are necessary to perform an exergy analysis of an unsteady adsorption step in an adsorption column or other adsorption process. In order to perform such an analysis, the accumulation of exergy on the surface of the sorbent, in an adsorbed phase with behavior different from that of the gas phase, must be able to be defined clearly. However, relative to bulk mixtures of electrolytic solvents and solutes (as covered in Chapter 3), the thermodynamics of adsorption are less commonly known. Here, the exergy of an adsorbed phase is derived from fundamental principles. Restrictions on adsorbed-phase equations of state and mixing rules, as well as the definition of the dead state, are discussed. The motivation for this chapter is to enable a detailed exergy analysis of the adsorption column from the post-combustion CO_2 capture system of Chapter 4; however, the expression derived here applies generally to any adsorption process.

5.1 Background from previous exergy analyses of adsorption processes

Exergy has been used as a metric, directly or indirectly, to analyze adsorption-based processes in a small number of previous studies. Banerjee et al. studied the exergy destroyed in a pressure-swing adsorption process for air separation [99], [100]. In their study, they quantified the exergy destruction in several system components at cyclic steady state, but did not analyze the transient operation in the column, and therefore did not quantify the exergy accumulated in the adsorbed phase.

Several studies have analyzed the exergy destruction during the dehumidification of air by silica gel. Lior and Al-Sharqawi focused on the flow of humid air through a desiccant-lined channel, to understand how the transient temperature, velocity, and composition gradients at the boundary of the desiccant affected exergy destruction [101]. Because of their particular system configuration, they could treat the adsorbed-phase properties as behaving like liquid water, and account for the exergy from the heat of adsorption as a simple heat transfer. They did not need to derive a general expression for the exergy of adsorbed species. Worek et al. tracked exergy destruction in a silica gel dehumidification batch cycle, instead of through a flowing channel [102]. This scenario bears more resemblance to the batch-cyclic processes used for carbon capture. However, in all of these studies, the presence of a single species (water) near its liquid saturation point greatly simplifies the process, allowing assumptions that are not possible for adsorbed mixtures of CO_2 and nitrogen.

Kearns and Webley have been the only ones, to our knowledge, to define the exergy of an adsorbed phase explicitly to perform an exergy analysis, and to do so in a way that is applicable to adsorbed mixtures of gases [103]. The system they modeled was an air-separation, pressure-swing adsorption process. For this process, certain simplifications in the choice of equations of state (linear isotherms, binary mixtures, ideal gases) are valid, and were applied during their derivation. Moreover, the exergy expression they applied was taken from standard, bulk-phase thermodynamics without justification.

The goal of the present work is to develop, from fundamental principles, an expression for the exergy of adsorbed phases that imposes no particular equation of state form. It should be noted that the expression derived here does reduce to Kearns and Webley's expression when their assumptions are invoked, despite the very different approach taken in the derivation.

5.2 Thermodynamic definitions relevant to an adsorbed phase

The thermodynamics of adsorption have been studied and written about extensively, starting with Gibbs in 1877 [104]. Here we summarize and discuss the results that are directly relevant to our application, namely the derivation of the exergy of adsorbed phases. For comprehensive discussion of the thermodynamics of adsorption, see the work of Young and Crowell [105], and Rudzinski and Everett [106], among others.

5.2.1 Defining the adsorbed phase

In order to discuss thermodynamic properties of an adsorbed phase, we need to have a definitive sense of where and what this phase is. We can think vaguely about the *adsorbed phase* as a region near the surface of a solid where gas molecules have agglomerated at a different number density than in the bulk gas phase, as shown in Figure 5.1a. However, this does not set clear boundaries between the three phases—solid (or sorbent), gas, and adsorbate. If we take an overall volume V^t that contains some solid, some bulk gas phase, and some adsorbed species, then the number density of a chemical species does not go through a detectable sharp change that would allow us to set the position of a phase boundary; the phases ease into each other. This means that it is not straightforward to split up the total volume V^t into three sub-volumes V^s, V^g, and V^a for the solid, gas, and adsorbed phases.

Gibbs [104] resolved this vagueness using a mathematical model: He introduced an artificial discontinuity—an interface—that is placed so as to account for all extensive properties of the chemical species with no loss of conserved quantities. We start with

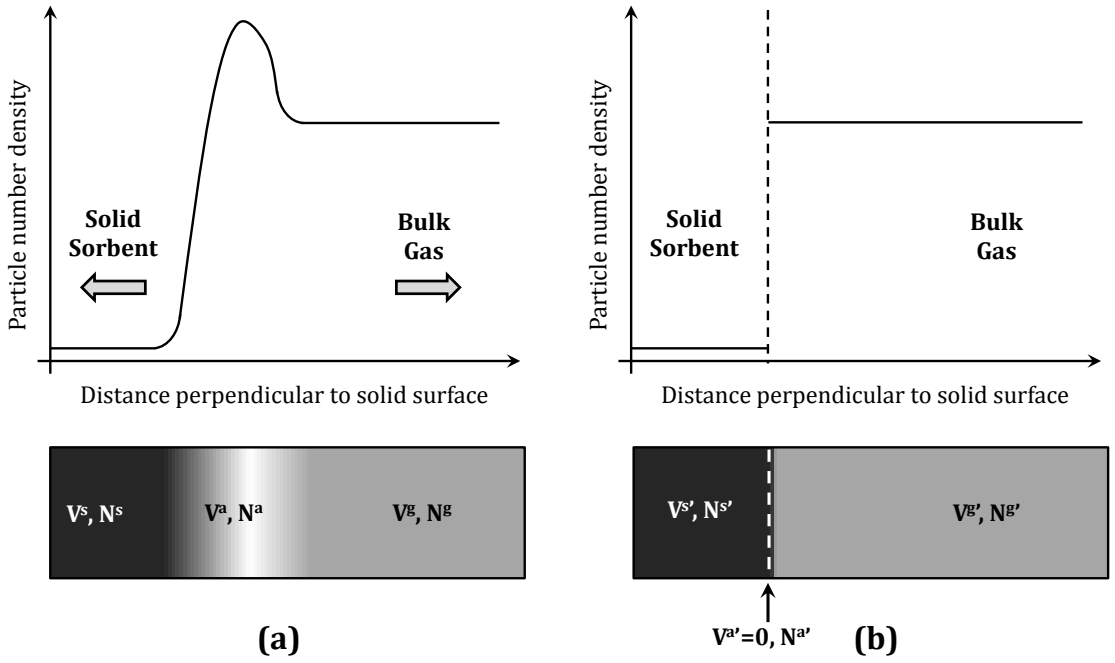

Figure 5.1: The gas-sorbent-adsorbate interphase region, represented either by a continuous gradient (in (a)) or by an interface (in (b)). In each of the lower rectangles, the shading represents the particle number density represented by the plot immediately above it. Lighter shading corresponds to a higher particle number density.

our volume V^t, which includes all three phases. Now imagine that instead of trying to create two interfaces to separate V^t into three volumes V^s, V^g, and V^a, we try instead to create a single interface between $V^{s\prime}$ and $V^{g\prime}$, as shown in Figure 5.1b. Taking $V^{s\prime}$ as a property of the solid, it must have the number density of the bulk solid everywhere—it must be homogeneous, since it is a phase. Similarly, $V^{g\prime}$ should then have everywhere the number density of the bulk gas, so there will be a distinct discontinuity in particle number density at the interface between the two phases.

The number of particles in each phase, $N^{s\prime}$ and $N^{g\prime}$, will therefore vary based on the size of $V^{s\prime}$ and $V^{g\prime}$—in other words, they will vary based on the chosen position of the interface. If we are tracking a species that exists mainly in the gas phase and negligibly in the solid phase, like the example shown in Figure 5.1, moving the interface to the left (into the solid) will result in a larger total number of particles, $N^{(g+s)\prime} = N^{g\prime} + N^{s\prime}$. Similarly, moving the interface to the right will result in a smaller number of particles $N^{(g+s)\prime}$. But the total number of particles inFigure 5.1b, $N^{t\prime}$, has to be equal to the total number of particles in Figure 5.1a, N^t, to ensure that matter is conserved. We can therefore think of a delta function of particle number density along the interface, accounting for the difference between N^t and $N^{t\prime}$. This difference is $N^{a\prime}$, the number of particles in the adsorbed phase, and its value will become smaller or larger as the interface is moved to the left or right, respectively.

When the expression *Gibbs dividing surface* is used, it refers to an interface that is positioned such that $N^a = 0$, so that all particles are assigned either to the gas phase or the solid phase. This is the basis for the measurement of the void fraction of porous media: a "non-adsorbing" gas is allowed to fill a previously cleaned and evacuated sample of porous solid in a rigid tank at a set temperature and pressure. By measuring the number of moles of gas that have entered the tank to fill the sample, the volume of gas is found using an equation of state for the gas phase. This volume is the one used to define the volumetric void fraction for the material, so this measurement effectively assigns all space either to the gas phase or to the solid phase.

In actual adsorption processes, there are usually several different species present in the gas phase, which may each adsorb to different degrees. This would result in a different location for the Gibbs dividing surface for each species. In order to set

a common reference, the void fraction of porous media is measured with a single component gas that is as lightly-adsorbing as possible, typically helium. This sets the position of the Gibbs dividing surface. For all other gaseous species on the same sorbent, the value of N^a is no longer zero, and there will be a delta function of particle number density at the interface. This quantity N^a is known as the *Gibbs excess adsorption*, and it determines the amount of the species that is considered to be in the adsorbed phase. The Gibbs definition of an adsorbed phase is thereby a zero-volume phase that contains the amount of species that has been assigned neither to the bulk gas phase nor to the clean, bulk solid.

5.2.2 Thermodynamic relations for the adsorbed phase

The discussion so far has been concerned only with defining the amount of chemical species that is assigned to the adsorbed phase. In order to define the exergy of this phase, we will also need to understand the thermodynamic relations that apply to it. The thermodynamics of these phases differ from the thermodynamics of bulk phases. Because adsorbed phases are modeled as zero-volume interfaces, the ways in which their internal energy can be modified are different from those of bulk phases. This is reflected in the adsorbed phase versions of the Gibbs equation (Eq. 5.1), the Euler relation (Eq. 5.2), and the Gibbs-Duhem equation (Eq. 5.3), all of which lack a pressure-volume product term. These equations can be found, with deeper discussion, in Myers [2].

Gibbs equation for adsorbed phases:

$$dU^a = TdS^a + \sum_{i=1}^{NS} \mu_i dN_i^a + \Phi dm^s \tag{5.1}$$

Euler relation for adsorbed phases:

$$U^a = TS^a + \sum_{i=1}^{NS} \mu_i N_i^a + \Phi m^s \tag{5.2}$$

Gibbs-Duhem equation for adsorbed phases:

$$m^s d\Phi = -S^a dT - \sum_{i=1}^{NS} N_i^a d\mu_i \tag{5.3}$$

Here the superscript a refers to the properties of the adsorbed phase, and NS refers to the total number of species. The parameter Φ that appears in these equations is known as the *surface potential*, and it accounts for the change in the chemical potential of the solid sorbent as a result of adsorption. Specifically, it is the difference between the chemical potential of the clean, evacuated sorbent, and the chemical potential of the sorbent after coming to equilibrium with the adsorbed phase (on a per-mass-of-sorbent basis):

$$\Phi = \frac{1}{\hat{M}^s}\left(\mu^{s,clean} - \mu^{s,post-ads}\right). \tag{5.4}$$

where $\hat{M}_s$ is the molar mass of the sorbent. Even though this property originates from a change in the chemical potential of the sorbent, it is a property of the adsorbed phase under the Gibbs dividing surface concept (which assigns all adsorption-related effects, including the chemical potential change of the sorbent, to the adsorbed phase). The surface potential Φ is also often represented in the literature as the product of a surface area A and a spreading pressure Π, by analogy with surface tension at interfaces [2], [107], [108]. In highly porous sorbents, the surface area is often ill-defined, so the use of the surface potential Φ is preferred.

5.3 Exergy of the adsorbed phase

5.3.1 System definition

A key concept underlies the definition of the phases using the Gibbs dividing surface in Section 5.2.2: The extensive properties of the adsorbed phase are defined only by a difference between the extensive properties of an equilibrated gas-sorbent-adsorbate system and those of the free bulk gas and clean sorbent phases. It is impossible

to derive any extensive property of the adsorbed phase without starting from the extensive properties of the full, three-phase system.

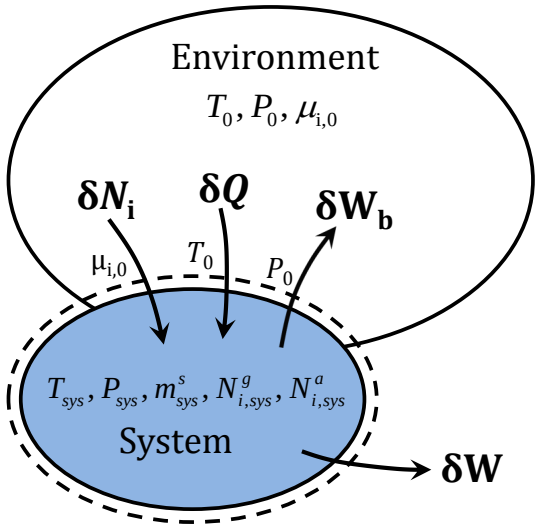

Figure 5.2: Definition of the system with all possible transfers. Note that the transfers cross the boundary between the system and the environment (indicated by the dashed line) at the environmental state.

For this reason, to derive the exergy of the adsorbed phase we first define a system that contains a mass m^s_{sys} of sorbent, an amount $N^g_{i,sys}$ of species i in the gas phase, and a Gibbs excess amount $N^a_{i,sys}$ of species i in the adsorbed phase. We will first derive an expression for the extensive exergy of this combined system. Then, we will solve for the exergy of the adsorbed phase by acknowledging that exergy is an extensive property, and that we can therefore subtract the exergy of the bulk gas and solid phases from the total exergy of the system:

$$X^a = X^t - (X^g + X^s)\,, \tag{5.5}$$

where the superscript a refers to the adsorbed phase, g refers to the gas phase in equilibrium with that adsorbed phase, s refers to the clean solid sorbent, and t refers to the total gas-sorbent-adsorbate system.

The system is initially at a temperature T_{sys}, at a pressure P_{sys}, and the chemical

potentials are equal across phases within the system boundary. The system is then allowed to interact with the environment, which is at a state T_o, P_o, and $\mu_{i,o}$, as shown in Figure 5.2. Only three forms of interactions are possible between the system and the environment: heat transfer (δQ), matter transfer (δN_i), and boundary work (δW_b). Additionally, we allow work (δW) to be extracted from the system while it interacts with the environment. The boundary of the system, indicated by a dashed line in Figure 5.2, is located such that all transfers cross the boundary at the environmental state (and any irreversibilities are therefore confined within the system boundary). For the purpose of this derivation, positive values of δQ and δN_i represent transfers into the system, while positive values of δW_b and δW represent transfers out of the system, as indicated by the arrows in Figure 5.2.

5.3.2 Exergy of the system

The exergy of any system is the maximum work that can be extracted while the system comes to equilibrium with the environment. Mathematically, this is defined by maximizing the path integral of δW from the system state to the environmentally equilibrated state, known as the dead state.

$$X^t = \max\left(\int_{SystemState}^{DeadState} \delta W\right) \tag{5.6}$$

To find an expression for δW we start by writing balance equations for the system defined in Figure 5.2.

Energy balance:

$$0 = dU^t + \delta W + \delta W_b - \delta Q - \sum_{i=1}^{NS} \bar{h}_{i,o}\delta N_i \tag{5.7}$$

Entropy balance:

$$\delta S_{gen} = dS^t - \frac{\delta Q}{T_o} - \sum_{i=1}^{NS} \bar{s}_{i,o}\delta N_i \tag{5.8}$$

We can combine Eqs. 5.7 and 5.8 by eliminating δQ and rewriting the resulting equation to isolate δW

$$\delta W = -dU^t - \delta W_b + T_o dS^t + \sum_{i=1}^{NS} \left(\bar{h}_{i,o} - T_o \bar{s}_{i,o}\right) \delta N_i - T_o \delta S_{gen}. \tag{5.9}$$

We recognize that the boundary work δW_b is given by $\delta W_b = P_o dV$ because the system boundary is located at the dead state (T_o, P_o, $\mu_{i,o}$). We also recognize that the expression $\bar{h}_{i,o} - T_o \bar{s}_{i,o}$ is the chemical potential of species i at the dead state $\mu_{i,o}$. By writing the conservation law for the amount of species i, we know that

$$\delta N_i = dN_i \tag{5.10}$$

where δN_i refers to the transfer of species i from the environment to the system, while dN_i refers to the accumulation of species i in the system. To be able to make this equality, we have to presuppose that the adsorption process is non-reactive (i.e., that no new species are created from species in the gas phase). This comes from the definition of an adsorption process: If gas species reacted with each other on the surface, the process is catalysis, and if gas species reacted with the surface of the solid to form a new compound, it is a surface reaction. In this section, we will additionally restrict the species i to those that already exist in the environment. The effect of relaxing this assumption will be examined in Section 5.3.7.

Making the substitutions for boundary work, chemical potential, and transfer of species, we rewrite Eq. 5.9

$$\delta W = -dU^t - P_o dV^t + T_o dS^t + \sum_{i=1}^{NS} \left(\mu_{i,o} dN_i\right) - T_o \delta S_{gen} \tag{5.11}$$

where the first four terms on the right hand side are now exact differentials and are therefore easily integrated. Integrating this expression from the system state to the

dead state results in

$$\int_{SystemState}^{DeadState} \delta W = (U_{sys}^t - U_o^t) + P_o(V_{sys}^t - V_o^t) - T_o(S_{sys}^t - S_o^t) - \sum_{i=1}^{NS} \mu_{i,o}(N_{i,sys}^t - N_{i,o}^t) - \int_{SystemState}^{DeadState} T_o \delta S_{gen} \tag{5.12}$$

From Eq. 5.12, it is clear that the useful work extracted from the system is maximized when the process path is reversible (i.e., $S_{gen} = 0$). We therefore arrive at an expression for the exergy of the system by imposing a reversible process:

$$X^t = (U_{sys}^t - U_o^t) + P_o(V_{sys}^t - V_o^t) - T_o(S_{sys}^t - S_o^t) - \sum_{i=1}^{NS} \mu_{i,o}(N_{i,sys}^t - N_{i,o}^t) \tag{5.13}$$

5.3.3 Exergy of the adsorbed phase

The expression for the exergy of the system in Eq. 5.13 can be applied to any system, adsorption-related or not, under the non-reactive constraint imposed. This result is already well known (among others, [109], [110]), although the path to deriving it here is somewhat different. Showing this derivation rigorously is important for appreciating its general applicability, including to systems that include a non-negligible adsorbed phase. This approach for deriving exergy of systems, and for the extension to non-environmental species in Section 5.3.7, can be seen in more detail in [29].

Expanding the terms in Eq. 5.13 for the gas-sorbent-adsorbate system, we can isolate the exergy of the adsorbed phase alone. For any extensive property Z, we know that

$$Z^t = Z^g + Z^s + Z^a \tag{5.14}$$

Expanding the terms in Eq. 5.13, we arrive at

$$\begin{aligned} X^t = &(U^g_{sys} + U^s_{sys} + U^a_{sys} - U^g_o - U^s_o - U^a_o) + \\ &P_o(V^g_{sys} + V^s_{sys} + V^a_{sys} - V^g_o - V^s_o - V^a_o) \\ &- T_o(S^g_{sys} + S^s_{sys} + S^a_{sys} - S^g_o - S^s_o - S^a_o) - \\ &\sum_{i=1}^{NS} \mu_{i,o}(N^g_{i,sys} + N^s_{i,sys} + N^a_{i,sys} - N^g_{i,o} - N^s_{i,o} - N^a_{i,o}) \end{aligned} \tag{5.15}$$

We can now remove the exergy of the bulk gas and sorbent phases from this combined expression. Applying Eq. 5.13 to the gas phase alone results in

$$X^g = \left(U^g_{sys} - U^g_0\right) + P_0\left(V^g_{sys} - V^g_0\right) - T_0\left(S^g_{sys} - S^g_0\right) - \sum_{i=1}^{NS} \mu_{i,0}\left(N^g_{i,sys} - N^g_{i,0}\right). \tag{5.16}$$

Here we note that we do not actually know the value of $N^g_{i,o}$ at the dead state, because an unknown amount of species i has left the system boundary over the course of equilibration with the environment, and an unknown amount of species i may have been transferred between the gas phase and the adsorbed phase during this process. However, using the Euler relation for the gas phase, we can find a relationship between the dead state quantities

$$U^g_o - T_o S^g_o + P_o V^g_o = \sum_{i=1}^{NS} \mu_{i,o} N^g_{i.o}, \tag{5.17}$$

which, when applied to Eq. 5.16, results in

$$X^g = U^g_{sys} + P_o V^g_{sys} - T_o S^g_{sys} - \sum_{i=1}^{NS} \mu_{i,o} N^g_{i,sys}. \tag{5.18}$$

The absence of extensive quantities at the dead state in Eq. 5.18 shows that it is not necessary to precisely know how much of species i has entered or left the gas phase, whether from the environment or from the adsorbed phase, during the

equilibration to the dead state.

We can apply the same reasoning to the solid sorbent. This results in two equivalent expressions for the sorbent's exergy:

$$X^s = (U^s_{sys} - U^s_o) + P_o(V^s_{sys} - V^s_o) - T_o(S^s_{sys} - S^s_o) - \sum_{i=1}^{NS} \mu_{i,0} \left(N^s_{i,sys} - N^s_{i,0}\right). \quad (5.19)$$

$$X^s = U^s_{sys} + P_o V^s_{sys} - T_o S^s_{sys} - \sum_{i=1}^{NS} \mu_{i,0} \left(N^s_{i,sys} - N^s_{i,0}\right). \quad (5.20)$$

Subtracting Eqs. 5.16 and 5.19 from Eq. 5.15 isolates the exergy of the adsorbed phase:

$$X^a = (U^a_{sys} - U^a_o) + P_o(V^a_{sys} - V^a_o) - T_o(S^a_{sys} - S^a_o) - \sum_{i=1}^{NS} \mu_{i,0} \left(N^a_{i,sys} - N^a_{i,0}\right). \quad (5.21)$$

By Gibbs' definition of an adsorbed phase, the volume of this phase is zero, whether at the system state or at the dead state, resulting in

$$X^a = (U^a_{sys} - U^a_o) - T_o(S^a_{sys} - S^a_o) - \sum_{i=1}^{NS} \mu_{i,0} \left(N^a_{i,sys} - N^a_{i,0}\right). \quad (5.22)$$

Finally, we can subtract the Euler relation for adsorbed phases (Eq. 5.2), applied at the dead state, from this expression to eliminate the extensive quantities at the dead state:

$$X^a = U^a_{sys} - T_o S^a_{sys} - \sum_{i=1}^{NS} \mu_{i,0} N^a_{i,sys} - \Phi_o m^s. \quad (5.23)$$

Equations 5.22 and 5.23 are general expressions for the exergy of the adsorbed phase. Both are equivalent, although Equation 5.23 may be preferred for ease of calculation. Apart from the statement that adsorption processes are non-reactive and can be characterized using a Gibbs dividing surface, we have made no restrictions on

the nature of the adsorbed phase. We have considered only environmental species so far, but this limitation will be relaxed in Section 5.3.7. Next, we discuss how to calculate the thermodynamic properties of the adsorbed phase (U, S, Φ).

Kearns and Webley's final expression for the exergy of adsorption systems [8] is compatible with this result. Applying their equations of state for the gas, sorbent, and adsorbed phases to Eq. 5.22 or 5.23 results in their final expression. This compatibility can be seen as mutual reinforcement for our work and theirs. The current work justifies Kearns and Webleys initial choice of expression for exergy, and their work is an example of Eq. 5.22 or 5.23 applied to an air separation adsorption system under certain modeling assumptions.

5.3.4 Properties for adsorbed phases: single component

Adsorption data are usually reported along isotherms, where the amount of a species adsorbed on a given mass of sorbent is measured for a range of pressures at a constant temperature. The functional forms for these adsorption isotherms, fit to experimental data, are the thermal equations of state for adsorbed phases (analogous to the P-v-T relationships of bulk phases). With some care in the choice of the functional form, the adsorption isotherm can therefore be used to derive thermodynamic properties.

When fitting an adsorption isotherm function to a set of adsorption data, a primary concern for researchers is understandably choosing a functional form that represents the observed data's behavior well. However, the need to use the isotherm as the basis for the calculation of thermodynamic properties imposes additional restrictions.

These additional restrictions all relate to being able to solve for the surface potential and its derivatives. Expressions for the surface potential, internal energy, entropy, and Gibbs free energy can be constructed from the thermodynamic relations listed in Section 5.2.2. Myers [2] shows these derivations in detail, and the key results are listed here in Table 5.1.

In order to be able to solve for the surface potential using the integral in Table 5.1, and then solve for all other properties of the adsorbed phase, two criteria must be satisfied. First, the adsorbed amount must be able to be defined at any T and P where

Table 5.1: Properties of single-component adsorbed species at T and P, adapted from Myers [2]. The tilde is used to indicate that the property is *semi-extensive*, because it is defined *per unit mass of sorbent*.

Function	Symbol	Expression
Surface potential	Φ	$-RT\int_0^f \tilde{N}^a d(\ln f)$
Gibbs free energy	$\tilde{G}^a$	$\tilde{N}^a \hat{g}^g_{T,P} + \Phi$
Enthalpy	$\tilde{H}^a$	$\tilde{N}^a \hat{h}^g_{T,P} - T^2 \frac{\partial}{\partial T}\left[\frac{\Phi}{T}\right]_P$
Internal energy	$\tilde{U}^a$	$\tilde{U}^a = \tilde{H}^a$
Entropy	$\tilde{S}^a$	$\frac{\tilde{H}^a - \tilde{G}^a}{T}$

state information is required. This sounds straightforward, but it is not unusual to find adsorption isotherm functional fits in the literature that are not temperature-dependent (i.e., that are fit to a single isotherm only). To be useful in a system model and exergy analysis, the adsorption isotherm should be a function of both T and P:

$$\tilde{N}^a = \tilde{N}^a(T, P). \tag{5.24}$$

where the tilde is used to indicate that the property is *semi-extensive*, because it is defined *per unit mass of sorbent*.

The second criterion concerns the low-pressure behavior of the adsorption isotherm for the calculation of Φ. Because of the nature of the integral for Φ listed in Table 1, even small errors in the low-pressure region can cause large errors in the value of Φ. Moreover, if the functional form of the isotherm has an infinite slope at the zero pressure limits, Φ cannot be calculated. Several commonly-used isotherm forms, such as Freundlich and Sips, have this zero-pressure slope issue, and cannot be used to calculate thermodynamic properties [19].

To be useful for calculating exergy, pure component isotherms forms must also fit the experimental data's behavior well, in particular in the low pressure region. Langmuir, Toth, and UNILAN are all forms which can be used for this purpose,

although the Langmuir form tends to fit experimental data less well in some regions than the latter two [20].

5.3.5 Properties for adsorbed phases: mixtures

There exist various approaches for finding adsorbed mixture information from pure species adsorption isotherms. For the calculation of exergy and any other thermodynamic information, it is critical that the chosen approach be thermodynamically consistent—that the Gibbs-Duhem equation for adsorbed phases (Eq. 5.3) be satisfied. Along an isotherm, this equation is known as the Gibbs adsorption isotherm:

$$d\Phi = -\sum_{i=1}^{NS} \tilde{N}_i^a d\mu_i \tag{5.25}$$

The Ideal Adsorbed Solution (IAS) concept developed by Myers and Prausnitz [92] provides a thermodynamically consistent framework for treating adsorbed mixtures. We will describe it first for ideal mixtures in both the gas and adsorbed phases, and assuming the ideal gas assumption holds for individual gas species. The procedure consists of finding, for each species i and at a defined temperature T, a single-component standard-state pressure P_i^* such that the surface potential Φ is found to be the same if calculated for each species:

$$\Phi = -RT \int_0^{P_1^*} \tilde{N}_1^a d(\ln P) = -RT \int_0^{P_2^*} \tilde{N}_2^a d(\ln P) = ... = -RT \int_0^{P_{NS}^*} \tilde{N}_{NS}^a d(\ln P) \tag{5.26}$$

The quantity P_i^* is used to find adsorbed-phase mole fractions in the adsorbed-phase analog to Raoult's Law

$$P y_i = P_i^* x_i \quad \{i = 1, 2, ..., NS\}. \tag{5.27}$$

where y_i is the mole fraction of species i in the gas phase, and x_i is its mole fraction in the adsorbed phase.

The combination of Equations 5.26 and 5.27 results in 2NS equations for 2NS +

1 unknowns (P_i^*'s, x_i's, and Φ). The final equation is given by

$$1 = \sum_{i=1}^{NS} x_i. \tag{5.28}$$

Algorithms for solving these coupled ideal-gas, ideal-mixture equations are given by O'Brien and Myers [93], [94]. Once the standard-state vapor pressures are found, the properties of the adsorbed-phase mixture can be calculated, including the total amount adsorbed $\tilde{N}^{a,total}$ and the thermodynamic functions:

$$\frac{1}{\tilde{N}^{a,total}} = \sum_{i=1}^{NS} \frac{x_i}{\tilde{N}_i^a(T, P_i^*)} \tag{5.29}$$

$$\hat{u}^a(T, P, \{y_i\}) = \sum_{i=1}^{NS} x_i \hat{u}_i^a(T, P_i^*) = \sum_{i=1}^{NS} x_i \frac{\tilde{U}_i^a(T, P_i^*)}{\tilde{N}_i^a(T, P_i^*)}, \tag{5.30}$$

$$\hat{s}^a(T, P, \{y_i\}) = \sum_{i=1}^{NS} x_i [\hat{s}_i^a(T, P_i^*) - R \ln x_i] = \sum_{i=1}^{NS} x_i \left[\frac{\tilde{S}_i^a(T, P_i^*)}{\tilde{N}_i^a(T, P_i^*)} - R \ln x_i \right]. \tag{5.31}$$

The equations discussed so far have been written for an ideal solution in the adsorbed phase and an ideal solution of ideal gases in the gas phase. In reality, not all gases behave ideally. For an extension to ideal solutions of real gases, Eqs. 5.26 and 5.27 would become, respectively,

$$\Phi = -RT \int_0^{f_1^*} \tilde{N}_1^a d(\ln f) = -RT \int_0^{f_2^*} \tilde{N}_2^a d(\ln f) = ... = -RT \int_0^{f_{NS}^*} \tilde{N}_{NS}^a d(\ln f) \tag{5.32}$$

where f_i^* now represents the single-component standard-state fugacity of species i at the temperature T, and

$$P y_i \phi_i = f_i^* x_i \quad \{i = 1, 2, ..., NS\}. \tag{5.33}$$

where ϕ_i is the fugacity coefficient of species i in the gas phase at the state defined by the system pressure P, the system temperature T, and the gas phase mole fractions $\{y_i\}$.

Furthermore, in reality not all mixtures form an ideal solution in the adsorbed phase, even if they are ideal mixtures in the gas phase. The measurement, prediction, and implementation of activity coefficients for the creation of non-ideal adsorbed solutions are discussed by [19], [24], and [25] (among others). In that case, the modified Raoult's Law equation would become

$$Py_i\phi_i = f_i^* x_i \gamma_i \quad \{i = 1, 2, ..., NS\}. \tag{5.34}$$

where γ_i is the activity coefficient of species i in the adsorbed phase.

The reason for starting from an ideal adsorbed solution, even if it does not represent all mixtures well, is that it provides the correct framework for extension to non-ideal solutions—it is thermodynamically consistent. When activity coefficients are measured for the gas mixtures in the system and at the dead state, they can be incorporated into this framework. In contrast, there exist other mixing procedures for adsorption that are not always thermodynamically consistent. A commonly used example is the extended Langmuir isotherm

$$\tilde{N}_i^a = \frac{N_{i,s} K_i P_i}{1 + \sum_{j=1}^{NS} K_i P_j}, \tag{5.35}$$

where P_i represents a partial pressure, and K_i and $N_{i,s}$ are characteristic parameters of the Langmuir form. This isotherm returns the amount of species i adsorbed when other gases j are also present. It is often used due to its ease of calculation, but unless the value of $N_{i,s}$ (the monolayer capacity) is the same for all species, it is not thermodynamically consistent [26]. If used to calculate exergy, a thermodynamically inconsistent isotherm or mixing rule will return nonsensical results that can violate the second law of thermodynamics.

5.3.6 Definition of the dead state

The dead state is the state of mutual equilibration of a system and the environment. When the environment is large, which is generally assumed to be the case in exergy calculations, the dead state is the same as the environmental state. The dead state for bulk phases is therefore generally defined by the environmental temperature T_o, pressure P_o, and chemical potentials $\mu_{i,o}$ for each species i in the environment.

The same concept—that the dead state refers to the state where the system is in equilibrium with the environment—holds true for the dead state of adsorbed phases. However, unlike bulk phases, the intensive properties T, P, and μ_i, are not the relevant parameters for setting the state of an adsorbed phase. Pressure is not an independent state property of adsorbed phases; it is a bulk-phase property. Instead, the state of an adsorbed phase is set by specifying the temperature T, the chemical potentials of each species μ_i, and the surface potential Φ. Therefore, the dead state for adsorbed phases is set not by T_o, $\mu_{i,o}$, and P_o as it is for bulk phases, but instead by T_o, $\mu_{i,o}$, and Φ_o, the surface potential at the dead state.

This means that to specify the dead state for adsorption, we must know not only the temperature of the environment and the chemical potential of each environmental species, but also how each environmental species adsorbs. This involves understanding both how pure environmental species adsorb as well as how their mixtures adsorb, as explained in Sections 4.4 and 4.5.

In practice, there are very few sorbents on which the adsorption of all environmental species has been characterized. Very common sorbents, like zeolite 13X or 5A, have been more widely studied, so these data generally exist (although, due to existing variability in sorbent nomenclature and sorbent preparation methods, data from different publications is not always cross-compatible). However, for new or specialized sorbents, a full dead state cannot be found if adsorption data do not exist for all environmental species. In this case, a *restricted* dead state (e.g. allowing the sorbent to equilibrate with the environmental compositions of known species) may be used, although this will give exergy values that differ from those where the full dead state is defined.

5.3.7 Adsorption of non-environmental species

In some adsorption processes, one or more of the gases being separated is a species that does not exist in the equilibrated environment. In many cases, such species can react to form environmental species. For example, methane in the environment will react with oxygen to form CO_2 and H_2O.

$$CH_4 \longrightarrow CO_2 + 2H_2O - \frac{3}{2}O_2 \tag{5.36}$$

Placing the oxygen on the right-hand side is an intentional choice; it places all non-environmental species on the left and all environmental species on the right. We can generalize that non-environmental species (A_j) will be converted to environmental species (A_i)

$$\nu_j A_j \longrightarrow \sum_{i=1}^{NS} \nu_{ij} A_i \tag{5.37}$$

where the ν's are signed stoichiometric coefficients. Incorporating this reaction in Eq. 10, which is the species balance for finding the total exergy of the gas-sorbent-adsorbate system, leads to

$$\delta N_i = dN_i + \sum_{j=1}^{NNES} \frac{\nu_{ij}}{\nu_j} dN_j \tag{5.38}$$

This equation marks the key difference between the exergy derivation restricted to environmental species, and the derivation allowing non-environmental species (that can react to become environmental species). Equation 5.11 for the useful work then becomes

$$\delta W = -dU^t - P_o dV^t + T_o dS^t + \sum_{i=1}^{NS} \mu_{i,o} dN_i + \sum_{j=1}^{NNES} \mu_{i,o} \frac{\nu_{ij}}{\nu_j} dN_j - T_o \delta S_{gen} \tag{5.39}$$

where $NNES$ refers to the number of non-environmental species. Recognizing that $N_{j,o}^t = 0$ by the definition of a non-environmental species, Eq. 13 for the exergy of

the total system becomes

$$X^t = (U^t_{sys} - U^t_o) + P_o(V^t_{sys} - V^t_o) - T_o(S^t_{sys} - S^t_o) - \sum_{i=1}^{NS} \mu_{i,o}(N^t_{i,sys} - N^t_{i,o}) - \sum_{j=1}^{NNES} \mu_{i,o}\frac{\nu_{ij}}{\nu_j} N^t_{j,sys}. \tag{5.40}$$

Finally, the exergy of an adsorbed phase that includes non-environmental species is given by

$$X^a = U^a_{sys} - T_o S^a_{sys} - \sum_{i=1}^{NS} \nu_{i,o} N^a_{i,sys} - \sum_{j=1}^{NNES} \mu_{i,o}\frac{\nu_{ij}}{\nu_j} N^a_{j,sys} - \Phi_o m^s. \tag{5.41}$$

for non-environmental species that can react to form environmental species. The extension to species that cannot react to form environmental species (mercury, for example) is possible but not treated here.

5.4 Exergy analysis of the adsorption column

The goal of developing the set of property relations described in this chapter was to enable the exergy analysis of an unsteady adsorption process. For example, this would be used to analyze the column from the VSA system in Chapter 4 during one of the four unsteady steps in the adsorption cycle (pressurization, adsorption, blowdown, and evacuation).

To this end, a set of re-usable property methods were written in Matlab for the thermodynamic properties of adsorbed phases, based on the adsorption isotherms for CO_2 and N_2 used in Haghpanah et al. [86], and using the Cantera open-source Matlab package for ideal gas properties [111]. These property methods are included in Appendix D.

Solving for the state of an adsorbed phase in a process model

In order to calculate the thermodynamic properties of an adsorbed phase, we must know its state fully. Thus far, we have been able to define its state relative to an ideal gas with which it is in equilibrium. However, in real adsorption processes, the adsorbed phase is rarely in equilibrium with the bulk gas phase in the column. Therefore, care must be taken when analyzing these systems to define the state properly.

In Section 5.3.5, we saw that calculating the surface potential Φ is key to knowing the state of the adsorbed phase. The set of equations to be solved for finding Φ were listed, along with references to algorithms for their solution, based on knowing the composition and temperature of the gas phase with which the adsorbed phase was to be equilibrated. These equations then returned the adsorbed phase composition. If the composition and temperature of the adsorbed phase are known instead, the state must be set by solving for Φ based on these properties instead (in essence, the reverse problem to that given in Section 5.3.5). An algorithm for solving for the state of the adsorbed phase, based on the sorbent loading, is given by O'Brien & Myers [94], and sample code for solving this problem is given in Appendix D.

5.4.1 Example application

A simple model problem was created to test the validity of the Matlab property methods written with this work. A "button-cell" approach to an adsorption column was used, where a button-cell represents a volume element in which the gas phase undergoes instantaneous mixing. Several button-cells are strung together to create a simple model for an adsorption column. The column is not represented by a set of partial differential equations to be solved by a set of numerical methods, but instead by a sequence of mixing, equilibration, and transfer steps written explicitly by the user and repeated for each new button-cell and for each new time step.

The advantage of this approach is its ease of tracking fluxes of matter and energy in the column on an element-per-element basis. It is thus well-suited to debugging, as each button-cell can be observed separately from the rest of the column, and conservation laws can be checked rigorously. The disadvantage of this approach is

that we will not necessarily be able to model more complex or stiff processes, such as an adsorption process with moving concentration fronts.

Each button-cell in this example is 10 mm in height, 5 mm in depth, and 1 mm in length, where the length is the dimension in the flow direction. One hundred button-cells are connected in series, resulting in an overall column length of 100 mm. Each cell has 50% of its volume available for gas to flow, and 50% filled with zeolite 13X sorbent. The column is held to be isobaric and isothermal, but the gas entering the column does not have to be at the same temperature as the column. The column is therefore cooled or heated as needed to preserve isothermal conditions during adsorption and desorption processes.

Each cell begins with an initial amount of substance in both the gas phase and in the adsorbed phase. They are set independently and are therefore not typically in equilibrium with each other. In this example, the cells were filled with only N_2 (no CO_2) to mimic the initial state in the adsorption system in Chapter 4. Each cell is held at 1.01325 bar and 303.15 K during the entire process. The gas phase is assumed to be an ideal gas, and its properties are found using the Cantera package for Matlab [111].

The transfer of matter from the gas phase to the adsorbed phase (and vice versa) is assumed to be governed by a diffusion process, with a diffusion constant equal to the binary diffusivity of the gas mixture (as found using the correlation given in Bird, Stewart, and Lightfoot [112]), across a gas diffusion layer of thickness 1 mm.

At the beginning of a time step, the flux between the gas and adsorbed phases is calculated based on Fick's law. Meanwhile, gas is introduced into the button cell. These are two transfers into or out of the cell. The gas phase in the cell is assumed to mix instantaneously, which means that the gas phase mole fractions in the cell are recalculated from these two transfers over the specified time step. Then, the transfer out of the current cell and into the next one is calculated by imposing that the cell must remain isobaric.

The gas introduced into the first cell of the column is fed at 0.5 m/s, is composed of 15% CO_2 and 85% N_2 by mole, and is at 313.75 K. The adsorption process is modeled to run for 100 s, with time steps of 0.1 s.

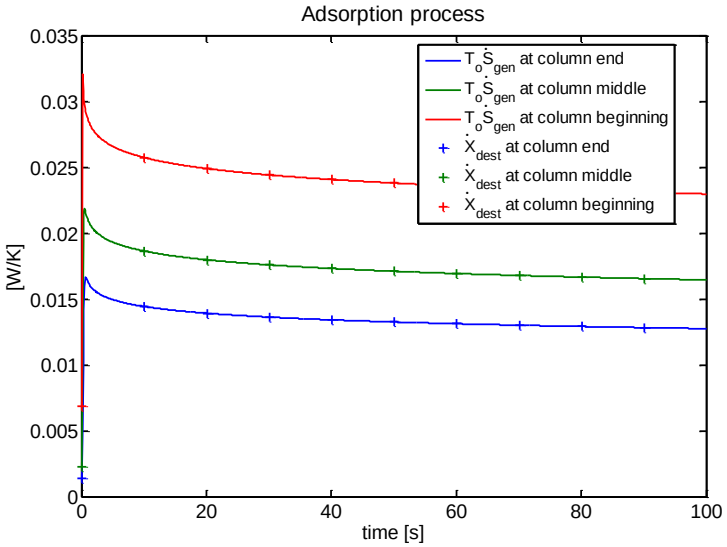

Figure 5.3: Exergy destruction, as calculated two different ways, in the first cell in the column, the cell at the midpoint, and the last cell in the column.

As seen in Figure 5.3, the exergy destruction can be calculated using the set of property methods developed from this chapter. The fact that exergy destruction has the same value when calculated in two independent ways (by calculating X_{dest} explicitly or by calculating $T_o S_{gen}$) lends credibility to these methods.

5.4.2 Applicability to complex column models

When the property methods used in Section 5.4.1 were used to perform an exergy analysis of the column modeled in Chapter 4 (a complex model with a WENO scheme in space and Matlab's ode23s in time), the results were unphysical. Specifically, when attempting to calculate the exergy destroyed during each of the four unsteady steps in the column (pressurization, adsorption, blowdown, evacuation), the resulting quantity was negative in two of the four steps (blowdown, evacuation). This is obviously incorrect, as it violates the second law of thermodynamics.

Despite many varied and repeated attempts, this unphysical behavior was not able to be reproduced in any other test case of the property methods. This includes

the test case shown above in Section 5.4.1, but also many other test cases involving adsorption and desorption, as well as equilibrium and non-equilibrium conditions between the gas and adsorbed phases. In other words, the second law was always obeyed in all other uses of these property methods.

It is possible that there remains an incompatibility between a modeling decision in the column model in Chapter 4, and in the ability to perform an exergy analysis. If so, that incompatibility has not yet been identified, and is left to a future study. However, some other important points have emerged from this search. First, because exergy destruction and entropy generation are closure terms on a balance equation, these quantities are very sensitive to any lack of closure in mass and energy balances. In models that rely on numerical solutions to partial differential equations, such as the column modeled in Chapter 4, this can sometimes be an issue. Second, for exergy analyses of adsorption systems, it is imperative to represent the adsorption in a thermodynamically consistent way (e.g., by using the Ideal Adsorbed Solution model [92]). Otherwise, the state cannot be precisely defined, and its properties cannot be calculated.

5.5 Summary

In this chapter we show the derivation, from basic principles, of the exergy of an adsorbed phase in order to enable the exergy analysis of unsteady adsorption steps in adsorption columns. The final result is given by Eq. 5.23 for cases where the adsorbed species exist in the environment, and by Eq. 5.41 for cases where they do not (but can react to form environmental species). During the derivation, no assumptions were made about the system's behavior, except for the validity of the Gibbs dividing surface concept to represent the adsorbed phase and the non-reactivity of the adsorbed species with the surface (and with each other). This expression can therefore be used in any adsorption process where these assumptions hold, to track the exergy and find the locations of its destruction.

After arriving at the expression for the adsorbed-phase exergy, the restrictions

for adsorbed-phase equations of state and mixing rules were discussed. Pure component adsorption isotherms must have a zero-pressure slope that is finite in order to be able to calculate the surface potential. Forming mixtures must be done in a thermodynamically consistent way, either using the Ideal Adsorbed Solution theory directly, or using it as a framework for thermodynamically-consistent activity coefficients. The information necessary to define the dead state was discussed. Although this is a derivation that was used here in the context of carbon capture systems, it is generally applicable to any adsorbed phase for which the Gibbs dividing surface definition applies.

Finally, the implementation into usable code form (in Matlab) of the theoretical derivations from this chapter is discussed. A simple example problem is presented to show the usability of the code, and existing limitations on expanding the analysis to more complex models is discussed.

Chapter 6

CO_2 Separation Using a Novel Oxyfuel Concept

This chapter introduces and analyzes a new type of natural gas burning power plant that can satisfy two criteria: (1) capturing 100% (or near 100%) of the CO_2 produced, while (2) keeping a high efficiency given this constraint. The proposed system uses a supercritical water oxyfuel combustor—combusting natural gas and oxygen in a supercritical water moderator—to produce the working fluid for the turbines. This builds on work done by Heberle [113] and Mobley [114], [115] concerning the theoretical and experimental analysis of oxyfuel combustion in supercritical water for electricity generation. In the current work, the product stream is expanded post-combustor through several turbine stages, condensed, and the remaining liquid water is pumped back up to the operating pressure. In this way, the system bears similarities to a Rankine cycle which is internally, rather than externally, fired. We have thus named it SuperCritical Auto-Thermal Rankine (SCATR).

Over the operation of the cycle, CO_2 is automatically separated from the water—at no additional energy penalty—by phase separation in the condenser. This allows for compression of the CO_2 produced to pipeline pressure for storage, fulfilling the first criterion of low atmospheric emissions. In this paper, a complete thermodynamic model of SCATR is used to find the overall efficiency of the system, including CO_2 compression. We show that high efficiencies are possible, thus fulfilling our second

criterion. An exergy breakdown and sensitivity analysis provide insight into the irreversibilities in the system, and the limits of the possible efficiency improvements.

6.1 Background

6.1.1 Motivation in the context of CO_2 capture

The two systems studied in the preceding chapters were both post-combustion CO_2 capture systems. Both had low exergy efficiencies, and would therefore incur large energy penalties on the power plant. While one approach to improving this reality is to identify inefficiencies in the capture system and eliminate them to the extent possible, there are only limited ways in which additional efficiency gains can be made through system integration with the rest of the plant.

An alternative approach is to re-think the entire concept for the power plant in such a way that the CO_2 separation becomes an intrinsic part of the cycle, and that much greater flexibility is given for exergy integration of different parts of the plant. Moreover, if the traditional-combustion approach to electricity generation is abandoned, the efficiency has the potential to be increased, by reducing the exergy destruction inherent in combustion processes. Both of these approaches are taken here in the development of a new concept for an electricity-generating cycle.

Relative to the amine absorption and the vacuum-swing adsorption systems considered earlier, this system is at a low level of technological maturity. This is an exploratory concept, with the goal of identifying efficiency gains that could be made by the development of this alternative strategy.

6.1.2 Survey of similar systems

In oxyfuel systems, natural gas or syngas is burned in a stream of highly enriched (>95%) oxygen, resulting in combustion products that are primarily CO_2 and water. The water is condensed, leaving a stream of high-purity CO_2 for industrial uses, enhanced oil recovery, or for storage—hence oxyfuel systems' main advantage over other carbon capture systems is their ability to separate CO_2 without introducing a

more complex post-combustion separation unit. Since the selective extraction of CO_2 from other gases has only limited efficacy past a certain level of CO_2 depletion from the flue gas, oxyfuel systems can also achieve 100% capture more easily than many other systems.

The energy penalty paid in oxyfuel systems is on the pre-combustion side, as they must necessarily include a system to enrich oxygen from air. This can be done via cryogenic air separation units (ASUs), or via ion transport membranes (ITMs). At this time, cryogenic ASUs, as mature technologies, are well understood and well optimized. By contrast, ITMs are still the focus of active research and are not yet scalable to support a power plant [116]. For the system presented in this paper, a cryogenic ASU was chosen in order to focus solely on the development of the power system, assuming a guaranteed source of enriched oxygen.

In an oxyfuel system, an inert moderating species is necessary to keep the combustion temperature below acceptable materials limits. (This role is usually filled by nitrogen when air is used as the oxidizer.) There has been a significant research effort towards using CO_2 and/or water as the combustion moderator in advanced carbon capture cycles. A representative selection of these cycles are listed in Table 6.1 and described here. For a more detailed overview of these and other cycles, please see review papers published by Kvamsdal [42] and Habib [117], as well as the second chapter of the book "Zero Emissions Power Cycles" by Yantovsky [118]. All of the systems listed in Table 6.1 include the capture of CO_2 and its subsequent compression to 100-300 bar, and air separation.

In 1995, Mathieu and Nihart introduced the MATIANT cycle, in which the moderator is CO_2 [120], [126]. This system is essentially a CO_2-Rankine system followed by a CO_2-moderated Brayton system. The CO_2 begins as a liquid, is compressed to high pressure (300 bar), heated by a recuperator, and expanded to an intermediate pressure of 40 bar. At this point, it is used as the moderator in the two-stage combustion of natural gas in oxygen. A variant, the E-MATIANT cycle, is a slightly simplified version in which the initial recuperative heating is done on pressurized gaseous CO_2, instead of liquid CO_2 (the Rankine portion having thus been eliminated) [119].

The Graz cycle is also one that has been studied in several incarnations [127], [128],

Table 6.1: Overview of systems similar to SCATR in the literature.

System name	Fuel	Moderator	T_{peak} [K] (P at T_{peak})	P_{peak} [bar] (T at P_{peak})	η [% LHV]
Matiant [119]	CH_4	CO_2	1573 (40 bar)	300 (873 K)	43-44
E-Matiant [120]	CH_4	H_2O	1573 (110 bar)	110 (1573 K)	45-47
S-Graz [121]	CH_4	H_2O	1673 (40 bar)	180 (823 K)	53.1
Gou-1 [122]	CH_4	H_2O	1573 (40 bar)	189.5 (815 K)	47.1
Gou-2 [122]	CH_4	H_2O	1573 (40 bar)	189.5 (817 K)	50.6
CES-1 [123]	CH_4	H_2O	1478 (13.8 bar)	124 (1070 K)	46.5
CES-2 [124]	Coal	H_2O	1700 (17.2 bar)	102 (1090 K)	39
SCOC-CC [121], [125]	CH_4	CO_2	1673 (40 bar)	120 (833 K)	49.8

[121]. Its most recent configuration, sometimes called the S-Graz cycle, is listed in Table 6.1. This system combusts methane in oxygen at 40 bar, with a moderator that is primarily steam. After expansion, the remaining enthalpy of the products is used to vaporize high-pressure (180 bar) water in an HRSG. This steam, once expanded through a turbine, is injected into the combustor along with some re-compressed combustion products to serve as moderator [121].

Gou et al. introduced two new variations on the water-moderated oxyfuel system in a 2006 paper: we refer to them as Gou-1 and Gou-2 [122]. Gou-1 has three pressure levels of expansion. The highest pressure (190 bar) is reached by steam only, which is expanded to 40 bar, at which point it becomes the moderator for the two-stage oxy-combustion of methane (the second stage happening at 2 bar). After final expansion of the products, the remaining enthalpy is used to heat the feedwater in an HRSG, and the water in the products is condensed and recycled.

Gou-2 is similar to Gou-1. The notable differences relate to the water flows. In Gou-2, all of the water is pumped to 190 bar, while in Gou-1 just over 60% of the water was pumped beyond 44 bar, the rest being injected directly into the intermediate-pressure combustor. Additionally, in Gou-2 some of the products are sent directly into the low-pressure combustor after the HRSG, so that only 64% of the products are sent into the condenser.

Clean Energy Systems (CES), a California-based company, developed a water-moderated oxyfuel combustion system that could use gasified coal [124] or natural

gas [123]. In both cases, water is pumped to a high pressure (124 bar for the methane system, 102 bar for the coal) and preheated by a recuperator. It is used as the moderator in a first combustion stage. After expansion of the products to an intermediate pressure (14 bar for methane, 17 for coal), more fuel and oxygen are injected for a second combustion stage. The coal system has a third combustion stage at 3 bar. In both systems, the enthalpy of the fully expanded products is used to preheat the feedwater, before sending the products to a condenser.

The Semi-Closed Oxy-Combustion Combined Cycle [125], [122] (SCOC-CC, also found in the literature as SCCC-CC for Semi-Closed Combined Cycle with Carbon Capture) is another advanced oxyfuel system worthy of mention due to its support from ENCAP, the European ENhanced CO_2 CAPture program. SCOC-CC can be thought of as a standard combined cycle with a few significant differences. The combustor in the Brayton cycle receives methane and oxygen, along with dry CO_2 recycled from the products stream. The remaining dry CO_2 is sent to storage.

All of the water-moderated cycles described operate below the critical point of water (P_{crit} = 221 bar, T_{crit} = 647 K); when high pressures are reached, the temperatures are kept low, and vice versa. With SCATR, we explore the use of supercritical water as the combustion moderating species. In addition to the intellectual motivation of studying a yet-unexplored space, we have technical reasons for pursuing this avenue of research. First, oxygen and hydrocarbon fuels are highly miscible in water in its supercritical phase [129], which makes it an appropriate medium for combustion. With this fact in mind, a laboratory-scale (50 kW), continuous-flow combustor has been built at Stanford University to characterize the combustion process in supercritical water at conditions similar to SCATR's. Initial results have shown successful combustion of methanol in this environment [113]. Mobley et al. analyzed a system that used the products of supercritical water oxidation to power a helium Brayton cycle via heat exchanger [114], [115]. With SCATR, we propose instead to study the use of the combustion products directly as a working fluid for a power system.

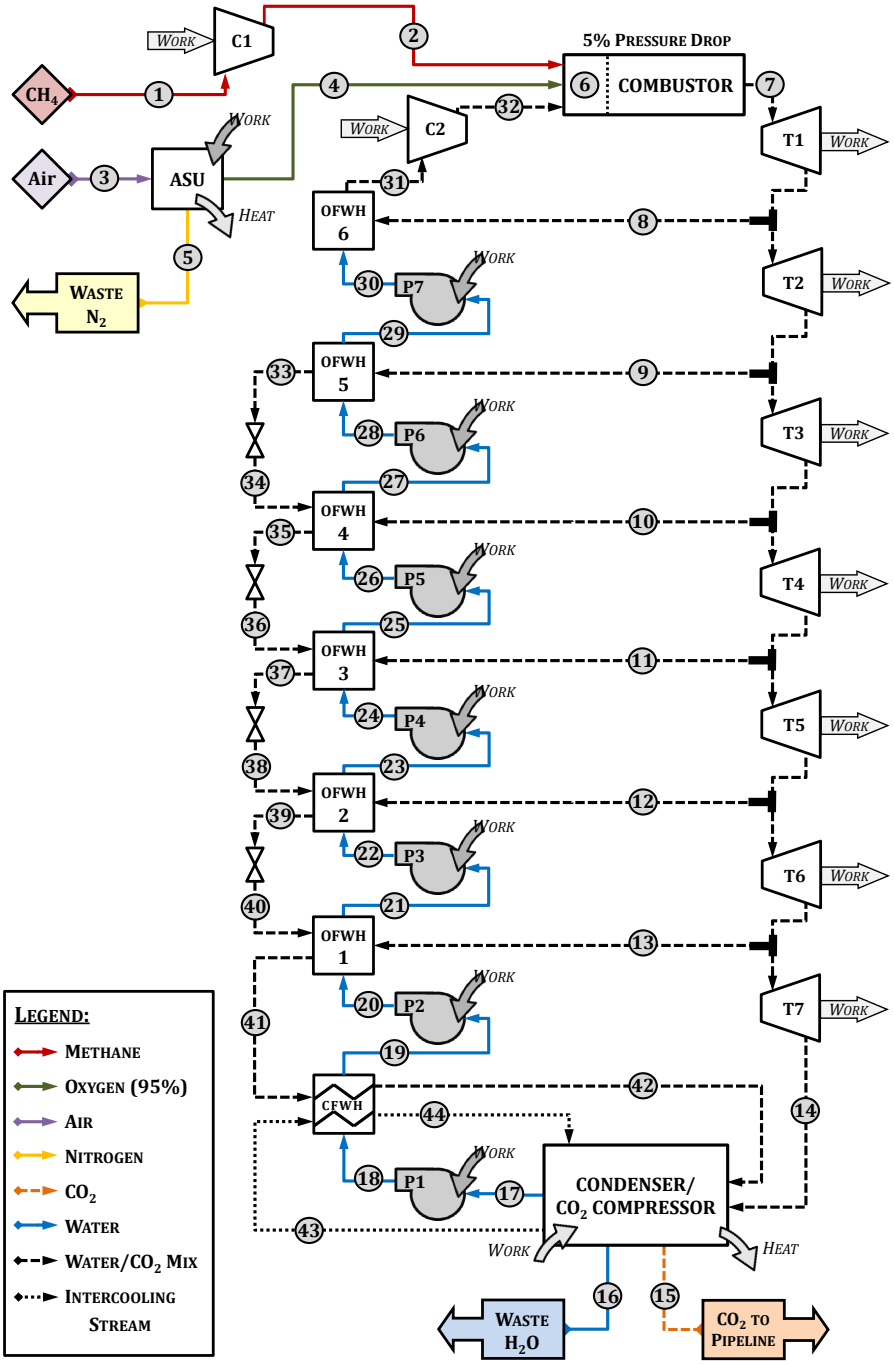

Figure 6.1: Schematic of the SCATR system. The inputs are a stoichiometric ratio of CH_4 and air at atmospheric conditions. The outputs are water at atmospheric conditions and CO_2 at 150 bar. Note that the condenser/CO_2-compressor subsystem is shown in detail in Figure 6.2.

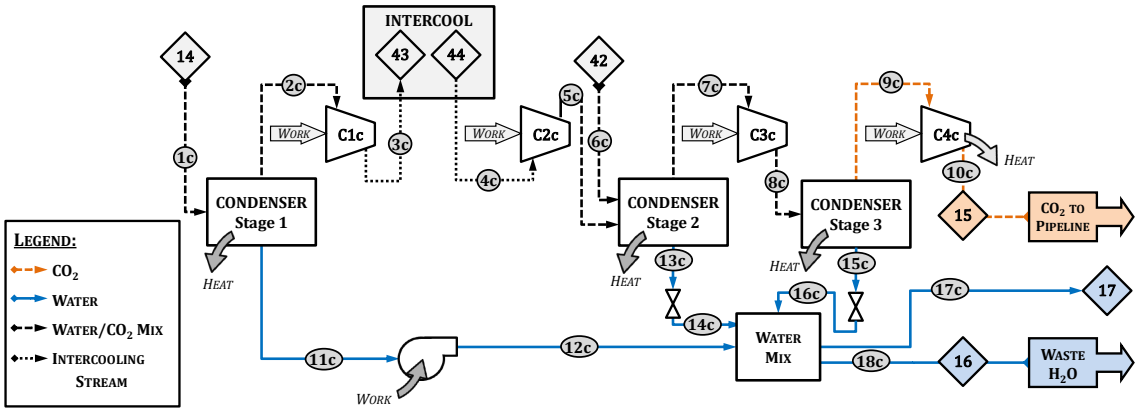

Figure 6.2: Schematic of the condenser/CO_2-compressor subsystem of the SCATR system. The outputs are water at atmospheric conditions and CO_2 at 150 bar. The numbered diamonds (14, 15, 16, 17, 42, 43, and 44) correspond to the stream numbers in Figure 6.1.

6.2 Design and modeling decisions

The design of the SCATR plant is shown in Figure 6.1 and Figure 6.2. It is a simple-cycle system that generates work through a multi-stage turbine expansion, with a peak pressure of 500 bar. The fuel used is methane. The oxidizer used is a stoichiometric amount of oxygen at 95% purity from a liquid oxygen ASU. The moderator for combustion is supercritical water. The CO_2 is separated from this stream in a deaerating condenser. The condenser produces a stream of water to recycle through the plant and a separate stream of CO_2 at a pressure that meets pipeline specifications [130]. Because water is a combustion product, some water is also rejected as waste from the plant. By extracting some of the hot fluid from the turbines and injecting into a series of feedwater heaters, the water recycled through the plant is brought to supercritical temperatures before it reaches the combustor. Each subsection of the plant is presented in more detail below. All states as labeled in Figure 6.1 and Figure 6.2 will be referenced with the designation S-# (for State-#).

6.2.1 Modeling thermodynamic properties

The primary fluid of interest in SCATR is a mixture of carbon dioxide and water (with some impurities, primarily argon and nitrogen), as produced by the combustion of methane in oxygen. The pressures reached in SCATR range from 4.5 kPa to 500 bar, and the temperatures range from 298.15 K to 1800 K. These states cover three phases: liquid, vapor, and supercritical. Because of the large differences in polarity and critical points for carbon dioxide and water (CO_2: T_{crit} = 304.1 K, P_{crit} = 73.8 bar; H_2O: T_{crit} = 647 K, P_{crit} = 221 bar), the mixture is far from ideal, and the representation of its properties needs to be given careful consideration.

The state-of-the-art representation of the CO_2-H_2O mixture was developed by Paulus and Penoncello in 2006 [131]. They built a multi-component fundamental relation explicit in Helmholtz free energy (a), with inputs of temperature (T), density(ρ), and overall composition (z). In the superheated vapor and supercritical fluid regions, this model is based on a linear combination of the fundamental relations for CO_2 and H_2O, with an added excess function to account for non-ideal mixing. The pure fluid fundamental relation for water was developed by Pruss and Wagner [132], and the one for CO_2 was developed by Span and Wagner [133]. Paulus and Penoncello then compiled experimental data that spanned temperatures of 323-1074 K, pressures up to 100 MPa, and the entire composition range. These data were used to develop the excess function, thus completing the mixture model.

Due to limited availability of vapor-liquid equilibrium (VLE) data, and lack of availability of subcooled liquid data, Paulus and Penoncello did not extend the Helmholtz-based model past the dew line. Instead, the pressure, specific volume, temperature, and composition (or $PvTx$) at the dew and bubble lines was found in Paulus and Penoncello's model using a Peng-Robinson cubic equation of state [134], using a binary interaction parameter of k_{ij} = 0.065 as derived from experimental data. The Paulus-Penoncello fundamental relation does not return any information for states in the two-phase or liquid region.

Paulus and Penoncello's fundamental relation is applicable to the saturated and superheated vapor phases, for pressures up to 100 MPa, and over the entire composition range. Moreover, the model is valid for finding the $PvTx$ values of the bubble

and dew lines over this space. This makes it by far the most complete model currently available for the mixture of CO_2 and water. It also has a high degree of accuracy over this range. The uncertainty in the calculated properties for the vapor phase is stated to be $\pm 0.1\%$ for the density, $\pm 2\%$ for the second virial coefficient, and $\pm 3\%$ for the excess enthalpy [131].

However, the Paulus-Penoncello fundamental relation cannot be used for all parts of the SCATR system. For the purposes of being able to integrate several different property models, as well as for its computational speed, Aspen Plus (7.1) was used to model the SCATR system. When selecting a property model in Aspen Plus, the accuracy and large range of Paulus and Penoncello's model make it a useful resource to use as a gauge of other property models' applicability to a CO_2-H_2O mixture.

Aspen does not include Paulus and Penoncello's mixture model for CO_2 and water in its choice of property models. We can, however, use the information from Paulus and Penoncello to choose an alternate property method. Paulus and Penoncello chose a Peng-Robinson equation of state to represent the VLE data in their model, and derived a binary interaction coefficient from a regression of collected experimental data. Based on this and on the justification in Figure 6.3, we also use a Peng-Robinson equation of state as implemented in Aspen Plus, while using Paulus and Penoncello's binary interaction parameter of $k_{ij} = 0.065$. This was implemented using the PR-BM property method in Aspen Plus, where *PR* stands for Peng-Robinson and *BM* refers to the Boston-Mathias extrapolation for high temperature gases.

Figure 6.3 shows the comparison of the saturated- and superheated-vapor side of the space, solved using the Paulus and Penoncello fundamental relation (implemented in Matlab) and the Peng-Robinson equation of state (in Aspen Plus). This is shown for a composition of 0.1 mole fraction of CO_2 and 0.9 mole fraction of H_2O, as this is an important composition for SCATR. As can be seen in this figure, the use of the Peng-Robinson equation of state is justified in the majority of the space shown. The key question is to ask whether it is justified at the states reached in SCATR, especially given that the region around the critical point is usually not well matched by Peng-Robinson. In Figure 6.4, we show the states for the matter transfers—the inlet and outlet states—of each process unit in SCATR. Although the near-critical region is

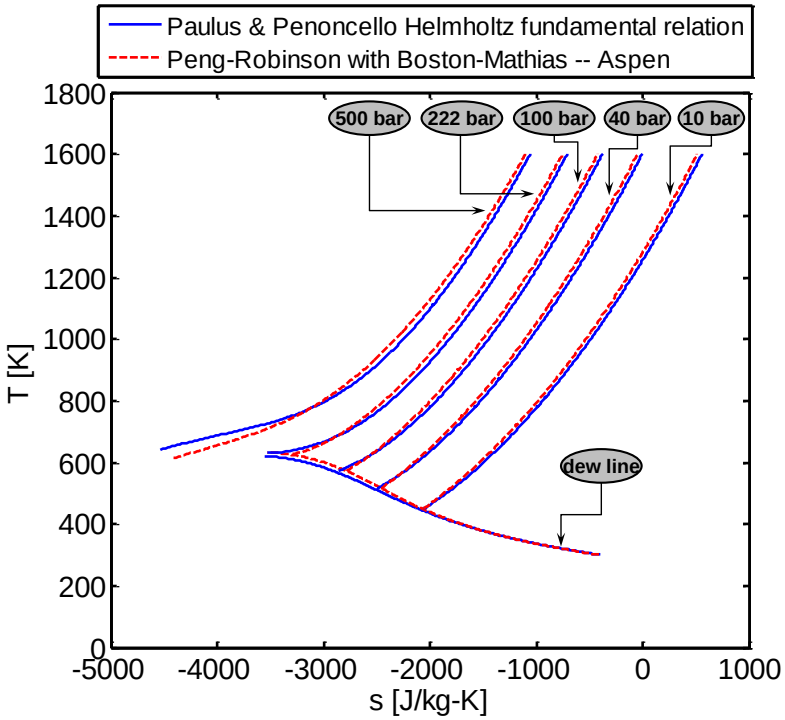

Figure 6.3: Comparison of the saturated- and superheated-vapor space using Paulus Penoncello's fundamental relation, and using the PR-BM method in Aspen Plus. This is shown for a mixture with 0.1 mole fraction CO_2 and 0.9 mole fraction H_2O. Note that the entropy values do not directly follow the $s = 0$ J/kg-K at $T = 0$ K requirement of the 3rd Law of thermodynamics. This is because Aspen Plus sets the *relative* entropy to be zero at a given reference state, and instead fulfills the 3rd Law requirement by adding the *absolute* entropy of these reference states when necessary (in particular, for chemical reactions).

certainly approached (and would be traversed inside of a device), the *transfers* are far enough from the critical point to justify the use of Peng-Robinson for this model.

We must also consider the liquid side of the space. Using a two-parameter cubic equation of state like Peng-Robinson to represent the entire property space of a fluid, including liquid, vapor, and the critical point, is not generally the most accurate approach. This is due to mathematical constraints on the cubic form: The actual behavior of an isotherm in P-v space (which is what a cubic equation of state aims to represent) would follow higher-order odd functions more closely than a simple cubic. Therefore, by using a two-parameter cubic equation of state, a gain in accuracy in one or two areas (where the *areas* under consideration are the liquid region, vapor region, and critical point) necessarily results in the loss of accuracy in others.

Cubics, however, are much easier to handle mathematically than higher-order equations, and thus have historically been in common use. Certain cubic equations of states are better at representing different areas: Peng-Robinson, for example, is particularly good at VLE, and specifically at achieving better estimates of the specific volume of the liquid phase given its specified gaseous complementary phase [135]. When using a "cubic equation-of-state based property model" however, Aspen Plus does not actually make sole use of a cubic, because of these known limitations. Instead, when the user chooses a property model named for a cubic equation of state, Aspen Plus applies the cubic directly only to the vapor and supercritical phases [63]. For the liquid side, it finds the specific volume using the Rackett equation of state—an empirically derived equation that finds the specific volume for a liquid as a function of reduced temperature T_r and critical compressibility factor Z_{crit} [136]. Finally, for pure or near-pure water, a set of steam tables (the NBS tables in this case) are used.

6.2.2 Air separation unit

The ASU for this plant produces liquid oxygen using a two-column distillation system. The choice of producing liquid oxygen instead of gaseous oxygen in this plant is explained by the high operating pressure of the combustor. Although the initial production of liquid oxygen is more energy-intensive than the production of gaseous

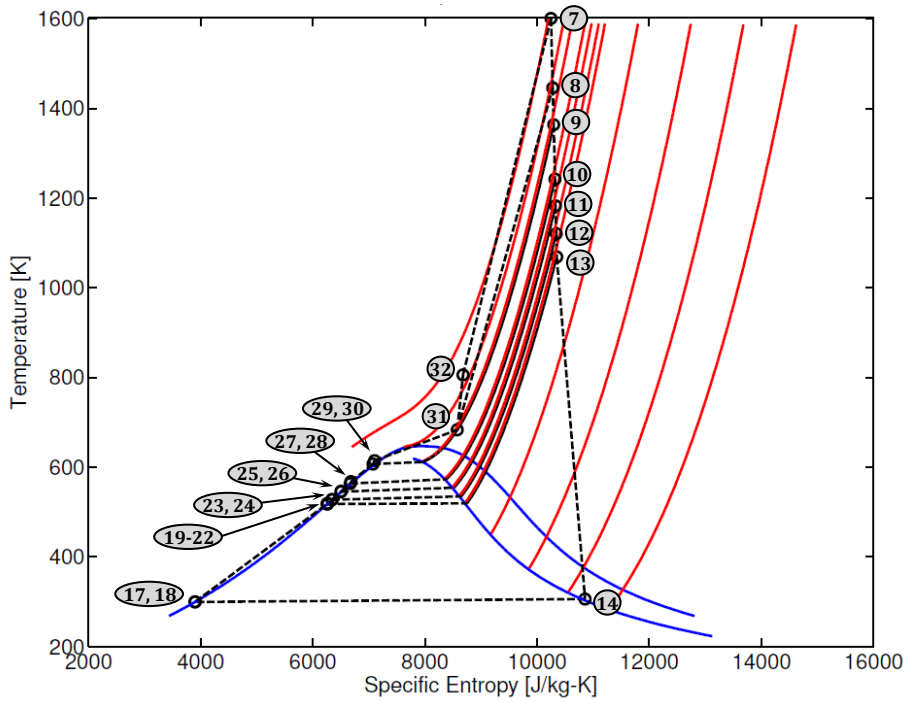

Figure 6.4: T-s diagram for the SCATR system operated at TIT = 1600 K, CIT = 750 K. The process path is shown by black dashed lines, with numeric labels corresponding to the state numbers in Figure 6.1. Two vapor domes are shown in blue. The complete (vapor and liquid) dome is shown for pure water, and the vapor side of the dome only is shown for a composition of 91%mol H_2O, 9%mol CO_2 (representing the working fluid). Isobars for the 91%mol H_2O mixture are shown in red for (starting at bottom): 1 kPa, 10 kPa, 1 bar, 10 bar, 40 bar, 55 bar, 75 bar, 100 bar, 175 bar, 250 bar, and 500 bar.

oxygen, the energy penalty required to subsequently compress gaseous oxygen to 500 bar is larger than the penalty to pump liquid oxygen to the same pressure. Consequently, at 1.385 MJ/kg-O_2, our liquid oxygen ASU's work requirement is in the range of values published by the IPCC for state-of-the-art, gaseous-oxygen producing air separators [116], if the gaseous products of the IPCCs ASUs were subsequently compressed to 500 bar. The specifics of the operation of the ASU are described in greater detail by Mobley et al. [114]. The composition of the enriched oxygen product from this ASU is, by mole, 95.0% O_2, 1.2% N_2, 3.8% Ar.

6.2.3 Combustor

Following the schematic in Figure 6.1, there are three inlets to the combustor: methane compressed to the combustor pressure of 500 bar (S-2), a stoichiometric amount of liquid oxygen at the same pressure from the ASU (S-4), and supercritical water (S-32). The water flow rate entering the combustor is adjusted to ensure that the combustion products exit the burner at a chosen turbine inlet temperature, which was varied over the range of 1450–1800 K. In Figure 6.1, S-6 refers to the unreacted mixed state (mixing the combustor inlet streams and allowing thermomechanical equilibration, but not chemical), while S-7 refers to the reacted products state.

The combustor is modeled here as a single, adiabatic component with a pressure drop of 5%, or 25 bar. The details of the combustor's internal design are not necessary for our purposes, since thermodynamically the products of combustion only depend on the inlet stream to the combustor and the operating conditions. The combustion products (S-7) are found using Gibbs free energy minimization allowing for minor combustion species. The composition of the products stream is shown in Table 6.2 for a specific set of operating conditions (turbine inlet temperature, or TIT, of 1600 K, and combustor inlet temperature, or CIT, of 750 K) to illustrate that this stream is composed largely of water, underscoring our reference to SCATR as a type of Rankine system.

Table 6.2: Composition of the working fluid exiting the combustor, for all species with mole fractions greater than 10^{-9}.

Species	Mole Fraction (%)
H_2O	90.63
CO_2	8.431
Ar	0.669
N_2	0.202
CO	1.605-2
H_2	5.582-2
O_2	1.984-5
NO	1.036-5

6.2.4 Multi-stage expansion

After the combustor, the products (S-7) are expanded through seven turbine stages. After each turbine stage, part of the flow is extracted to preheat the recycled feedwater. Extractions are taken at pressures of 250 bar (S-8), 175 bar (S-9), 100 bar (S-10), 75 bar (S-11), 55 bar (S-12), and 40 bar (S-13). These pressures were chosen to facilitate the feedwater heating, as discussed below. The pressure of the final stage, as in a standard Rankine system, is set by the pressure of the condenser, which is 4.5 kPa assuming cooling water is available to bring the condenser temperature to 298.15 K (25°C). All turbines were treated as adiabatic with polytropic efficiencies of 90%.

6.2.5 Condenser and CO_2 separator

The condenser and CO_2 separator in SCATR are interconnected processes, and cannot be described independently. This is due to the nature of oxyfuel systems: Their advantage over other carbon capture systems is that, by having combustion products that are primarily water and CO_2, the highly non-condensable CO_2 can be separated from the products stream directly by condensing the water. In SCATR specifically, this advantage goes a step further. Because SCATR is a Rankine-type system, through which liquid water must cycle, the condensation is an intrinsic (and integral) part of

the power-generation system. This is different from typical coal- or gas-based oxyfuel systems, where the condenser must be added as a separate CO_2-separation module without serving a purpose in the power generation.

The schematic for the condenser/separator process is shown in Figure 6.2. This unit will also be referred to by the acronym CPU, for CO_2 Purification Unit. In Figure 6.2, the fully expanded products stream (S-1c) exits the last turbine stage and enters the first condenser stage. At each of the condenser stages, which are cooled to 25°C, the liquid water is separated and brought to atmospheric pressure (either by pumping—in the first condenser stage, or by throttling—in the later, higher pressure condenser stages). Some fraction of this water is recycled through the plant (S-17c), while a smaller fraction is released as waste from the plant (S-18c). The fraction of the total condensed water recycled through the plant depends on the combustor operating point, but varies between 80-85%.

After each condenser stage, the remaining CO_2-rich vapor is gradually compressed and further purified. Compression to 40 bar is achieved via intercooled, two-stage compression (compressors C1c and C2c on Figure 6.2). The intercooling is achieved by using the cold, recycled feedwater (S-18 on Figure 6.1) to cool the intermediate pressure stream (S-3c on Figure 6.2, or equivalently S-43 on Figure 6.1). This allows the vapor to return to the condenser (S-4c on Figure 6.2, or S-44 on Figure 6.1) at a colder temperature for compression, while also helping to preheat the feedwater. After compression to 40 bar, the vapor (S-5c) is mixed with stream S-6c (equivalently S-42 on Figure 6.1), which is also a CO_2-enriched stream at 40 bar. The mixed stream is taken through a second condenser stage, and then compressed to 55 bar for a third and final condensation stage. The resulting CO_2-rich gas (S-9c) has now reached CO_2 pipeline specifications for water content (500 ppm). It is finally compressed to a pipeline pressure of 150 bar by a two-stage intercooled compressor (C4c), so that a pipeline-ready stream of CO_2 (S-10c) is released from the plant. All pumps and compressor stages were treated as adiabatic (with the exception of intercooling between stages), with a polytropic efficiency of 90%.

It should be noted that, while all other minor species (CO, O_2, NO_x, etc.) in the CO_2 stream meet pipeline specifications, the mole fraction of argon that remains

(originally from the ASU) is higher at 7.2% than the specified limit of 4% for non-condensable gases. One possible solution is to add a side column to the cryogenic ASU, which, while more cost-intensive, would have minimal effect on the plant efficiency. Argon, a valuable product, could be sold to offset some of these costs. Alternately, this could be remedied by adding a cryogenic CO_2 condenser system after the water condenser. Several such systems have been modeled and analyzed by Posch and Haider [137], with results showing that their proposed CPU has a work requirement that is directly comparable to SCATR's existing condenser/compressor unit (0.61 MJ/kg-CO_2 for SCATR, and a range of 0.52-0.70 MJ/kg-CO_2 for Posch and Haider's systems). Therefore, adding this functionality would have no effect on SCATR's efficiency. Similarly, the waste water that flows out of SCATR's condenser still has some trace CO_2 dissolved in it (310 ppm). This value would be relevant while siting the plant, as the effluent should not be routed into an area where this concentration of CO_2 would cause problems to the local ecosystem.

6.2.6 Feedwater heating

The recycled feedwater leaving the condenser (S-17) goes through a series of preheating and pumping stages that mirror the turbine expansion stages. The goal of these devices is to bring the feedwater to supercritical conditions, in both temperature and pressure, before it is injected into the combustor. The preheating is achieved by one closed feedwater heater (CFWH), followed by six open feedwater heaters (OFWH), with a pumping stage between each preheating stage. All pumps and compressors were treated as adiabatic, with polytropic efficiencies of 90%.

In the OFWHs, hot combustion products extracted from the end of each turbine stage are mixed with the feedwater. For the final (hottest) stage of feedwater heating, OFWH 6, the resulting mixture is in a single, supercritical phase. However, the lower pressure stages of feedwater heating (OFWH 1-5) result in a two-phase mixture, with CO_2 and other non-condensable combustion products primarily in the vapor stream. To ensure that only liquid is sent through the pumps, these phases are separated. The vapor stream is throttled and, because it still has significant enthalpy, it is cascaded

to mix in the feedwater stage at the next lowest pressure.

The mass flow extracted from each turbine stage and injected into each OFWH was determined based on a target state for the vapor vented from the OFWH. For OFWH 5, that target was a mole fraction of 10% CO_2 in the vented vapor (which corresponds to a vapor fraction of 0.5-3% for that feedwater heater, depending on the specific case of SCATR being modeled). For OFWHs 1-4, that target was a mole fraction of 15% CO_2 in the vented vapor (which corresponds to a vapor fraction of 1-5% for these OFWHs). The turbine extractions therefore serve to heat the feedwater to saturation, and then to separate the non-condensable gases.

Before the OFWHs, a significant amount of feedwater heating is done by a closed feedwater heater (CFWH). There are two hot streams: the final stage of cascaded vapor vented from OFWH 1 (S-41), and the CO_2-rich stream sent from the condenser for intercooling (S-43, see Section 6.2.5). These were both used to pre-heat the cold stream (the feedwater). The heat exchange between these three streams was modeled using the MHEATX block in Aspen Plus. This block allows a good integration of multiple hot and cold streams, by performing an internal pinch analysis in a counter-flow heat exchanger to best match the combination of available hot and cold streams. The optimized operation of this heat exchanger, with an imposed 10 K minimum approach temperature, can be seen in a T-h diagram in Figure 6.5. The hot side plotted on this figure is a composite of both hot streams. A 5% pressure drop was included for each of the three streams in the CFWH.

The purpose of this series of feedwater heaters and pumps is, as stated earlier, to bring the feedwater to a supercritical state before injection into the combustor. Therefore, as long as the critical point is surpassed, the feedwater heaters could theoretically be used to preheat the water even further. Raising the final preheating temperature (the temperature of S-32) will have the effect of raising the combustor inlet temperature (the temperature of S-6), thus changing the operation of the combustor. The combustor inlet temperature was allowed to vary over the range 700-950 K by changing the final preheating temperature.

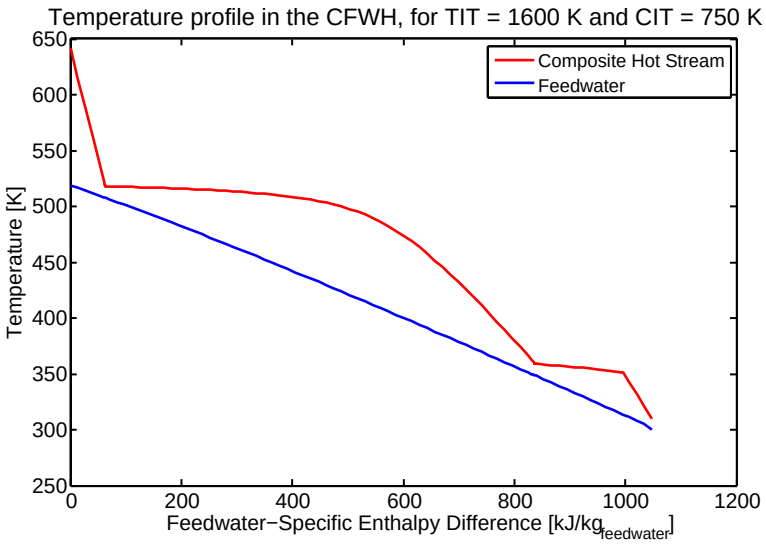

Figure 6.5: Temperature profile in the closed feedwater heater for the SCATR system operated at TIT = 1600 K and CIT = 750 K. The "composite" label for the hot side refers to the fact that two hot streams are used to pre-heat the feedwater. These two streams are combined via an internal pinch analysis in the Aspen Plus block MHEATX. A 10 K minimum approach temperature was set.

6.3 Results and discussion

Depending on its operating point, the SCATR system was found to have efficiencies ranging from 43.8% to 46.9% relative to the exergy of methane. This corresponds to a range of 45.4% to 48.6% on an LHV basis, or 40.9% to 43.8% on an HHV basis. All values include losses due to air separation, as well as CO_2 capture and compression. An exergy analysis was used to identify the remaining potential for system improvement. The general performance of SCATR at a fixed operating point will be discussed first, followed by an investigation of the effect of varying process conditions on the system efficiency.

6.3.1 Specific case: CIT = 750 K, TIT = 1600 K

All results in this section are relevant to the SCATR system operated with a combustor inlet temperature of 750 K and a turbine inlet temperature of 1600 K. Both of these values are in the ranges of temperatures considered for the sensitivity analysis in the next sub-section. At this operating point, SCATR has an exergy efficiency of 45.2%. A power flow of SCATR is shown in Table 6.4 for a 500 MW power plant. The thermodynamic states reached are shown on a T-s diagram in Figure 6.4, as well as in tabular form in Table 6.3. The breakdown of the fuel exergy use is shown, in bar graph form, in Figure 6.6.

As seen in Table 6.4, there are four main tasks for which power is supplied to the system: air separation, fuel compression, feedwater pressurization, and CO_2 compression. The feedwater pressurization process is separated into two parts: the liquid pumping that is done between feedwater heating stages, and the final compression stage to the combustor pressure of 500 bar. Whereas liquid water is largely incompressible, the water during the final pressurizing stage has already been pumped to a supercritical pressure of 250 bar, and has subsequently been preheated to a supercritical temperature of 683 K. Supercritical water, while showing less variability in specific volume than water vapor, is much more compressible than liquids. This variability results in the notable difference between the power required for pumping the feedwater to 250 bar and that required for the final compression to 500 bar.

Table 6.3: Thermodynamic state information for SCATR. The state numbers correspond to those in Figure 6.1.

State	**1**	**2**	**3**	**4**	**5**	**6**	**7**	**8**	**9**
$\dot{m}$ [kg/s]	21.33	21.33	374.8	90.08	284.7	480.67	480.6	126.4	27.27
P [bar]	1.013	500	1.013	500	1.013	500	475	250	175
T [K]	298.2	941.8	298.2	296.0	296.6	750.1	1600.0	1445.8	1364.0
mol% CO_2	0	0	0	0	0	2.925	8.557	8.557	8.557
State	**10**	**11**	**12**	**13**	**14**	**15**	**16**	**17**	**18**
$\dot{m}$ [kg/s]	9.48	9.21	4.32	37.95	266.0	63.48	47.93	224.6	224.6
P [bar]	100	75	55	42	0.045	150	1	1	42
T [K]	1242.3	1182.7	1120.8	1068.9	306.0	297.8	298.5	299.4	299.7
mol% CO_2	8.557	8.557	8.557	8.557	8.557	89.70	0.031	0	0
State	**19**	**20**	**21**	**22**	**23**	**24**	**25**	**26**	**27**
$\dot{m}$ [kg/s]	224.6	224.6	200.9	200.9	204.6	204.6	210.7	210.7	218.5
P [bar]	40	42	40	55	55	75	75	100	100
T [K]	519.0	517.9	518.0	518.5	527.3	528.1	545.1	546.3	563.5
mol% CO_2	0	0	0.047	0.047	0.182	0.182	0.308	0.308	0.490
State	**28**	**29**	**30**	**31**	**32**	**33**	**34**	**35**	**36**
$\dot{m}$ [kg/s]	218.5	242.8	242.8	369.2	369.2	3.00	3.00	4.64	4.64
P [bar]	175	175	250	250	500	175	100	100	75
T [K]	567.7	607.0	614.6	683.4	806.0	607.0	568.8	563.5	545.7
mol% CO_2	0.490	1.198	1.198	3.545	3.545	10.39	10.39	15.20	15.20
State	**37**	**38**	**39**	**40**	**41**	**42**	**43**	**44**	
$\dot{m}$ [kg/s]	7.80	7.80	8.43	8.43	70.01	70.01	83.72	83.72	
P [bar]	75	55	55	40	40	38	1	0.95	
T [K]	545.1	526.9	527.3	511.9	518.0	310.0	641.2	351.0	
mol% CO_2	15.86	15.86	15.33	15.33	5.951	5.951	38.19	38.19	

Table 6.4: Power flow of SCATR for TIT = 1600 K, CIT = 750 K, under steady state conditions for a 500 MW plant. Power outputs are listed as positive; power inputs are listed as negative.

Component(s)	Power (MW)
ASU	-124.77
CH_4 Compressor	-46.34
Turbines	818.47
Feedwater Pumps	-11.00
Final Feedwater Compressor	-61.45
CO_2 Compressors	-74.90
Net	500.0

The power requirement for air separation is consistent with state-of-the-art values available for cryogenic ASUs [116], and will only change if improvements can be made in the air separation process. This is beyond the scope of this research. The CO_2 compression was done in a five-stage, intercooled process. The power requirement could possibly be improved by adding more stages of intercooling, for the dual advantages of having a compression process that is nearer isothermal and of condensing more water from the gas mixture before compression. However, a large number of stages are not likely to be realistic in practice, nor will it give significant marginal efficiency benefits. Finally, while the fuel compressor was not intercooled, this was done consciously to take advantages of the higher temperatures reached during compression, to maintain the temperature of the mixed reactants stream above the critical temperature of water. The power supplied for the compressor's operation reflects this.

Shifting away from strictly focusing on power and instead focusing on the exergy transfers and destruction, we look at Figure 6.6. The first, tallest bar shows the net work generated by SCATR as a percentage of the exergy of the methane supplied to it, and therefore corresponds to the exergy efficiency of the plant. The other bars show exergy destruction in various plant components. It follows that decreasing the irreversibility in these components would result in a larger work output, and

thus a higher system efficiency—therefore, a discussion of sources of irreversibility is necessary.

The second bar indicates that 24% of the fuel exergy was destroyed in the combustion process. This is the single largest exergy sink in the system, which is why a sensitivity analysis was conducted to determine how the operating point of the combustion would affect the irreversibility. This analysis is discussed in detail in the next section.

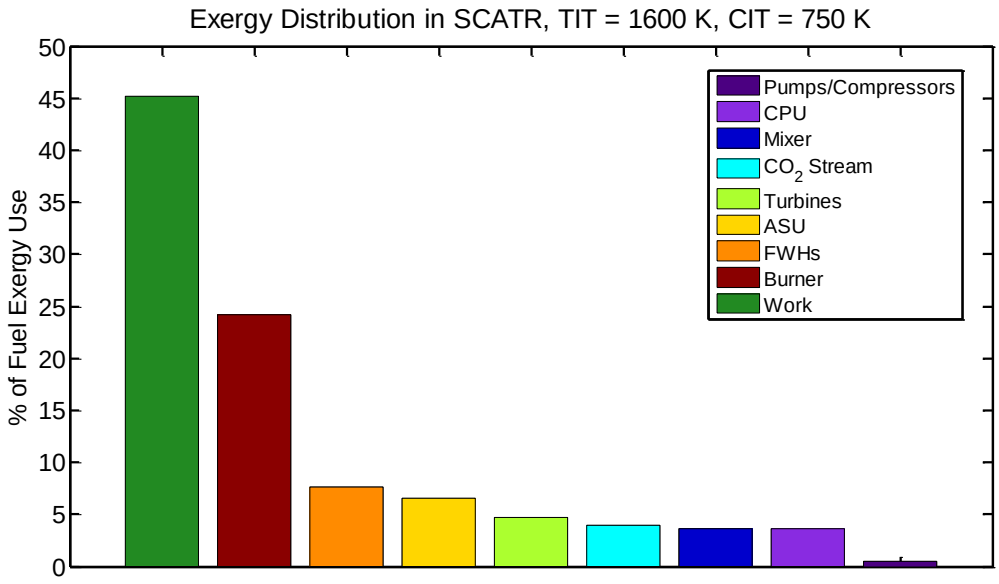

Figure 6.6: Exergy distribution in SCATR, for the case where TIT = 1600 K and CIT = 750 K. The first bar (in green) shows the work extracted from the system, and the sixth bar (in cyan) shows the exergy in the pressurized CO_2 stream. All other bars show exergy destruction due to system irreversibilities. The colors correspond to the ones used in Figure 6.8 and Figure 6.9.

The third bar, or second-largest exergy sink, is the feedwater heating at 7.6% of fuel exergy. Given that changing the combustion operating point (namely, the combustor inlet temperature) will require increased or decreased amounts of feedwater heating, we can expect that this amount of exergy destruction will change accordingly. The next section studies these changes relative to the change in combustion

irreversibility.

The remaining exergy destruction bars reflect system components without much potential improvement remaining, at this level of modeling. The ASU, as stated earlier, is operating at a level comparable with the IPCC's state-of-the-art units. The exergy destroyed through the turbines, pumps, and compressors is a function of the polytropic efficiency alone, which was already assumed to be high in this work (and would therefore be unlikely to improve). Finally, the CO_2 separation and compression is already done in a multi-stage, intercooled way—suggesting limited minimal benefit of adding further stages.

6.3.2 Sensitivity to the combustion operating point

Previously published work by Teh has shown that the fraction of fuel exergy destroyed in combustion can be reduced either by increasing the combustor inlet temperature (CIT), or by increasing the combustor outlet temperature (i.e., turbine inlet temperature, TIT) [138]. This is a particularly interesting finding for combustion-based systems because the exergy loss from combustion is otherwise often treated as unassailable, and is therefore ignored for the purposes of system improvement.

That said, a reduction in combustion irreversibility doesn't necessarily translate into an overall improved system efficiency—the operation of the particular system's other components also play a role, which means that the system must be studied as a whole. For SCATR, the CIT was allowed to vary between 700 K and 950 K, and the TIT between 1450 K and 1800 K. These two operating points can be varied independently by adjusting the mass flow rate of water recycled through the plant (for a fixed mass flow rate of fuel and oxygen). The lower CIT limit of 700 K ensures that the combustor inlet stream remains well above the critical temperature of water (T_{crit} = 647 K), thus avoiding phase transitions even locally. For the CIT variation, the TIT was fixed at 1600 K, and for the TIT variation, the CIT was fixed at 750 K (these fixed values correspond to the ones used in the specific case discussed in the previous sub-section). In each case considered, a full exergy breakdown of the plant was recorded in order to understand the exergy destruction tradeoffs between system

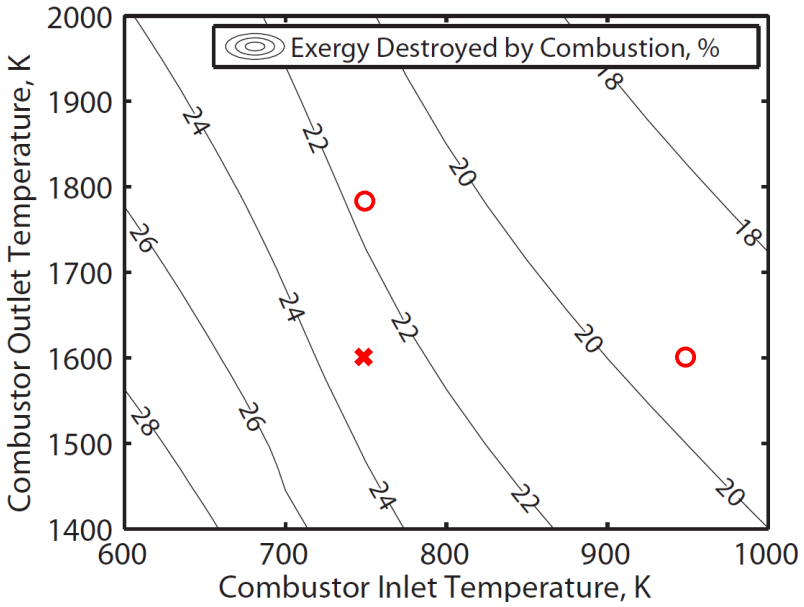

Figure 6.7: Combustion exergy destruction (% of fuel exergy) as a function of reactant and product temperature at 500 bar. The "x" marks the current operating point, and the two circles mark the two possibilities discussed for further improvements. The independence between combustor inlet and outlet is achieved by varying the mass flow rate of water, the moderating species.

components.

Combustion inlet temperature (CIT) variation

The results of the CIT variation are shown in Figure 6.8. Figure 6.8a shows the exergy breakdown including all system components, and Figure 6.8b focuses only on the components undergoing noteworthy changes as a result of the change in CIT. We first notice that there is indeed a marked reduction in combustion irreversibility as a result of increasing the CIT, from 25.2% of fuel exergy at 700 K to 21.1% at 950 K. However, the system exergetic efficiency shows no corresponding increase—in fact, it decreases slightly from 45.4% at 700 K to 44.3% at 950 K.

The main culprit here is the exergy destroyed in the series of feedwater heaters, and particularly in the final (hottest) stage of feedwater heating, as is seen in Fig. 6b. To achieve a higher CIT in SCATR, more hot products must be extracted after the first turbine expansion stage to preheat the feedwater. The lower pressure, colder extractions are not affected because the outlets of those feedwater heaters are already at a saturated liquid state (such that the temperature could not be raised further in these stages). The additional extraction needed to raise the CIT is such that it results in an increase of irreversibility in the final feedwater heater that counters, and exceeds, the irreversibility decrease in combustion. This suggests that SCATR should be operated at a CIT that is high enough to ensure a supercritical phase throughout the stream, but no higher (700–750 K).

Turbine inlet temperature (TIT) variation

The results of the TIT variation are shown in Figure 6.9. Once again, Figure 6.9a shows the exergy breakdown of SCATR including all system components, and Figure 6.9b shows the exergy destroyed in the components undergoing the largest change as a result of the temperature variation. The TIT in SCATR was increased by holding constant the mass flow rates of fuel and oxygen, as well as the states achieved during the feedwater heating process, while varying the mass flow rate of water recycled through the plant.

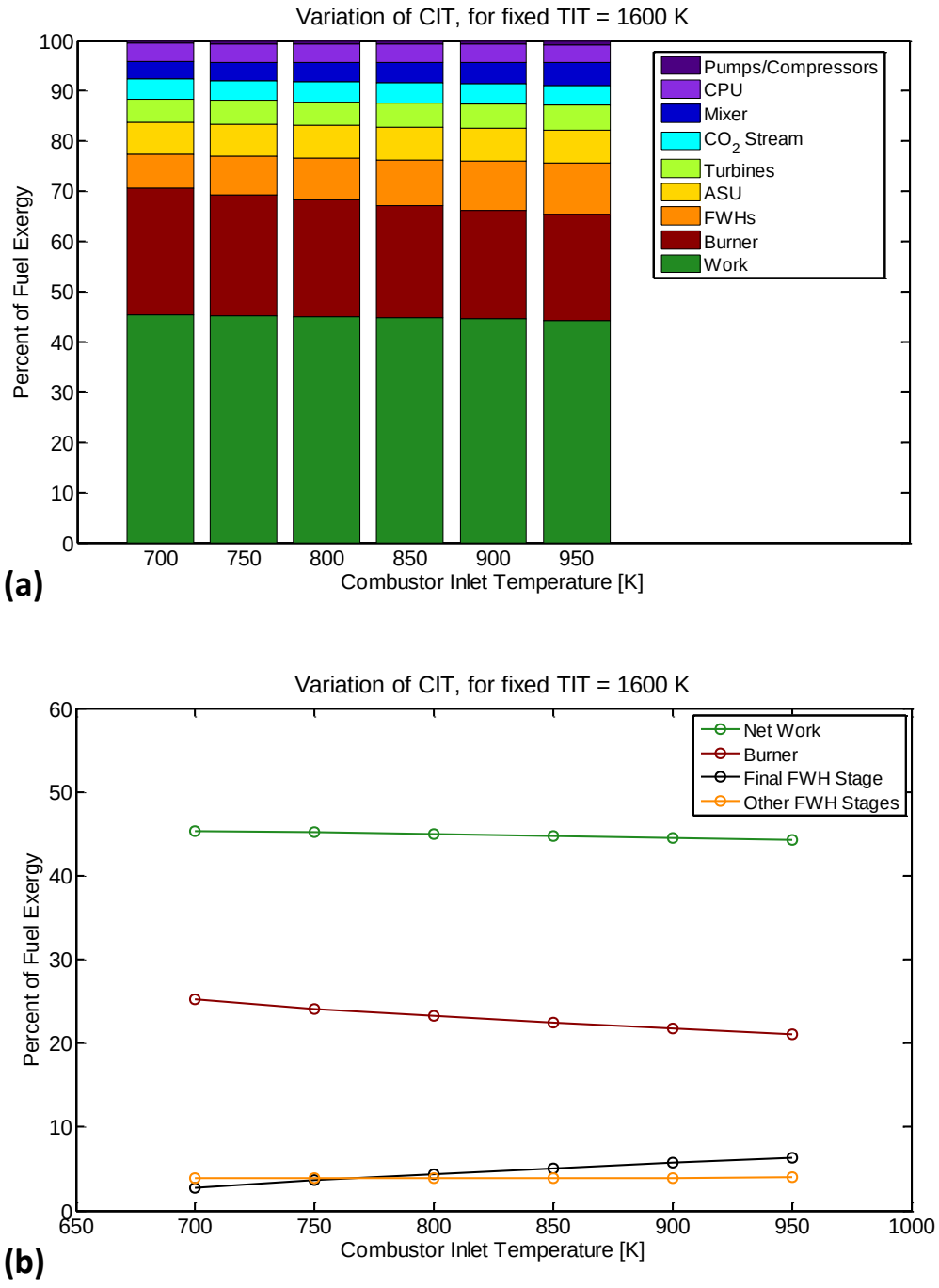

Figure 6.8: Exergy distribution in SCATR, as a percentage of fuel exergy, as a result of varying the CIT while holding the TIT fixed at 1600 K. (a) shows all exergy destruction and outflow in SCATR, and (b) focuses on the most significant changes resulting from the CIT variation.

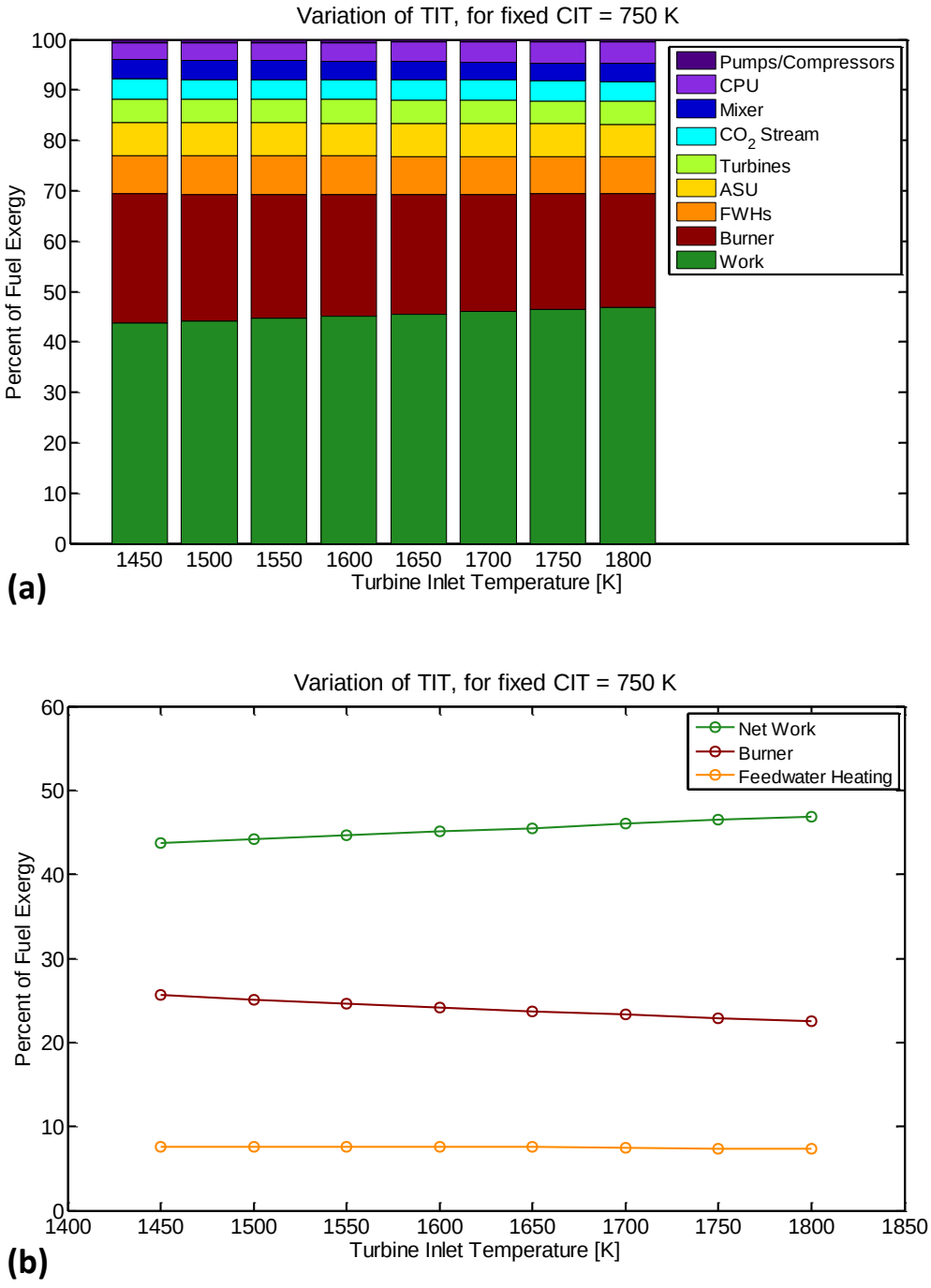

Figure 6.9: Exergy distribution in SCATR, as a percentage of fuel exergy, as a result of varying the TIT while holding the CIT fixed at 750 K. (a) shows all exergy destruction and outflow in SCATR, and (b) focuses on the most significant changes resulting from the TIT variation.

The fraction of fuel exergy destroyed in combustion is seen to decrease as the TIT increases, from 25.6% of fuel exergy at 1450 K to 22.5% at 1800 K. Unlike in the CIT variation case, there is no significant increase in irreversibility in other system components as a result of the TIT increase (only a slight increase in the condenser, which now receives expanded products at a slightly higher specific enthalpy). Therefore, nearly all of the exergy regained in the combustor goes directly to the systems exergy efficiency, which increases from 43.8% at a TIT of 1450 K to 46.9% at a TIT of 1800 K.

For highest system efficiencies then, the CIT should be kept as low as possible while maintaining a supercritical state for the water (in the range of 700-750 K), while the TIT should be raised as high as allowable under materials constraints.

It is interesting to note that the combustion irreversibility actually decreases by a smaller amount for each 100 K increase in TIT than it does for a 100 K increase in CIT. Though the relationship is not linear, there was an average decrease of 1.7% fuel exergy destruction in the combustor for each 100 K increase in CIT over the range of temperatures considered, but only a decrease of 0.9% of fuel exergy destruction per 100 K of TIT increase. Looking only at the combustor, increasing CIT would have seemed like the best way to reduce irreversibility, but at a system level it is clear that increasing TIT has a better effect. This speaks to the need to complete a full system analysis when adjusting the operating point of a single component.

6.4 Conclusions and comparison to other advanced cycles

SCATR is introduced here as a concept for a natural-gas-fired power plant with the potential to reach high efficiencies with intrinsic CO_2 capture. The system modeling and analysis show that system efficiencies of 43.8% to 46.9% relative to the exergy of methane are possible, including all penalties for CO_2 capture and compression to 150 bar. This corresponds to a range of 45.4% to 48.6% on an LHV basis, or

40.9% to 43.8% on an HHV basis. This is comparable to other advanced, water-moderated oxyfuel systems presented in the literature and listed in Section 6.1.2. It is also exactly comparable to efficiency values for NGCC power plants including CO_2 capture and compression (see for example the 42.8%HHV efficiency of Case 14 in the DOE/NETL's Fossil Energy Baseline report).

It is certainly possible, however, that a system like SCATR could have a smaller footprint than an NGCC power plant. This would be likely because SCATR has a single cycle (as opposed to a combined cycle including a large HRSG), because its working fluid is very dense relative to combustion products of natural gas in air, and because of the integration of the CO_2 separation/compression process as an intrinsic part of the cycle. A more definitive statement on this issue would require a techno-economic evaluation with a good awareness of the choice of system components, which is left to a future study. However, the work here would establish the necessary first step in such an analysis.

Chapter 7

Conclusions and Recommendations

This dissertation focused on the evaluation of CO_2 capture systems via the process of exergy analysis. The need for the implementation of carbon capture systems in the electricity sector as a supplement to other greenhouse gas emissions reductions techniques is clear, and was outlined in Chapter 1. However, these systems cause a significant reduction in the electricity output of the power plant. Therefore, new systems are being developed while older, existing ones are improved upon. This has led to a need for a rigorous way to compare sometimes very different systems, on an even basis, in order to understand the direction future research and investment should take.

Exergy analysis can provide a way to perform this comparison, because exergy—which is the measure of the potential work that could be extracted from a resource—can be defined for any transfer to any system. Processes and subprocesses that destroy more exergy are thereby identified as being in need of improvement. Existing post-combustion capture systems were indicated to have exergy efficiencies in the range of 10-25%. Therefore, performing a detailed exergy analysis of these systems was a useful next step to identify the reasons for these low values. This was done for two post-combustion system, an amine absorption system and a vacuum-swing adsorption system. A third system, which used a novel oxycombustion process for burning natural gas and oxygen in a medium of supercritical water, was then studied. One motivation behind this final system was to see whether significant efficiency

gains could be made on the overall power plant by reducing the exergy destruction in combustion. Given the significant decreases in plant exergy efficiency caused by post-combustion capture systems, it could be advantageous to develop systems such as this one, in which the CO_2 separation is an intrinsic part of the process, if it can result in higher plant efficiencies.

7.1 Conclusions and recommendations for process improvement

Over the course of this dissertation, it was found that for the post-combustion capture system using absorption in MEA, the exergy efficiency was even lower than the range of 10-25% anticipated from earlier studies. This mismatch with the expected efficiency values was due to ambiguously defined system boundaries and ambiguously defined reference streams for the separation process. As expected, it was found that a majority of the exergy destruction occurred in the two columns (absorber and stripper). More unexpected was the fact that a significant part of the exergy destruction occurred in the mixing and condensing of the steam extracted from the power cycle for the reboiler—in other words, in the integration of the carbon capture system with the rest of the power plant. The path towards reducing the exergy destruction in the absorber and stripper is already known from other studies, but has only been implemented to small degrees thus far. This involves reducing the driving forces in both columns, so that less exergy destruction occurs (transfers across larger driving gradients result in greater irreversibility). The path towards reducing the exergy destruction in the steam extraction, however, lies in better integrating the CO_2 capture system with the rest of the power plant.

Amine absorption systems are relatively well understood: they are at a high level of technological maturity, and they have been analyzed in relative detail in many different studies. By contrast, post-combustion capture systems using vacuum-swing adsorption are typically less well understood. The modeling and optimization focus for these systems in the past has largely been on the operation of the absorption

column—which states are reached, and for how long—rather than on the rest of the system. As a result, even when analyzing a state-of-the-art system that had specifically been optimized to minimize the work required, remaining potential for efficiency gain was found. This efficiency gain would result from intercooling a vacuum pump process. The technical feasibility of this would need to be discussed with adsorption plant designers and operators. The first recommendation for these processes, therefore, is that a better understanding of the operation of other parts of the system should be gained beyond the column itself. If intercooling were to be used, the efficiency gains made would be significant (≈5 points), and the electrical power needed for the operation of the capture system would be reduced accordingly.

Furthermore, a large part of the exergy destruction in the VSA system occurred in the adsorption column itself. However, the theoretical and modeling tools available to analyze the underlying causes for this irreversibility were found lacking, and were therefore extended. This is discussed in Section 7.2 below.

The third system, SCATR, was developed, modeled, and analyzed as an exploratory concept to raise overall system efficiencies while also separating CO_2. In the end, the resulting efficiencies were relatively high (comparable to an NGCC plant with CO_2 capture), but only limited additional gains could be made. Although potential for improvement of the overall system exergy efficiency was identified in the combustor, very little of that exergy was recoverable as work output from the system.

One of the key uses for results of an exergy analysis is to improve the *integration* of system components. Here, this was addressed to some extent for each of these systems. However, it would be advisable to take this farther, especially in the case of the two post-combustion capture systems. There is value in studying them independently from the remainder of the power plant: This is how large existing inefficiencies (including $\eta_x < 10\%$ for the MEA system) are identified, targeted, and hopefully improved. However, in order to achieve the final goal of having a reduced impact on the electricity output for the plant, the efficiency improvements must be implemented at the integrated, full-plant level.

7.2 Recommendations for modeling needs

A recurring theme during the process evaluation was that of defining a system clearly. This is a straightforward concept, but it does not always get implemented correctly, in particular when using the same binary "minimum exergy of separation" even for separation systems that also separate water, or that have matter transfers into or out of the system at a state that is very different from the environmental state. Careful accounting is needed if different systems are to be compared fairly.

Several issues arose during this dissertation regarding the modeling tools and considerations that are necessary for a detailed exergy analysis. The issue of thermodynamic consistency was revisited on several occasions, both in the mixing rules and isotherm forms that are valid for finding the properties of adsorbed species, and in the implementation of the electrolyte-NRTL method in Aspen Plus. In the *ab*sorption case, the current state of property methods available in Aspen Plus was discussed, with recommendations about which to use to perform exergy analyses of electrolyte systems.

In the *ad*sorption case, the entirety of Chapter 5 can be seen as a recommendation on how to treat thermodynamics of adsorbed species, and can be used as a starting point for future studies. In the vacuum-swing adsorption system studied, a significant part of the exergy destruction was in the adsorption column itself. In order to analyze the adsorption column in more detail, the thermodynamics relevant to the system needed to be better understood. Chapter 5 provides the tools for future exergy analyses of adsorption-based systems in which there is significant accumulation of pure or mixed species in the surface phase. These tools take the form of the theoretical derivation and final expressions, given in Chapter 5, and a set of re-usable property methods written in Matlab for the thermodynamic properties of adsorbed phases, given in Appendix D. These can be used with the existing Cantera open-source property package for ideal gas properties [111].

The fact that the working fluid in the new system in Chapter 6 consisted of a supercritical mixture of water and CO_2 also meant that thermodynamic property methods had to be evaluated carefully. In this case, the issue was not so much one

of thermodynamic consistency, but of taking care to recognize highly non-ideal areas and of modeling them appropriately.

In each of the three systems studied here, there existed significant departures from ideality in thermodynamic property behavior. In order to correctly model and evaluate systems, accurate representation of the thermodynamic properties are essential. As we have seen here, this is especially true when the relevant thermodynamic properties are entropy or exergy.

Appendix A

States and Transfers: MEA System

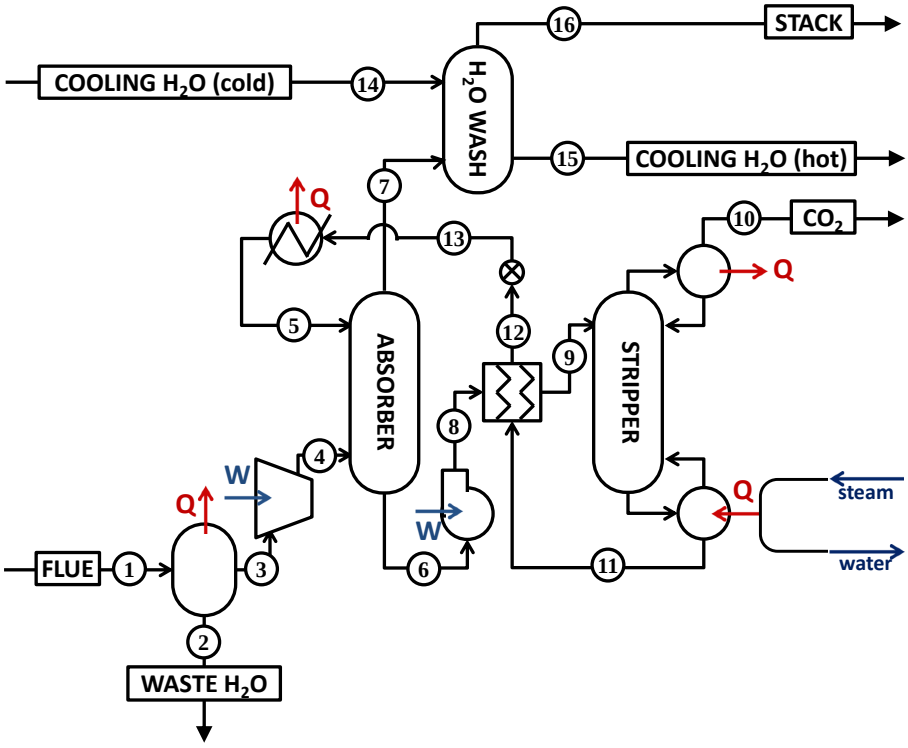

Figure A.1: Diagram of the MEA absorption carbon capture system modeled.

Table A.1: State information in the Aspen Plus model of the MEA system (using ELECNRTL and Hilliard's property parameters [3]). State numbers correspond to labels in Figure A.1. Note that the outlet states for the waste streams (2, 15, 16) are listed here at the temperature that corresponds to the DOE/NETL Baseline values. When performing an exergy analysis however, these streams are cooled to the environmental temperature T_o.

State	1	2	3	4	5	6	7	8
y_i (mol frac)								
H_2O	1.537E-1	1.000E+0	5.465E-2	5.465E-2	8.880E-1	8.772E-1	1.920E-1	8.772E-1
CO_2	1.350E-1	7.404E-10	1.508E-1	1.508E-1	3.050E-13	6.127E-11	1.494E-2	6.144E-11
MEA	0.000E+0	0.000E+0	0.000E+0	0.000E+0	4.821E-2	3.046E-3	9.401E-5	3.047E-3
MEA^+	0.000E+0	0.000E+0	0.000E+0	0.000E+0	3.197E-2	5.990E-2	0.000E+0	5.990E-2
$MEACOO^-$	0.000E+0	0.000E+0	0.000E+0	0.000E+0	3.145E-2	5.174E-2	0.000E+0	5.174E-2
HCO_3^-	0.000E+0	8.081E-7	0.000E+0	0.000E+0	2.850E-4	8.087E-3	0.000E+0	8.088E-3
CO_3^{-2}	0.000E+0	5.624E-11	0.000E+0	0.000E+0	1.141E-4	3.646E-5	0.000E+0	3.640E-5
H^+	0.000E+0	8.082E-7	0.000E+0	0.000E+0	3.157E-10	1.225E-8	0.000E+0	1.227E-8
OH^-	0.000E+0	7.509E-12	0.000E+0	0.000E+0	1.978E-7	7.949E-9	0.000E+0	7.949E-9
O_2	2.380E-2	5.317E-7	2.659E-2	2.659E-2	0.000E+0	9.167E-8	2.653E-2	9.167E-8
N_2	6.793E-1	7.917E-6	7.588E-1	7.588E-1	0.000E+0	1.425E-6	7.573E-1	1.425E-6
Ar	8.200E-3	1.997E-7	9.160E-3	9.160E-3	0.000E+0	3.396E-8	9.142E-3	3.396E-8
h (kJ/kg)	-3.097E+3	-1.582E+4	-2.402E+3	-2.378E+3	-1.236E+4	-1.218E+4	-1.929E+3	-1.218E+4
s (kJ/kg-K)	1.626E-1	-8.920E+0	1.840E-1	2.122E-1	-8.344E+0	-8.037E+0	4.040E-2	-8.037E+0
$\dot{m}$ (kg/s)	85.73	58.44	27.29	27.29	2280.91	2192.88	96.03	2192.88
T (°C)	58.0	34.5	34.5	57.6	40.0	52.3	62.2	52.3
P (MPa)	0.101	0.101	0.101	0.120	0.101	0.111	0.101	0.203

State	9	10	11	12	13	14	15	16
y_i (mol frac)								
H_2O	8.754E-1	1.591E-2	8.849E-1	8.848E-1	8.848E-1	1.000E+0	1.000E+0	4.749E-2
CO_2	6.054E-3	9.840E-1	4.479E-10	2.277E-12	2.280E-12	0.000E+0	6.377E-11	1.760E-2
MEA	1.163E-2	1.087E-8	5.008E-2	5.014E-2	5.014E-2	0.000E+0	1.544E-5	2.815E-14
MEA^+	5.345E-2	0.000E+0	3.251E-2	3.257E-2	3.257E-2	0.000E+0	3.784E-6	0.000E+0
$MEACOO^-$	4.890E-2	0.000E+0	3.214E-2	3.202E-2	3.202E-2	0.000E+0	2.789E-8	0.000E+0
HCO_3^-	4.534E-3	0.000E+0	3.603E-4	4.169E-4	4.169E-4	0.000E+0	3.741E-6	0.000E+0
CO_3^{-2}	5.457E-6	0.000E+0	8.258E-6	6.647E-5	6.647E-5	0.000E+0	1.533E-8	0.000E+0
H^+	7.380E-8	0.000E+0	4.512E-8	1.197E-9	1.198E-9	1.737E-9	1.639E-8	0.000E+0
OH^-	1.345E-8	0.000E+0	8.022E-8	1.813E-7	1.814E-7	1.737E-9	7.791E-10	0.000E+0
O_2	9.112E-8	3.296E-6	1.112E-19	0.000E+0	0.000E+0	0.000E+0	5.225E-7	3.128E-2
N_2	61.416E-6	5.123E-5	1.000E-30	0.000E+0	0.000E+0	0.000E+0	7.990E-6	8.929E-1
Ar	3.376E-8	1.221E-6	5.343E-23	0.000E+0	0.000E+0	0.000E+0	1.948E-7	1.078E-2
h (kJ/kg)	-1.200E+4	-8.975E+3	-1.203E+4	-1.222E+4	-1.222E+4	-1.586E+4	-1.578E+4	-6.487E+2
s (kJ/kg-K)	-7.518E+0	-3.582E-2	-7.602E+0	-8.137E+0	-8.137E+0	-9.051E+0	-8.770E+0	9.070E-2
$\dot{m}$ (kg/s)	2201.77	3.86	138.70	138.70	138.70	131.43	135.64	23.55
T (°C)	100.0	21.0	113.9	59.0	59.0	25.0	45.7	32.0
P (MPa)	0.193	0.160	0.170	0.162	0.101	0.101	0.101	0.101

Table A.2: Energy transfers in the MEA system model.

Device	Heat or Work (MW)
Flue gas cooler $\dot{Q}$	163.938
Reboiler $\dot{Q}$	588.572
Condenser $\dot{Q}$	199.051
Lean solvent cooler $\dot{Q}$	18.043
Blower $\dot{W}$	20.261
Pump $\dot{W}$	0.605

Appendix B

VSA system parameters

These parameters are taken from Haghpanah et al. 2013 [86], and any additional parameters can be found there as well.

Adsorption parameter	Value	Units
$q_{s\alpha,CO2}$	3.09	mol/kg$_{sorbent}$
$q_{s\beta,CO2}$	2.54	mol/kg$_{sorbent}$
$q_{s\alpha,N2}$	5.84	mol/kg$_{sorbent}$
$q_{s\beta,N2}$	0.00	mol/kg$_{sorbent}$
$K_{0\alpha,CO2}$	8.65E-7	m$^3_{gas}$/mol
$K_{0\beta,CO2}$	2.63E-8	m$^3_{gas}$/mol
$K_{0\alpha,N2}$	2.50E-6	m$^3_{gas}$/mol
$K_{0\beta,N2}$	0.00	m$^3_{gas}$/mol
$\Delta U_{a\alpha,CO2}$	-36.641	kJ/mol
$\Delta U_{a\beta,CO2}$	-35.690	kJ/mol
$\Delta U_{a\alpha,N2}$	-15.800	kJ/mol
$\Delta U_{a\beta,N2}$	0.000	kJ/mol

Property	Value	Units
Column length	1	m
Column inner radius	0.1445	m
Column void fraction, ε	0.37	$\frac{m^3_{gas}}{m^3_{column}}$
Sorbent density	1130	kg/m^3
Specific heat capacity of sorbent	1070	J/kg-K
Effective thermal conductivity	0.09	J/m-K-s
Flue gas pressure	1	bar
Flue gas temperature	298.15	K
Flue gas CO_2 content	0.15	$\frac{kmol_{CO_2}}{kmol_{gas}}$
Flue gas N_2 content	0.85	$\frac{kmol_{CO_2}}{kmol_{gas}}$
CO_2 capture percentage	90	%
CO_2 purity in product	90	%
Gas viscosity, μ	1.72E-5	kg/m-s
Isentropic efficiency of vac. pumps	0.72	—
High pressure	1	bar
Intermediate pressure	0.09	bar
Low pressure	0.02	bar
Pressurization duration	20	s
Adsorption duration	94.89	s
Blowdown duration	122.84	s
Evacuation duration	189.46	s

Appendix C

Adsorbed phase exergy example

Exergy is a state property of a substance and its environment. To help understand how this property behaves, the exergy of various substances is plotted in Figure C.2. The exergy of four gases is plotted as a function of pressure, for five different temperatures, on the left-hand side (Figure C.2 a, c, e, and g). These gases are, respectively, dry air (molar composition 78.08% N_2, 20.94% O_2, 0.934% Ar, and 380 ppm CO_2), pure nitrogen, pure carbon dioxide, and a representation of dry flue gas from a coal-fired power plant (molar composition 85% N_2, 15% CO_2). The dead state has the composition of dry air, a pressure of 1 bar, and a temperature of 298.15 K. The gas phase can be treated as an ideal gas for the states considered, and gas-phase properties are calculated using the Cantera open-source package for Matlab [111].

On the right-hand side (Figure C.2 b, d, f, and h) is plotted the exergy of the adsorbed phase that is in equilibrium with each of these gases on zeolite 13X. The exergy of these gases is calculated as derived in Chapter 5, assuming an ideal adsorbed solution, and using pure-component adsorption isotherms from the literature. The O_2 and N_2 isotherms are taken from Baksh et al. [139]. The CO_2 isotherm is taken from Haghpanah et al. [86] and are listed in Appendix B. Functional forms of adsorption isotherms for argon at low pressure on zeolite 13X are surprisingly difficult to find, but studies of air separation using this zeolite indicate that argon isotherms match oxygen closely, especially when compared to nitrogen or CO_2 [139]. For the purpose of this illustration, the argon adsorption isotherm is taken to be the same as for oxygen.

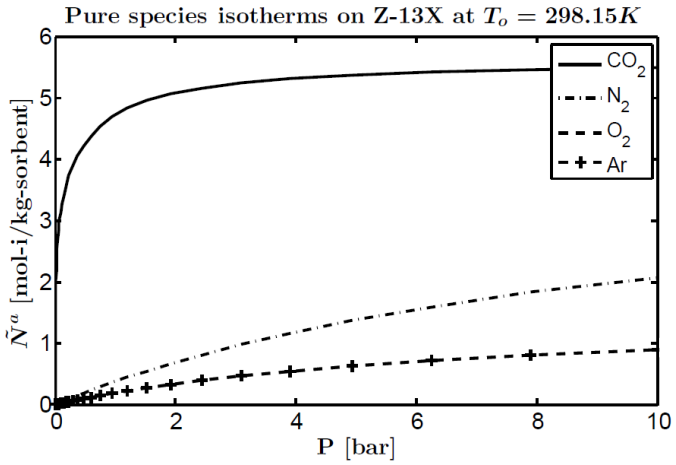

Figure C.1: Adsorption isotherms on Zeolite 13X at 298.15 K, used in the calculation of dead-state properties.

The isotherms for the environmental gases at the dead state temperature are shown in Figure C.1.

Except at the dead state where it is zero, exergy is always a positive quantity, regardless of whether the system is at a higher or lower temperature, pressure, or mole fraction than the dead state. In Figure C.2, the zero-exergy state is seen in two instances: for gaseous air at 1 bar and 298.15 K, and for adsorbed air at 1 bar and 298.15 K. Note that the mole fraction of the air in the adsorbed phase will not be the same as the mole fraction of air in the gas phase. Instead, the adsorbed air has the same chemical potential as the gaseous air; the mole fractions in the adsorbed phase vary with temperature and pressure and are found using the Ideal Adsorbed Solution procedure described in Chapter 5.

For all species and phases, the value of the exergy reaches a minimum at the state that is nearest to the dead state. Mixtures that have compositions that are nearer to the dead state's have overall lower exergy. The pure nitrogen plots are only somewhat different from the air plots because air is primarily nitrogen. Similarly, the gaseous CO_2 has much larger exergy than any other species or mixture plotted because the mole fraction of CO_2 at the dead state is so low. This is well understood for the exergy of gas phases. However, the adsorbed CO_2 shows a different behavior: its

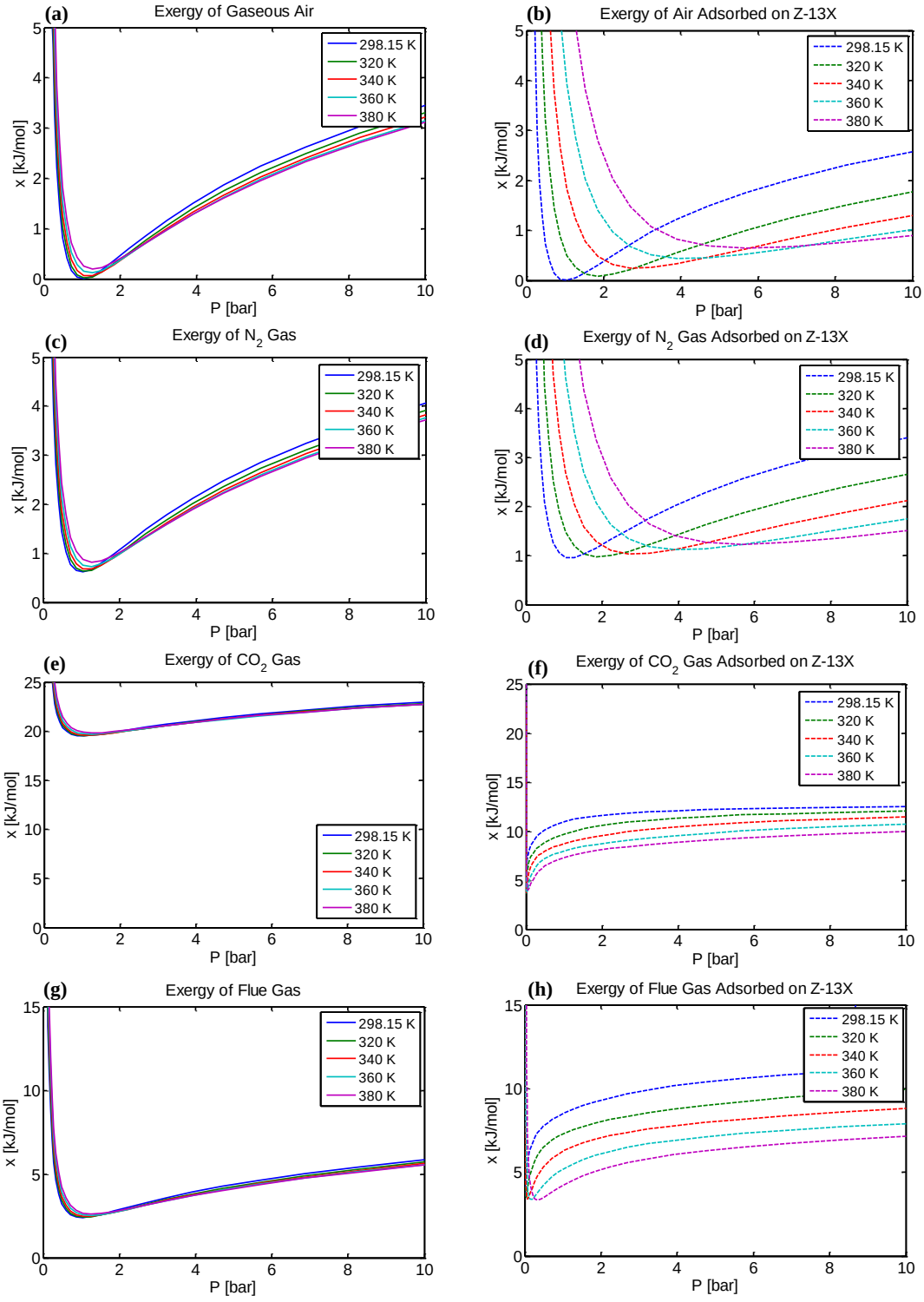

Figure C.2: Exergy of various gases and gas mixtures, and exergy of the adsorbed phase in equilibrium with these gases.

exergy is considerably lower than that of the gaseous CO_2. This can be understood by noting that CO_2 adsorbs very strongly onto zeolite 13X such that, even when in contact with 380 ppm CO2 air, the adsorbed phase will still have a high mole fraction of CO_2. Therefore pure CO_2 adsorbed on zeolite 13X is not nearly as different from air adsorbed on zeolite 13X as pure CO_2 gas is from gaseous air—adsorbed CO2's exergy is lower than that of gaseous CO_2.

A similar reasoning can be used to understand the flue gas plots. Flue gas (85% N_2, 15% CO_2) is mainly nitrogen so its gas-phase exergy, while slightly larger than that of pure nitrogen, behaves similarly. Flue gas adsorbed on zeolite 13X, by contrast, will be much more enriched in CO_2, so this phase's exergy behaves more like pure CO_2 than like pure nitrogen.

Appendix D

Matlab code for adsorbed phase properties

D.1 For solving for the Ideal Adsorbed Solution mixture state

D.1.1 "Forward"

```
function [Pstand, qvec, x] = FastIAS(Tsys, Pvec, varargin)
%%%%%%%%%%%%%%%%%%%%%%%%%%%%%%%%%%%%%%%%%%%%%%%%%%%%%%%%%%%%%%%%%%%%%%%%
% [Pstand, qvec, x] = FastIAS(Tsys, Pvec, varargin)
%
% Function that makes a thermodynamically consistent mixture for
% adsorbed species. Can use activity coefficients if available;
% otherwise will set them to 1.
%
% Currently exists only in a state that assumes dual-site Langmuir
% isotherms for the pure species, in the form that Haghpanah et al. 2013
% use (i.e. explicit in c_i instead of P_i).
%
% Based on the algorithm as laid out by O'Brien and Myers, 1985 (although
% with a different isotherm form).
%
% INPUTS:   System T [K]
%           Vector of partial pressures in gas phase [Pa]
```

```
%           Activity coefficients if available [unitless]
%
% OUTPUTS:  Vector of standard state pressures for each component [Pa]
%           Vector of loadings for each component [kmol-i/kg-sorbent]
%           Mole fractions in the adsorbed phase [unitless, and redundant
%               on Nvec, but might still be handy]
%
% A. Calbry-Muzyka
% 15 Jan. 2014
%%%%%%%%%%%%%%%%%%%%%%%%%%%%%%%%%%%%%%%%%%%%%%%%%%%%%%%%%%%%%%%%%%%%%%%%

% Make the species references available.
global iN2 iCO2 iO2 iAr Ru
% Make the dual-site Langmuir parameters available to all functions.
% All can be vectors, using the gas-specific indices above.
global b0 d0 Nsatb Nsatd DUb DUd

% Check to see if we have activity coefficients or not:
if nargin == 3
    alpha = varargin{1};                % This should be a vector.
else
    alpha = ones(length(Pvec),1);       % IDEAL ADSORBED SOLUTION DEFAULT.
end

% Find out how many species we have:
N           = length(Pvec);

%%%%%%%%%%%%%%%%%%%%%%%%%%%%%%%%%%%%%%%%%%%%%%%%%%%%%%%%%%%%%%%%%%%%%%%%%%%%
%% Fast IAS. Assume that we have dual-site Langmuir for pure comps.
%%%%%%%%%%%%%%%%%%%%%%%%%%%%%%%%%%%%%%%%%%%%%%%%%%%%%%%%%%%%%%%%%%%%%%%%%%%%
Psys            = sum(Pvec);                    % [Pa]
y               = Pvec./Psys;                   % unitless
Kbi             = b0.*exp(-DUb./(Ru.*Tsys));   % [m3/kmol]
Kdi             = d0.*exp(-DUd./(Ru.*Tsys));   % [m3/kmol]

% Make the code much faster by pre-eliminating species that aren't there
% (i.e. that have a partial pressure of zero).
N_short         = 0;
for i = 1:N
    if ( Pvec(i) ~= 0 )
        N_short                 = N_short + 1;
        Pvec_short(N_short)     = Pvec(i);
        alpha_short(N_short)    = alpha(i);
        Nsatb_short(N_short)    = Nsatb(i);
        Nsatd_short(N_short)    = Nsatd(i);
        Kbi_short(N_short)      = Kbi(i);
        Kdi_short(N_short)      = Kdi(i);
```

```
        y_short(N_short)        = y(i);
        species_storage(N_short) = i;
    end
end

% Initial guess for Pstand (based on Henry's Law limit)
for i = 1:N_short
    Pstand0(i)   = Psys*( sum((Nsatb_short.*Kbi_short + ...
        Nsatd_short.*Kdi_short).*y_short) ...
        ./ (Nsatb_short(i)*Kbi_short(i) + Nsatd_short(i)*Kdi_short(i)) );
end

% Initialize vectors.
J       = zeros(N_short,N_short);
gvec    = zeros(N_short,1);

% Set the initial guess for Newton-Raphson.
Pstand_short  = Pstand0';
Nstand_short  = zeros(N_short,1);

MAXITER = 50;               % Max allowed iterations for Newton-Raphson
TOLER   = 10e-9;            % Tolerance required for Newton-Raphson
err     = 1;                % Start err > TOLER to enter loop
k       = 1;                % Newton-Raphson loop counter
while (err > TOLER)
    for j = 1:N_short         % j is the column of the NxN system
        for i = 1:N_short-1       % i is the row of the NxN system
            if (i == j)
                J(i,j) = Nsatb_short(i)*Kbi_short(i)/( ...
                    Ru*Tsys+(Kbi_short(i)*Pstand_short(i)) ) ...
                    + Nsatd_short(i)*Kdi_short(i)/( ...
                        Ru*Tsys+(Kdi_short(i)*Pstand_short(i)) );
            elseif (i+1 == j)
                J(i,j) = -( Nsatb_short(i+1)*Kbi_short(i+1)/( ...
                    Ru*Tsys+(Kbi_short(i+1)*Pstand_short(i+1)) )...
                    + Nsatd_short(i+1)*Kdi_short(i+1)/( ...
                        Ru*Tsys+(Kdi_short(i+1)*Pstand_short(i+1)) ) );
            end
            % Define the g vector here too:
            % Define the function psi first:
            psi = @(a) Nsatb_short(a).*log(1 + ...
                Pstand_short(a).*Kbi_short(a)./(Ru*Tsys))...
                + Nsatd_short(a).*log(1 + Pstand_short(a).*Kdi_short(a)./(Ru*Tsys));
            % Now use it to find gvec
            gvec(i)     = psi(i) - psi(i + 1);
        end
        % Bottom row of Jacobian:
```

```
        J(N_short,j)      = (-Psys*y_short(j)) / (alpha_short(j)*Pstand_short(j)^2);
        % Define the end of the g vector here too:
        gvec(N_short)     = -1 + sum(Psys.*y_short./(Pstand_short'.*alpha_short));
    end

    % Make a Newton-Raphson step:
    correct          = J\(-gvec);
    Pstandold        = Pstand_short;
    Pstand_short     = Pstandold + correct;
    k = k + 1;       % to see how many iterations it takes

    % Define the convergence criterion:
    err = sum(abs(correct./Pstand_short));

    % Put in checks to make this more rigorous:
    if (k ≥ MAXITER)
        disp('Newton-Raphson is taking too long. Something is wrong.')
        break
    else
        for i = 1:N_short
            if (Pstand_short(i) ≤ 0)
                disp('Newton-Raphson running off. Using bisection now.')
                Pstand_short(i) = Pstandold(i)/2;
            end
        end
    end

end

%%%%%%%%%%%%%%%%%%%%%%%%%%%%%%%%%%%%%%%%%%%%%%%%%%%%%%%%%%%%%%%%%%%%%%%%%%%%%%%
%% Return all other information from IAS now that Pstand is found.
%%%%%%%%%%%%%%%%%%%%%%%%%%%%%%%%%%%%%%%%%%%%%%%%%%%%%%%%%%%%%%%%%%%%%%%%%%%%%%%
% Find adsorbed phase mole fractions:
x_short       = Pvec_short./(Pstand_short'.*alpha_short);
% Find the standard state loading for each species:
Nstand_short  = Nsatb_short.*Kbi_short.*Pstand_short'./(Ru*Tsys + ...
    Kbi_short.*Pstand_short')...
    + Nsatd_short.*Kdi_short.*Pstand_short'./(Ru*Tsys + Kdi_short.*Pstand_short');
% Find the total loading:
Nt      = 1/(sum(x_short./Nstand_short));
% Find the individual species loading:
Nvec_short    = Nt.*x_short;

%% Now make the vector the normal size again.
Pstand   = zeros(N,1);
Nvec     = zeros(N,1);
x        = zeros(N,1);
```

```
for i = 1:N_short
    long_index = species_storage(i);
    Pstand(long_index) = Pstand_short(i);
    Nvec(long_index)   = Nvec_short(i);
    x(long_index)      = x_short(i);
end

% Return the vector of loadings.
qvec = Nvec;

end
```

D.1.2 "Backward"

```
function [Pstand, Psys, y] = FastIAS_fromNs(Tsys, qvec, varargin)
%%%%%%%%%%%%%%%%%%%%%%%%%%%%%%%%%%%%%%%%%%%%%%%%%%%%%%%%%%%%%%%%%%%%%%%%
% [Pstand, Psys, y] = FastIAS_fromNs(Tsys, qvec, varargin)
%
% Function that makes a thermodynamically consistent mixture for
% adsorbed species. Can use activity coefficients if available;
% otherwise will set them to 1.
%
% Returns the vector of standard pressures of the given set of adsorption
% loadings, as well as the system pressure and gas mole fractions that
% would be in equilibrium with that set of loadings (all for a given
% temperature).
%
% Mainly useful for calculating thermodynamic properties of adsorbed
% phases that are NOT in equilibrium with the bulk gas phase (eg. due to
% mass transfer resistance). We need to know standard pressures and
% temperature of each substance in the adsorbed phase mixture.
%
% Currently exists only in a state that assumes dual-site Langmuir
% isotherms for the pure species, in the form that Reza uses (i.e.
% explicit in c_i instead of P_i).
%
% Based on the algorithm as laid out by O'Brien and Myers, 1985,
% and O'Brien and Myers, 1988 (although with a different isotherm form).
%
% INPUTS:   System T [K]
%           Vector of loadings [kmol-i/kg-sorbent]
%           Activity coefficients if available [unitless]
%
```

```
% OUTPUTS:  Vector of standard state pressures for each component [Pa]
%           System pressure [Pa]
%           Mole fractions in the gas phase [unitless]
%
% A. Calbry-Muzyka, Jan. 15, 2014
%%%%%%%%%%%%%%%%%%%%%%%%%%%%%%%%%%%%%%%%%%%%%%%%%%%%%%%%%%%%%%%%%%%%%%%%%%%

% Make the species references available.
global iN2 iCO2 Ru
% Make the dual-site Langmuir parameters available to all functions.
% All can be vectors, using the gas-specific indices above.
global b0 d0 Nsatb Nsatd DUb DUd

% Rename qvec to Nvec:
Nvec            = qvec;             % [kmol-i/kg-sorbent]

% Check to see if we have activity coefficients or not:
if nargin == 3
    alpha = varargin{1};             % This should be a function handle, eventually.
    disp('This function cannot take in non-unity activity coefficients yet. Talk ...
        to Adelaide.')
    return
else
    alpha = ones(length(Nvec),1);   % IDEAL ADSORBED SOLUTION DEFAULT.
end

% Find out how many species we have:
N               = length(Nvec);

%%%%%%%%%%%%%%%%%%%%%%%%%%%%%%%%%%%%%%%%%%%%%%%%%%%%%%%%%%%%%%%%%%%%%%%%%%%
%% Fast IAS. Assume that we have dual-site Langmuir for pure comps.
%%%%%%%%%%%%%%%%%%%%%%%%%%%%%%%%%%%%%%%%%%%%%%%%%%%%%%%%%%%%%%%%%%%%%%%%%%%
Ntot            = sum(Nvec);                    % [kmol/kg-sorbent]
x               = (Nvec./Ntot)';                   % mole frac in adsorbed phase
Kbi             = b0.*exp(-DUb./(Ru.*Tsys));    % [m3/kmol]
Kdi             = d0.*exp(-DUd./(Ru.*Tsys));    % [m3/kmol]

% First put in a check that the loadings given are actually possible.
if Ntot > (Nsatb + Nsatd)
    disp('The sorbent loading exceeds the saturation capacity of this material.')
    return
end

% Initial guess for Pstand (based on Henry's Law limit)
Pstand0 = zeros(N,1);
for i = 1:N
    Pstand0(i)   =  ( Ntot*Ru*Tsys ) / ( Nsatb(i)*Kbi(i) + Nsatd(i)*Kdi(i) );
```

```
end

J       = zeros(N,N);
gvec    = zeros(N,1);
Pstand  = Pstand0;          % Set the initial guess for Newton-Raphson.

MAXITER = 100;
TOLER   = 10e-9;
err     = 1;
k       = 1;                % k is the Newton-Raphson loop counter
while (err > TOLER)
    for j = 1:N         % j is the column of the NxN system
        for i = 1:N-1       % i is the row of the NxN system
            if (i == j)
                J(i,j) = Nsatb(i)*Kbi(i)/( Ru*Tsys+(Kbi(i)*Pstand(i)) ) + ...
                    Nsatd(i)*Kdi(i)/( Ru*Tsys+(Kdi(i)*Pstand(i)) );
            elseif (i+1 == j)
                J(i,j) = -( Nsatb(i+1)*Kbi(i+1)/( Ru*Tsys+(Kbi(i+1)*Pstand(i+1)) ...
                    ) + ...
                    Nsatd(i+1)*Kdi(i+1)/( Ru*Tsys+(Kdi(i+1)*Pstand(i+1)) ) );
            end
            % Define the g vector here too:
            % Define the function psi first:
            psi = @(a) Nsatb(a).*log(1 + Pstand(a).*Kbi(a)./(Ru*Tsys)) + ...
                Nsatd(a).*log(1 + Pstand(a).*Kdi(a)./(Ru*Tsys));
            gvec(i)     = psi(i) - psi(i + 1);
        end
        % Define a function for standard state loading:
        Nstand_vec    = @(Pstand) Nsatb.*Kbi.*Pstand./(Ru*Tsys + Kbi.*Pstand) + ...
            Nsatd.*Kdi.*Pstand./(Ru*Tsys + Kdi.*Pstand);
        % Now make the bottom row of the Jacobian:
        % ASSUMES THAT THE ACTIVITY COEFFICIENTS ARE CONSTANT.
        Nstandvec     = Nstand_vec(Pstand);
        J(N,j)      = -x(j)/((Nstandvec(j))^2) * ...
            ( Nsatb(j)*Kbi(j)*Ru*Tsys/((Ru*Tsys + Kbi(j)*Pstand(j))^2) + ...
            Nsatd(j)*Kdi(j)*Ru*Tsys/((Ru*Tsys + Kdi(j)*Pstand(j))^2));
        % Define the end of the g vector here too:
        % ONCE AGAIN, ASSUMES THAT ACTIVITY COEFFICIENTS ARE CONSTANT.
        gvec(N)     = sum(x./Nstandvec) - 1/Ntot;
    end
    % Make a Newton-Raphson step:
    correct     = J\(-gvec);
    Pstandold   = Pstand;
    Pstand      = Pstandold + correct;
    k = k + 1;                  % to see how many iterations it takes
    % Define the convergence criterion:
    err = sum(abs(correct./Pstand));
```

```
    % Put in checks to make this more rigorous:
    if (k ≥ MAXITER)
        disp('Newton-Raphson is taking too long. Something is wrong.')
        break
    else
        for i = 1:N
            if (Pstand(i) ≤ 0)
                disp('Newton-Raphson running off. Using bisection now.')
                Pstand(i) = Pstandold(i)/2;
            end
        end
    end

end


%%%%%%%%%%%%%%%%%%%%%%%%%%%%%%%%%%%%%%%%%%%%%%%%%%%%%%%%%%%%%%%%%%%%%%%%%%%
%% Return all other information from IAS now that Pstand is found.
%%%%%%%%%%%%%%%%%%%%%%%%%%%%%%%%%%%%%%%%%%%%%%%%%%%%%%%%%%%%%%%%%%%%%%%%%%%
% Find gas phase partial pressures:
Pi   = zeros(N,1);
for i = 1:N
    Pi(i)    = Pstand(i)*x(i)*alpha(i);          % Pa
end
% Find total system pressure:
Psys     = sum(Pi);                             % Pa
% Find gas phase mole fractions:
y        = Pi./Psys;                            % unitless


end
```

D.2 For finding thermodynamic properties at a known state

D.2.1 Surface potential and Gibbs free energy

```
function Phi_i = Phi_i_L2(T, Pstand, iSpecies)
%%%%%%%%%%%%%%%%%%%%%%%%%%%%%%%%%%%%%%%%%%%%%%%%%%%%%%%%%%%%%%%%%%%%%%%%%%%
% Phi_i = Phi_i_L2(T, Pstand, iSpecies)
```

```
%
% Returns the semi-extensive (per mass sorbent) surface potential of the
% adsorbed phase (J/kg), ASSUMING DUAL-SITE LANGMUIR form of the isotherm,
% and an ideal gas vapor phase.
%
% INPUTS: T_system, the standard state pressure of the species, and the index
% of the species for which the property is wanted.
% NECESSARY GLOBALS: Langmuir parameters.
% OUTPUTS: Phi_i (J/kg-sorbent), the surface potential of a pure species.
%
% A. Calbry-Muzyka
% 21 Jan. 2014
%%%%%%%%%%%%%%%%%%%%%%%%%%%%%%%%%%%%%%%%%%%%%%%%%%%%%%%%%%%%%%%%%%%%%%%%%%%

global To Po xo mu_o Phio iN2 iCO2 Ru
global b0 d0 Nsatb Nsatd DUb DUd

% Make vectors for Arrhenius terms.
b_i          = b0.*exp(-DUb./(Ru.*T));                % m3/kmol
d_i          = d0.*exp(-DUd./(Ru.*T));                % m3/kmol

% Find Phi for species i.
Phi_i = -Ru*T*Nsatb(iSpecies)*log( 1 + b_i(iSpecies)*Pstand/(Ru*T) ) - ...
    Ru*T*Nsatd(iSpecies)*log( 1 + d_i(iSpecies)*Pstand/(Ru*T) );

end
```

```
function DGa_i = DGa_i_L2(T, Pstand, iSpecies)
%%%%%%%%%%%%%%%%%%%%%%%%%%%%%%%%%%%%%%%%%%%%%%%%%%%%%%%%%%%%%%%%%%%%%%%%%%%
% DGa_i = DGa_i_L2(T, Pstand, iSpecies)
%
% Returns the semi-extensive (per mass sorbent) Gibbs free energy of the
% adsorbed phase (J/kg-sorbent), ASSUMING DUAL-SITE LANGMUIR form of the
% isotherm, relative to an ideal gas reference phase.
%
% Based on the relations from Myers 2002.
%
% INPUTS: T_system, the standard state pressure of the species, and the index
% of the species for which the property is wanted.
% NECESSARY GLOBALS: Langmuir parameters
% OUTPUTS: Delta G of the adsorbed species i, per mass of sorbent
%          (J/kg-sorbent), where Delta_Ga = Ga - G(ideal gas @ Po and same T)
%
% Remember: Use to get back to Ga by adding to G_gas, not as Ga directly.
%
```

```
% A. Calbry-Muzyka
% 21 Jan. 2014
%%%%%%%%%%%%%%%%%%%%%%%%%%%%%%%%%%%%%%%%%%%%%%%%%%%%%%%%%%%%%%%%%%%%%%%%%%%%

global To Po xo mu_o Phio iN2 iCO2 Ru
global b0 d0 Nsatb Nsatd DUb DUd

% Make vectors for Arrhenius terms.
b_i          = b0.*exp(-DUb./(Ru.*T));                % m3/kmol
d_i          = d0.*exp(-DUd./(Ru.*T));                % m3/kmol

% Use the dual-site Langmuir isotherm to find Na_i, in kmol-i/kg-sorbent
% at the standard state (i.e. at the vapor pressure).
Nastand_i = Nsatb(iSpecies)*b_i(iSpecies)*Pstand/(Ru*T + b_i(iSpecies)*Pstand) + ...
    Nsatd(iSpecies)*d_i(iSpecies)*Pstand/(Ru*T + d_i(iSpecies)*Pstand);

% Assuming an ideal gas vapor phase:
if Nastand_i == 0
    DGa_i = 0;      % Otherwise log(0) = -inf and this function returns NaN.
else
    DGa_i = Nastand_i*Ru*T*log(Pstand/Po) + Phi_i_L2(T,Pstand,iSpecies);
end

end
```

```
function Dga_imol = Dga_imol_L2(T, Pstand, iSpecies)
%%%%%%%%%%%%%%%%%%%%%%%%%%%%%%%%%%%%%%%%%%%%%%%%%%%%%%%%%%%%%%%%%%%%%%%%%%%%
% Dga_imol = Dga_imol_L2(T, Pstand, iSpecies)
%
% Returns the intensive (per kmol of species i) Gibbs free energy of the
% adsorbed phase (J/kmol-i), ASSUMING DUAL-SITE LANGMUIR form of the
% isotherm, relative to an ideal gas reference phase.
%
% INPUTS: T_system, the standard state pressure of the species, and the
% index of the species for which the property is wanted.
% NECESSARY GLOBALS: Langmuir parameters
% OUTPUTS: Delta g of the adsorbed species i (J/kmol-i), where
%           Delta_ga = ga - g(idealgas @ Po and same T)
%
% Remember: Use to get back to ga by adding to g_gas, not as ga directly.
%
% A. Calbry-Muzyka
% 21 Jan. 2014
%%%%%%%%%%%%%%%%%%%%%%%%%%%%%%%%%%%%%%%%%%%%%%%%%%%%%%%%%%%%%%%%%%%%%%%%%%%%
```

```
global To Po xo mu_o Phio iN2 iCO2 Ru
global b0 d0 Nsatb Nsatd DUb DUd

% Make vectors for Arrhenius terms.
b_i          = b0.*exp(-DUb./(Ru.*T));                % m3/kmol
d_i          = d0.*exp(-DUd./(Ru.*T));                % m3/kmol

% Use the dual-site Langmuir isotherm to find Na_i, in kmol-i/kg-sorbent
% at the standard state (i.e. at the vapor pressure).
Nastand_i = Nsatb(iSpecies)*b_i(iSpecies)*Pstand/(Ru*T + b_i(iSpecies)*Pstand) + ...
    Nsatd(iSpecies)*d_i(iSpecies)*Pstand/(Ru*T + d_i(iSpecies)*Pstand);

% Find Dga_i from DGa_i (which is in J/kg-sorbent):
DGa_i = DGa_i_L2(T,Pstand,iSpecies);
Dga_imol = DGa_i * (1/Nastand_i);

end
```

```
function ga_mol = ga_mol_L2(T, Pstand_vec, x_vec, fluid, varargin)
%%%%%%%%%%%%%%%%%%%%%%%%%%%%%%%%%%%%%%%%%%%%%%%%%%%%%%%%%%%%%%%%%%%%%%%%%%%%
% ga_mol = ga_mol_L2(T, Pstand_vec, x_vec, fluid, varargin)
%
% Returns the molar Gibbs free energy [J/kmol-mix] of an adsorbed phase mixture,
% ASSUMING DUAL-SITE LANGMUIR form of the isotherm, and assuming ideal gas vapor ...
    phase.
%
% Note that this uses the Cantera open-source package to solve for ideal
% gas properties. This is not necessary, but then you will need to update
% this file.
%
% INPUTS: T_system, vector of standard pressures of all species in the mixture [Pa],
%           vector of actual adsorbed phase mole frac, and a fluid object.
%           HAS THE OPTION OF SENDING A VECTOR OF ACTIVITY COEFFICIENTS AFTER.
% NECESSARY GLOBALS: Langmuir parameters for ALL ADSORBED SPECIES, and Po.
% OUTPUTS: g (not Δ g) of the adsorbed phase [J/kmol-mix]
%
% A. Calbry-Muzyka
% 21 Jan. 2014
%%%%%%%%%%%%%%%%%%%%%%%%%%%%%%%%%%%%%%%%%%%%%%%%%%%%%%%%%%%%%%%%%%%%%%%%%%%%

global To Po xo mu_o Phio iN2 iCO2 Ru
global b0 d0 Nsatb Nsatd DUb DUd

% Find the number of species:
N            = length(Pstand_vec);                        % Number of species
```

```
% Check to see if we have activity coefficients or not:
if nargin == 5
    alpha = varargin{1};             % This should be a vector.
else
    alpha = ones(N,1);   % IDEAL ADSORBED SOLUTION DEFAULT.
end

%% First, find adsorbed phase properties as departure functions from id. gas.
Dga_vec     = zeros(1,N);
ga_vec      = zeros(1,N);
IG_g_mol    = zeros(1,N);
gas_y       = zeros(1,N);
for i = 1:N

    % Find the individual component's properties
    Dga_vec(i)  = Dga_imol_L2(T,Pstand_vec(i),i);           % in J/kmol-i.
    % Now, we'll move from the Δ functions to the absolute functions.
    % Set the state for the REFERENCE gas (not the equilibrium gas!!).
    % This is a gas at T of the system, x of the ADSORBED PHASE, and Po (the
    % dead state pressure, since that is what is used to integrate to find DG
    % and therefore DS).
    % Because we are still just finding the pure species props though,
    % we are going to keep the mole fractions to single species.
    % We will do the mixing later.
    gas_y(i)        = 1;
    set(fluid,'T',T,'P',Po,'X',gas_y);
    IG_g_mol(i)     = gibbs_mole(fluid);                    % J/kmol-i
    % Now, add the ideal gas ref state to make an absolute
    % (cross-comparable with gas phase) Gibbs free energy:
    ga_vec(i)       = Dga_vec(i) + IG_g_mol(i);             % J/kmol-i

    % Reset the gas phase composition for the next species:
    gas_y       = zeros(1,N);

end

% SOLVE FOR THE ABSOLUTE MOLAR GIBBS FREE ENERGY OF THE ADSORBED MIXTURE.
ga_mol      = 0;                            % J/kmol-mix
% Here is where the mixing happens:
for i = 1:N
    if (x_vec(i) ≠ 0)
        ga_mol = ga_mol + x_vec(i)*( ga_vec(i) + Ru*T*log(alpha(i)*x_vec(i)) );  ...
            % J/kmol-mix
    end
end

end
```

D.2.2 Enthalpy and internal energy

```
function DHa_i = DHa_i_L2(T, Pstand, iSpecies)
%%%%%%%%%%%%%%%%%%%%%%%%%%%%%%%%%%%%%%%%%%%%%%%%%%%%%%%%%%%%%%%%%%%%%%%%%%%%
% DHa_i = DHa_i_L2(T, Pstand, iSpecies)
%
% Returns the semi-extensive (per mass sorbent) enthalpy of the
% adsorbed phase (J/kg), ASSUMING DUAL-SITE LANGMUIR form of the isotherm,
% relative to an ideal gas reference phase.
%
% Based on the relations from Myers 2002.
%
% INPUTS: T_system, the standard state pressure of the species, and the index
% of the species for which the property is wanted.
% NECESSARY GLOBALS: Langmuir parameters.
% OUTPUTS: Delta H of the adsorbed species i, per mass of sorbent
%          (J/kg-sorbent), where Delta Ha is Ha - H(idealgas @ same T)
%
% Remember: Use to get back to a Ha from H_gas, not as Ha directly!!
%
% A. Calbry-Muzyka
% 21 Jan. 2014
%%%%%%%%%%%%%%%%%%%%%%%%%%%%%%%%%%%%%%%%%%%%%%%%%%%%%%%%%%%%%%%%%%%%%%%%%%%%

global To Po xo mu_o iN2 iCO2 Ru
global b0 d0 Nsatb Nsatd DUb DUd

% Make vectors for Arrhenius terms.
b_i          = b0.*exp(-DUb./(Ru.*T));                % m3/kmol
d_i          = d0.*exp(-DUd./(Ru.*T));                % m3/kmol

% Use the dual-site Langmuir isotherm to find Na_i on each site,
% in kmol-i/kg-sorbent at the standard state (i.e. at the vapor pressure).
Na_ib = Nsatb(iSpecies)*b_i(iSpecies)*Pstand/(Ru*T + b_i(iSpecies)*Pstand);
Na_id = Nsatd(iSpecies)*d_i(iSpecies)*Pstand/(Ru*T + d_i(iSpecies)*Pstand);

% Now find DHa_i, assuming an ideal gas vapor phase:
DHa_i = (DUb(iSpecies) - Ru*T)*Na_ib + (DUd(iSpecies) - Ru*T)*Na_id;

end
```

```
function Dha_imol = Dha_imol_L2(T, Pstand, iSpecies)
%%%%%%%%%%%%%%%%%%%%%%%%%%%%%%%%%%%%%%%%%%%%%%%%%%%%%%%%%%%%%%%%%%%%%%%%%%%%
```

```
% Dha_imol = Dha_imol_L2(T, Pstand, iSpecies)
%
% Returns the intensive (per kmol of species i) enthalpy of the
% adsorbed phase (J/kmol-i), ASSUMING DUAL-SITE LANGMUIR form of the isotherm,
% relative to an ideal gas reference phase.
%
% INPUTS: T_system, the standard state pressure of the species, and the index
% of the species for which the property is wanted.
% NECESSARY GLOBALS: Langmuir parameters
% OUTPUTS: Delta h of the adsorbed species i (J/kmol-i), where
%           Delta ha is ha - h(idealgas @ Po and same T)
%
% Remember: Use to get back to h_a from h_gas, not as h_a directly!!
%
% A. Calbry-Muzyka
% 21 Jan. 2014
%%%%%%%%%%%%%%%%%%%%%%%%%%%%%%%%%%%%%%%%%%%%%%%%%%%%%%%%%%%%%%%%%%%%%%%%%%%

global To Po xo mu_o Phio iN2 iCO2 Ru
global b0 d0 Nsatb Nsatd DUb DUd

% Make vectors for Arrhenius terms.
b_i          = b0.*exp(-DUb./(Ru.*T));                % m3/kmol
d_i          = d0.*exp(-DUd./(Ru.*T));                % m3/kmol

% Use the dual-site Langmuir isotherm to find Na_i, in kmol-i/kg-sorbent
% at the standard state (i.e. at the vapor pressure).
Nastand_i = Nsatb(iSpecies)*b_i(iSpecies)*Pstand/(Ru*T + b_i(iSpecies)*Pstand) + ...
    Nsatd(iSpecies)*d_i(iSpecies)*Pstand/(Ru*T + d_i(iSpecies)*Pstand);

% Find Dha_i from DHa_i (which is in J/kg-sorbent):
DHa_i = DHa_i_L2(T,Pstand,iSpecies);            % [J/kmol-mix]
Dha_imol = DHa_i * (1/Nastand_i);               % [J/kmol-mix]

end
```

```
function ha_mol = ha_mol_L2(T, Pstand_vec, x_vec, fluid)
%%%%%%%%%%%%%%%%%%%%%%%%%%%%%%%%%%%%%%%%%%%%%%%%%%%%%%%%%%%%%%%%%%%%%%%%%%%
% ha_mol = ha_mol_L2(T, Pstand_vec, x_vec, fluid)
%
% Returns the molar enthalpy [J/kmol-mix] of an adsorbed phase mixture,
% ASSUMING DUAL-SITE LANGMUIR form of the isotherm, and assuming ideal gas
% vapor phase.
%
% Note that this uses the Cantera open-source package to solve for ideal
```

```
% gas properties. This is not necessary, but then you will need to update
% this file.
%
% INPUTS: T_system, vector of standard pressures of all species in the mixture
%          [Pa], vector of actual adsorbed phase mole frac, and a fluid object.
%           WOULD NEED TO SEND IN ACTIVITY COEFFS AS A FUNCTION; DOES NOT
%           YET HAVE THE ABILITY TO RECEIVE THEM.
% NECESSARY GLOBALS: Langmuir parameters for ALL ADSORBED SPECIES, and Po.
% OUTPUTS: h (not Δ h) of the adsorbed phase [J/kmol-mix]
%
% A. Calbry-Muzyka
% 21 Jan. 2014
%%%%%%%%%%%%%%%%%%%%%%%%%%%%%%%%%%%%%%%%%%%%%%%%%%%%%%%%%%%%%%%%%%%%%%%%%%%

global To Po xo mu_o Phio iN2 iCO2 Ru
global b0 d0 Nsatb Nsatd DUb DUd

% Find the number of species:
N           = length(Pstand_vec);                       % Number of species

%% First, find adsorbed phase properties as departure functions from id. gas.
Dha_vec     = zeros(1,N);
ha_vec      = zeros(1,N);
IG_h_mol    = zeros(1,N);
gas_y       = zeros(1,N);
for i = 1:N

    % Find the individual component's properties
    Dha_vec(i)  = Dha_imol_L2(T,Pstand_vec(i),i);           % in J/kmol-i.
    % Now, we'll move from the Δ functions to the absolute functions.
    % Set the state for the REFERENCE gas (not the equilibrium gas!!).
    % This is a gas at T of the system, x of the ADSORBED PHASE, and Po (the
    % dead state pressure, since that is what is used to integrate to find DG
    % and therefore DS).
    % Because we are still just finding the pure species props though,
    % we are going to keep the mole fractions to single species.
    % We will do the mixing later.
    gas_y(i)        = 1;
    set(fluid,'T',T,'P',Po,'X',gas_y);
    IG_h_mol(i)     = enthalpy_mole(fluid);                   % J/kmol-i
    % Now, add the ideal gas ref state to make an absolute
    % (cross-comparable with gas phase) Gibbs free energy:
    ha_vec(i)       = Dha_vec(i) + IG_h_mol(i);             % J/kmol-i

    % Reset the gas phase composition for the next species:
    gas_y       = zeros(1,N);
```

```
end

% SOLVE FOR THE ABSOLUTE MOLAR ENTHALPY OF THE ADSORBED MIXTURE.
% Here is where the ideal solution assumption is made: hmix = 0.
ha_mol      = 0;                            % J/kmol-mix
for i = 1:N
    if (x_vec(i) ~= 0)
        ha_mol = ha_mol + x_vec(i)*( ha_vec(i) );  % J/kmol-mix
    end
end

end
```

```
function ua_mol = ua_mol_L2(T, Pstand_vec, x_vec, fluid)
%%%%%%%%%%%%%%%%%%%%%%%%%%%%%%%%%%%%%%%%%%%%%%%%%%%%%%%%%%%%%%%%%%%%%%%%%%%%
% ua_mol = ua_mol_L2(T, Pstand_vec, x_vec, fluid)
%
% Returns the molar internal energy [J/kmol-mix] of an adsorbed phase mixture,
% ASSUMING DUAL-SITE LANGMUIR form of the isotherm, and assuming ideal gas vapor ...
    phase.
%
% From relation in Myers 2002. Remember that this is a zero-volume phase!
%
% INPUTS: T_system, vector of standard pressures of all species in the mixture [Pa],
%           vector of actual adsorbed phase mole frac, and a fluid object.
%           WOULD NEED TO SEND IN ACTIVITY COEFFS AS A FUNCTION; DOES NOT
%           YET HAVE THE ABILITY TO RECEIVE THEM.
% NECESSARY GLOBALS: None here.
% OUTPUTS: u (not Δ u) of the adsorbed phase [J/kmol-mix]
%
% A. Calbry-Muzyka
% 21 Jan. 2014
%%%%%%%%%%%%%%%%%%%%%%%%%%%%%%%%%%%%%%%%%%%%%%%%%%%%%%%%%%%%%%%%%%%%%%%%%%%%

%% Note that ua_mol = ha_mol, because va_mol = 0.
ua_mol = ha_mol_L2(T, Pstand_vec, x_vec, fluid);

end
```

D.2.3 Entropy

```
function DSa_i = DSa_i_L2(T, Pstand, iSpecies)
%%%%%%%%%%%%%%%%%%%%%%%%%%%%%%%%%%%%%%%%%%%%%%%%%%%%%%%%%%%%%%%%%%%%%%%%%%%%
% DSa_i = DSa_i_L2(T, Pstand, iSpecies)
%
% Returns the semi-extensive (per mass sorbent) entropy of the
% adsorbed phase (J/kg-K), ASSUMING DUAL-SITE LANGMUIR form of the isotherm,
% relative to an ideal gas reference phase.
%
% INPUTS: T_system, the standard state pressure of the species, and the index
% of the species for which the property is wanted.
% NECESSARY GLOBALS: None here (they all get called by the DHa_i and DGa_i
%           functions instead).
% OUTPUTS: Delta S of the adsorbed species i, per mass of sorbent
%          (J/K-kg-sorbent), where DeltaSa is Sa - S(idealgas @ Po and same T)
%
% Remember: Use to get back to a Sa, not as Sa directly!!
%
% A. Calbry-Muzyka
% 21 Jan. 2014
%%%%%%%%%%%%%%%%%%%%%%%%%%%%%%%%%%%%%%%%%%%%%%%%%%%%%%%%%%%%%%%%%%%%%%%%%%%%

% Find values for DHa_i and DGa_i first from our functions:
DHa_i = DHa_i_L2(T, Pstand, iSpecies);
DGa_i = DGa_i_L2(T, Pstand, iSpecies);

% Then, use the fact that G = H-TS to find DSa_i:
DSa_i = (1/T)*(DHa_i - DGa_i);

end
```

```
function Dsa_imol = Dsa_imol_L2(T, Pstand, iSpecies)
%%%%%%%%%%%%%%%%%%%%%%%%%%%%%%%%%%%%%%%%%%%%%%%%%%%%%%%%%%%%%%%%%%%%%%%%%%%%
% Dsa_imol = Dsa_imol_L2(T, Pstand, iSpecies)
%
% Returns the intensive (per kmol of species i) entropy of the
% adsorbed phase (J/kmol-i), ASSUMING DUAL-SITE LANGMUIR form of the isotherm,
% relative to an ideal gas reference phase.
%
% INPUTS: T_system, the standard state pressure of the species, and the index
% of the species for which the property is wanted.
% NECESSARY GLOBALS: Langmuir parameters
% OUTPUTS: Delta s of the adsorbed species i (J/kmol-i), where
%           Delta sa is sa - s(idealgas @ Po and same T)
%
% Remember: Use to get back to s_a from s_gas, not as s_a directly!!
```

```
%
% A. Calbry-Muzyka
% 21 Jan. 2014
%%%%%%%%%%%%%%%%%%%%%%%%%%%%%%%%%%%%%%%%%%%%%%%%%%%%%%%%%%%%%%%%%%%%%%%%%%%%

global To Po xo mu_o Phio iN2 iCO2 Ru
global b0 d0 Nsatb Nsatd DUb DUd

% Make vectors for Arrhenius terms.
b_i          = b0.*exp(-DUb./(Ru.*T));                % m3/kmol
d_i          = d0.*exp(-DUd./(Ru.*T));                % m3/kmol

% Use the dual-site Langmuir isotherm to find Na_i, in kmol-i/kg-sorbent
% at the standard state (i.e. at the vapor pressure).
Nastand_i = Nsatb(iSpecies)*b_i(iSpecies)*Pstand/(Ru*T + b_i(iSpecies)*Pstand) + ...
    Nsatd(iSpecies)*d_i(iSpecies)*Pstand/(Ru*T + d_i(iSpecies)*Pstand);

% Find Dsa_i from DSa_i (which is in J/kg-sorbent):
DSa_i = DSa_i_L2(T,Pstand,iSpecies);
Dsa_imol = DSa_i * (1/Nastand_i);

end
```

```
function sa_mol = sa_mol_L2(T, Pstand_vec, x_vec, fluid)
%%%%%%%%%%%%%%%%%%%%%%%%%%%%%%%%%%%%%%%%%%%%%%%%%%%%%%%%%%%%%%%%%%%%%%%%%%%%
% sa_mol = sa_mol_L2(T, Pstand_vec, x_vec, fluid)
%
% Returns the molar entropy [J/K-kmol-mix] of an adsorbed phase mixture,
% ASSUMING DUAL-SITE LANGMUIR form of the isotherm, and assuming ideal gas vapor ...
    phase.
%
% Note that this uses the Cantera open-source package to solve for ideal
% gas properties. This is not necessary, but then you will need to update
% this file.
%
% INPUTS: T_system, vector of standard pressures of all species in the mixture [Pa],
%           vector of actual adsorbed phase mole frac, and a fluid object.
%           WOULD NEED TO SEND IN ACTIVITY COEFFS AS A FUNCTION; DOES NOT
%           YET HAVE THE ABILITY TO RECEIVE THEM.
% NECESSARY GLOBALS: Langmuir parameters for ALL ADSORBED SPECIES, and Po.
% OUTPUTS: s (not Δ s) of the adsorbed phase [J/K-kmol-mix]
%
% A. Calbry-Muzyka
% 21 Jan. 2014
%%%%%%%%%%%%%%%%%%%%%%%%%%%%%%%%%%%%%%%%%%%%%%%%%%%%%%%%%%%%%%%%%%%%%%%%%%%%
```

```
global To Po xo mu_o Phio iN2 iCO2 Ru
global b0 d0 Nsatb Nsatd DUb DUd

%% First, find the enthalpy and Gibbs free energy of this state:
ga_mol      = ga_mol_L2(T,Pstand_vec,x_vec,fluid);          % J/kmol-mix
ha_mol      = ha_mol_L2(T,Pstand_vec,x_vec,fluid);          % J/kmol-mix

%% Now, solve for the molar entropy of this mixture:
sa_mol      = (1/T)*(ha_mol - ga_mol);                      % J/K-kmol-mix

end
```

D.2.4 Exergy

```
function xa_mol = xa_mol_L2(T, Pstand_vec, x_vec, qtot, fluid)
%%%%%%%%%%%%%%%%%%%%%%%%%%%%%%%%%%%%%%%%%%%%%%%%%%%%%%%%%%%%%%%%%%%%%%%%%%%
% xa_mol = xa_mol_L2(T, Pstand_vec, x_vec, qtot, fluid)
%
% Returns the molar exergy [J/kmol-mix] of the
% adsorbed phase, ASSUMING DUAL-SITE LANGMUIR form of the isotherm,
% and an ideal gas vapor phase.
%
% Note that this uses the Cantera open-source package to solve for ideal
% gas properties. This is not necessary, but then you will need to update
% this file.
%
% INPUTS: T_system, vector of standard pressures of all species in the mixture [Pa],
%           vector of actual adsorbed phase mole frac, total loading
%           [kmol/kg], and a fluid object.
%           WOULD NEED TO SEND IN ACTIVITY COEFFS AS A FUNCTION; DOES NOT
%           YET HAVE THE ABILITY TO RECEIVE THEM.
% NECESSARY GLOBALS: Langmuir parameters for ALL ADSORBED SPECIES.
% OUTPUTS: x (not Δ x) of the adsorbed phase [J/kmol-mix]
%
% A. Calbry-Muzyka
% 21 Jan. 2014
%%%%%%%%%%%%%%%%%%%%%%%%%%%%%%%%%%%%%%%%%%%%%%%%%%%%%%%%%%%%%%%%%%%%%%%%%%%

global To Po xo mu_o Phio iN2 iCO2 Ru
global b0 d0 Nsatb Nsatd DUb DUd

%% First, find values for ua_mol and sa_mol.
```

```
ua_mol      = ua_mol_L2(T, Pstand_vec, x_vec, fluid);       % [J/kmol-mix]
sa_mol      = sa_mol_L2(T, Pstand_vec, x_vec, fluid);       % [J/kmol-mix]

%% Now, find the molar exergy of this state.
xa_mol      = ua_mol - To*sa_mol - dot(mu_o,x_vec) - (1/qtot)*Phio;      % ...
    [J/kmol-mix]

end
```

Appendix E

Nomenclature

All symbols are listed with labels and suggested units where relevant.

E.1 Environmental state

- T_o: environmental temperature, 298.15 K
- P_o: environmental pressure, 101325 Pa
- y_{o,N_2}: N_2 mole fraction, 0.753641
- y_{o,O_2}: O_2 mole fraction, 0.202157
- y_{o,H_2O}: H_2O mole fraction, 0.034820
- $y_{o,Ar}$: Ar mole fraction, 0.009015
- y_{o,CO_2}: CO_2 mole fraction, 0.000367

E.2 Roman symbols

- a: activity (Chapter 3)
- A: column cross-sectional area, m^2 (Chapter 4)

- A: Helmholtz function, J (Chapter 6)
- C_i: volumetric concentration of species i, kmol-i/m^3-gas
- c: specific heat capacity (for an incompressible substance), J/kg-K
- c_p: constant-pressure specific heat capacity, J/kg-K
- c_v: constant-volume specific heat capacity, J/kg-K
- D_L: axial dispersion coefficient, m^2/s
- f: fugacity, Pa
- G: Gibbs function, J
- H: enthalpy, J
- $K_{\alpha,\beta}$: adsorption constant, m^3-gas/kmol-i
- K_{eq}: equilibrium constant
- K_z: thermal conductivity, J/m-K-s
- m: mass, kg
- M: molality, kmol/kg (Chapter 3)
- $\hat{M}$: molar mass, kg/kmol
- N: amount of species, kmol
- P: pressure, Pa
- q: sorbent loading, kmol-adsorbed/kg-sorbent
- Q: heat transfer, J
- r_p: adsorption pellet size, m
- R or $\hat{R}$: ideal gas constant, J/kmol-K

- S: entropy, J/K
- t: time, s
- T: temperature, K
- U: internal energy, J
- $\mathbf{v}$: interstitial velocity, m/s
- V: volume, m^3
- W: work, J
- X: exergy, J
- x: mole fraction (in the liquid or adsorbed phase, if multiple phases are present)
- y: mole fraction (in the gas phase, if multiple phases are present)
- z: coordinate for length of column, m (Chapter 4)

E.3 Greek symbols

- α: effective loading, kmol-CO_2/kmol-MEA (Chapter 3)
- γ: activity coefficient (Chapter 3); ratio of specific heats (Chapter 4)
- ε: volumetric void fraction
- η: efficiency (e.g., η_x for exergy efficiency, η_s for isentropic efficiency)
- μ: chemical potential, J/kmol
- μ_g: gas viscosity, kg/m-s
- ν: stoichiometric coefficient
- ϕ: fugacity coefficient

- ρ: density, kg/m^3
- Φ: surface potential, J/kg-sorbent
- ψ: mass-specific flow exergy, J/kg (or mole-specific, $\hat{\psi}$, J/kmol
- ω: lumped species transfer parameter, 1/s

E.4 Subscripts, superscripts, and accents

- a: adsorbed phase
- $actual$: in reality (as in $X_{sep,actual}$, the actual exergy of separation)
- b: at the boundary (as in T_b)
- $comp$: of compression
- $crit$: at the critical point
- $dest$: destroyed
- e: excess
- eq: at equilibrium
- g: gas phase
- gen: generated
- HP: high pressure
- i: of species i
- IP: intermediate pressure
- LC: local contribution term
- LP: low pressure

- o: environmental state
- PDH: Pitzer-Debye-Huckel term
- Q: with heat transfer
- s: sorbent phase
- s: at saturation (subscript in isotherm expression)
- sep: of separation (as in $X_{min,sep}$, the minimum exergy of separation)
- W: with work
- α and β: adsorption site types (Chapter 4)
- $\hat{\cdot}$: molar
- $\dot{\cdot}$: rate
- $\tilde{\cdot}$: per mass of sorbent, 1/kg-sorbent
- *: reference state

E.5 Acronyms or abbreviations

- Ads.: adsorption step in a VSA cycle
- ASU: air separation unit
- BD: blowdown step in a VSA cycle
- CCS: carbon capture and sequestration
- CFWH: closed feedwater heater
- CIT: combustor inlet temperature
- COE: cost of electricity

- CPU: CO_2 purification unit
- DOE: U.S. Department of Energy
- Evac.: evacuation step in a VSA cycle
- EPRI: Electric Power Research Institute
- FGD: flue gas desulfurization
- HHV: higher heating value, J/kg
- HRSG: heat recovery steam generator
- IAS: Ideal Adsorbed Solution
- IEA: International Energy Agency
- IGCC: integrated gasification, combined cycle power plant
- IL: ionic liquid
- IPCC: Intergovernmental Panel on Climate Change
- LDF: linear driving force
- LHV: lower heating value, J/kg
- MDEA: methyl diethanolamine
- MEA: monoethanolamine
- MOF: metal-organic framework
- NETL: U.S. National Energy Technology Laboratory
- NGCC: natural gas, combined cycle power plant
- NNES: number of *non-environmental* species
- NRTL: non-random, two-liquid activity coefficient model

- NS: number of species (in Chapter 5, number of *environmental* species)
- ODE: ordinary differential equation
- OFWH: open feedwater heater
- PC: pulverized coal plant
- PDE: partial differential equation
- PR-BM: Peng-Robinson equation of state with Boston-Mathias extrapolations
- Press.: pressurization step in a VSA cycle
- PSA: pressure-swing adsorption
- PVSA: pressure-vacuum-swing adsorption
- PZ: piperazine
- SCATR: supercritical, auto-thermal Rankine
- TIT: turbine inlet temperature
- TRL: Technology Readiness Level
- TSA: temperature-swing adsorption
- VSA: vacuum-swing adsorption
- WENO: weighted, essentially non-oscillatory scheme

Bibliography

[1] U.S. Department of Energy, Office of Fossil Energy, NETL. *Cost and Performance Baseline for Fossil Energy Plants: Bituminous Coal and Natural Gas to Electricity Final Report, Revision 2a.* DOE/NETL-2010/1397, 2013.

[2] A. L. Myers. Thermodynamics of adsorption in porous materials. *AIChE Journal*, 48(1):145–160, 2002.

[3] Marcus Hilliard. *A Predictive Thermodynamic Model for an Aqueous Blend of Potassium Carbonate, Piperazine, and Monoethanolamine for Carbon Dioxide Capture from Flue Gas.* PhD thesis, University of Texas at Austin, Austin, TX, 2008.

[4] IEA. *Energy Technology Perspectives 2015: Mobilising Innovation to Accelerate Climate Action.* OECD/IEA, Paris, 2015.

[5] Christopher B Field and Maarten Van Aalst. *Climate Change 2014: Impacts, Adaptation, and Vulnerability*, volume 1. IPCC Working Group II, 2014.

[6] Deanna M D'Alessandro, Berend Smit, and Jeffrey R Long. Carbon dioxide capture: Prospects for new materials. *Angewandte Chemie International Edition*, 49(35):6058–6082, 2010.

[7] IEA. *CO_2 emissions from fuel combustion: Highlights (2014 Edition).* OECD/IEA, Paris, 2014.

[8] EIA. Frequently Asked Questions: How much of U.S. carbon dioxide emissions are associated with electricity generation?, 2015. [Online; accessed 8-November-2015].

[9] Saeed Danaei Kenarsari, Dali Yang, Guodong Jiang, Suojiang Zhang, Jianji Wang, Armistead G Russell, Qiang Wei, and Maohong Fan. Review of recent advances in carbon dioxide separation and capture. *RSC Advances*, 3(45):22739–22773, 2013.

[10] Shinya Kishimoto, Takuya Hirata, Masaki Iijima, Tsuyoshi Ohishi, Kazuo Higaki, and Ronald Mitchell. Current status of MHI's CO_2 recovery technology and optimization of CO_2 recovery plant with a PC fired power plant. *Energy Procedia*, 1(1):1091–1098, 2009.

[11] Karl Stéphenne. Start-up of world's first commercial post-combustion coal fired CCS project: Contribution of Shell Cansolv to SaskPower Boundary Dam ICCS project. *Energy Procedia*, 63:6106–6110, 2014.

[12] Fred Kozak, Arlyn Petig, Ed Morris, Richard Rhudy, and David Thimsen. Chilled ammonia process for CO_2 capture. *Energy Procedia*, 1(1):1419–1426, 2009.

[13] Stefan Bachu. CO_2 storage in geological media: role, means, status and barriers to deployment. *Progress in Energy and Combustion Science*, 34(2):254–273, 2008.

[14] PNK De Silva and PG Ranjith. A study of methodologies for CO_2 storage capacity estimation of saline aquifers. *Fuel*, 93:13–27, 2012.

[15] Toshiyasu Sakakura, Jun-Chul Choi, and Hiroyuki Yasuda. Transformation of carbon dioxide. *Chemical Reviews*, 107(6):2365–2387, 2007.

[16] Peter Markewitz, Wilhelm Kuckshinrichs, Walter Leitner, Jochen Linssen, Petra Zapp, Richard Bongartz, Andrea Schreiber, and Thomas E Müller. Worldwide innovations in the development of carbon capture technologies and the utilization of CO_2. *Energy & Environmental Science*, 5(6):7281–7305, 2012.

[17] Kai Man Kerry Yu, Igor Curcic, Joseph Gabriel, and Shik Chi Edman Tsang. Recent advances in CO_2 capture and utilization. *ChemSusChem*, 1(11):893–899, 2008.

[18] Bernhard Mayer, Maurice Shevalier, Michael Nightingale, Jang-Soon Kwon, Gareth Johnson, Mark Raistrick, Ian Hutcheon, and Ernie Perkins. Tracing the movement and the fate of injected CO_2 at the IEA GHG Weyburn-Midale CO_2 Monitoring and Storage project (Saskatchewan, Canada) using carbon isotope ratios. *International Journal of Greenhouse Gas Control*, 16:S177–S184, 2013.

[19] SaskPower. CCS Performance data exceeding expectations at world-first Boundary Dam Power Station Unit #3, 2015. [Online; accessed 8-November-2015].

[20] Aquistore. CO_2 Injection Begins at Aquistore, 2015. [Online; accessed 19-May-2015].

[21] Bert Metz, Ogunlade Davidson, Heleen de Coninck, Manuela Loos, Leo Meyer, et al. *IPCC Special Report on Carbon Dioxide Capture and Storage*. Cambridge University Press, 2005.

[22] Howard Herzog, Jerry Meldon, and Alan Hatton. Advanced post-combustion CO_2 capture. *Clean Air Task Force*, pages 1–39, 2009.

[23] John Davison. Performance and costs of power plants with capture and storage of CO_2. *Energy*, 32(7):1163–1176, 2007.

[24] Edward S Rubin, Hari Mantripragada, Aaron Marks, Peter Versteeg, and John Kitchin. The outlook for improved carbon capture technology. *Progress in Energy and Combustion Science*, 38(5):630–671, 2012.

[25] Edward Rubin, George Booras, John Davison, Clas Ekstrom, Mike Matuszewski, Sean McCoy, and Chris Short. *Toward a common method of cost estimation for CO_2 capture and storage at fossil fuel power plants*. Task Force on CCS Costing Methods, 2013.

[26] U.S. Department of Energy Office of Fossil Energy: Clean Coal Research Program. *2012 Technology Readiness Assessment—Carbon Capture, Utilization, and Storage (CCUS).* National Energy Technology Laboratory (NETL), 2012.

[27] Global CCS Institute. *The Global Status of CCS.* Global Carbon Capture and Storage Institute, Melbourne, Australia, 2014.

[28] Abhoyjit S Bhown and Brice C Freeman. Analysis and status of post-combustion carbon dioxide capture technologies. *Environmental Science & Technology*, 45(20):8624–8632, 2011.

[29] Adam Simpson. *Decision making in energy: advancing technical, environmental, and economic perspectives.* PhD thesis, Stanford University, Palo Alto, CA, 2010.

[30] M. Gouy. Sur l'énergie utilisable. *J. de Phys.*, 2(VIII):501–518, 1889.

[31] Kurt Zenz House, Charles F Harvey, Michael J Aziz, and Daniel P Schrag. The energy penalty of post-combustion CO_2 capture & storage and its implications for retrofitting the US installed base. *Energy & Environmental Science*, 2(2):193–205, 2009.

[32] Jennifer Wilcox. *Carbon Capture.* Springer, New York, 2012.

[33] H.B. Callen. *Thermodynamics and an Introduction to Thermostatistics.* John Wiley & Sons, New York, 2nd edition, 1985.

[34] Hendrick C. Van Ness. Thermodynamics in the treatment of vapor/liquid equilibrium (VLE) data. *Pure & Appl. Chem.*, 67(6):859–872, 1995.

[35] Kurt Zenz House, Antonio C Baclig, Manya Ranjan, Ernst A van Nierop, Jennifer Wilcox, and Howard J Herzog. Economic and energetic analysis of capturing CO_2 from ambient air. *Proceedings of the National Academy of Sciences*, 108(51):20428–20433, 2011.

[36] Patricia Luis. Exergy as a tool for measuring process intensification in chemical engineering. *Journal of Chemical Technology and Biotechnology*, 88(11):1951–1958, 2013.

[37] IL Leites, DA Sama, and N Lior. The theory and practice of energy saving in the chemical industry: some methods for reducing thermodynamic irreversibility in chemical technology processes. *Energy*, 28(1):55–97, 2003.

[38] Kristin Jordal. Benchmarking of power cycles with CO_2 capture: The impact of the selected framework. *International Journal of Greenhouse Gas Control*, 2(4):468–477, 2008.

[39] Gary Rochelle, Eric Chen, Stephanie Freeman, David Van Wagener, Qing Xu, and Alexander Voice. Aqueous piperazine as the new standard for CO_2 capture technology. *Chemical Engineering Journal*, 171(3):725–733, 2011.

[40] Adam P Simpson and AJ Simon. Second law comparison of oxy-fuel combustion and post-combustion carbon dioxide separation. *Energy Conversion and Management*, 48(11):3034–3045, 2007.

[41] Yolanda Lara, Ana Martínez, Pilar Lisbona, Irene Bolea, Ana González, and Luis M Romeo. Using the second law of thermodynamics to improve CO_2 capture systems. *Energy Procedia*, 4:1043–1050, 2011.

[42] Hanne M. Kvamsdal, Kristin Jordal, and Olav Bolland. A quantitative comparison of gas turbine cycles with capture. *Energy*, 32(1):10–24, 2007.

[43] Jean Li Yuen Fong, Clare Anderson, Barry Hooper, Gongkui Xiao, Paul Webley, and Andrew Hoadley. Multi-objective optimisation of hybrid CO_2 capture processes using exergy analysis. *Conference on Process Integration, Modelling and Optimisation for Energy Saving and Pollution Reduction*, 39:1501–1506, 2014.

[44] Isabel Guedea, Carlos Lupiañez, and Luis M Romeo. Exergetic comparison of different oxyfuel technologies. *International Journal of Energy and Environmental Engineering*, 2:35–47, 2011.

[45] B Erlach, M Schmidt, and G Tsatsaronis. Comparison of carbon capture IGCC with pre-combustion decarbonisation and with chemical-looping combustion. *Energy*, 36(6):3804–3815, 2011.

[46] Christian Kunze, Karsten Riedl, and Hartmut Spliethoff. Structured exergy analysis of an integrated gasification combined cycle (IGCC) plant with carbon capture. *Energy*, 36(3):1480–1487, 2011.

[47] Ivar S Ertesvåg, Hanne M Kvamsdal, and Olav Bolland. Exergy analysis of a gas-turbine combined-cycle power plant with precombustion co 2 capture. *Energy*, 30(1):5–39, 2005.

[48] Luis M Romeo, Sergio Usón, Antonio Valero, and Jesús M Escosa. Exergy analysis as a tool for the integration of very complex energy systems: The case of carbonation/calcination CO_2 systems in existing coal power plants. *International Journal of Greenhouse Gas Control*, 4(4):647–654, 2010.

[49] Xiangping Zhang, Xuezhong He, and Truls Gundersen. Post-combustion carbon capture with a gas separation membrane: parametric study, capture cost, and exergy analysis. *Energy & Fuels*, 27(8):4137–4149, 2013.

[50] FH Geuzebroek, LHJM Schneiders, GJC Kraaijveld, and PHM Feron. Exergy analysis of alkanolamine-based CO_2 removal unit with AspenPlus. *Energy*, 29(9):1241–1248, 2004.

[51] Zeinab Amrollahi, Ivar S Ertesvåg, and Olav Bolland. Thermodynamic analysis on post-combustion CO_2 capture of natural-gas-fired power plant. *International Journal of Greenhouse Gas Control*, 5(3):422–426, 2011.

[52] Zeinab Amrollahi, Ivar S Ertesvåg, and Olav Bolland. Optimized process configurations of post-combustion CO_2 capture for natural-gas-fired power plant: Exergy analysis. *International Journal of Greenhouse Gas Control*, 5(6):1393–1405, 2011.

[53] Gary T Rochelle et al. Amine scrubbing for CO_2 capture. *Science*, 325(5948):1652–1654, 2009.

[54] Kathryn Smith, Gongkui Xiao, Kathryn Mumford, Jeffri Gouw, Indrawan Indrawan, Navin Thanumurthy, Dimple Quyn, Robyn Cuthbertson, Aravind Rayer, Nathan Nicholas, et al. Demonstration of a concentrated potassium carbonate process for CO_2 capture. *Energy & Fuels*, 28(1):299–306, 2013.

[55] Satish Reddy, Jeff Scherrfius, Stefano Freguia, and Christopher Roberts. *Fluor's Econamine FG Plus Technology: An Enhanced Amine-Based CO_2 Capture Process*. Fluor Enterprises, Aliso Viejo, CA, Second National Conference on Carbon Sequestration, NETL/DOE, Alexandria VA, 2003.

[56] Stephanie A Freeman, Ross Dugas, David H Van Wagener, Thu Nguyen, and Gary T Rochelle. Carbon dioxide capture with concentrated, aqueous piperazine. *International Journal of Greenhouse Gas Control*, 4(2):119–124, 2010.

[57] Raphael Idem, Malcolm Wilson, Paitoon Tontiwachwuthikul, Amit Chakma, Amornvadee Veawab, Adisorn Aroonwilas, and Don Gelowitz. Pilot plant studies of the CO_2 capture performance of aqueous MEA and mixed MEA/MDEA solvents at the University of Regina CO_2 capture technology development plant and the Boundary Dam CO_2 capture demonstration plant. *Industrial & engineering chemistry research*, 45(8):2414–2420, 2006.

[58] Fred Closmann, Thu Nguyen, and Gary T Rochelle. MDEA/Piperazine as a solvent for CO_2 capture. *Energy Procedia*, 1(1):1351–1357, 2009.

[59] Joan F Brennecke and Burcu E Gurkan. Ionic liquids for CO_2 capture and emission reduction. *The Journal of Physical Chemistry Letters*, 1(24):3459–3464, 2010.

[60] Fluor. *Improvement in power generation with post-combustion capture of CO_2, Report Number PH4/33*. IEA Greenhouse Gas R&D Programme, 2004.

[61] Satish Reddy, Dennis Johnson, and John Gilmartin. Fluor's econamine fg plus sm technology for co2 capture at coal-fired power plants. In *Power Plant Air Pollutant Control Mega Symposium*, pages 25–28, 2008.

[62] John M Prausnitz, Rudiger N Lichtenthaler, and Edmundo Gomes de Azevedo. *Molecular thermodynamics of fluid-phase equilibria*. Pearson Education, 1998.

[63] Aspen Plus. Aspen Physical Property Methods. *Aspen Technology Inc., Cambridge, MA, USA*, 2013.

[64] Chau-Chyun Chen. *Computer simulation of chemical processes with electrolytes*. PhD thesis, Massachusetts Institute of Technology, Cambridge, MA, 1980.

[65] Chau-Chyun Chen, Herbert I Britt, JF Boston, and LB Evans. Local composition model for excess Gibbs energy of electrolyte systems. Part I: Single solvent, single completely dissociated electrolyte systems. *AIChE Journal*, 28(4):588–596, 1982.

[66] Henri Renon and John M Prausnitz. Local compositions in thermodynamic excess functions for liquid mixtures. *AIChE journal*, 14(1):135–144, 1968.

[67] Yuhua Song and Chau-Chyun Chen. Symmetric electrolyte nonrandom two-liquid activity coefficient model. *Industrial & Engineering Chemistry Research*, 48(16):7788–7797, 2009.

[68] Charles W. White III. *Aspen Plus Simulation of CO_2 Recovery Process: Final Report*. DOE/NETL-2002/1182, National Energy Technology Laboratory, Morgantown, WV, 2002.

[69] Anusha Kothandaraman. *Carbon dioxide capture by chemical absorption: a solvent comparison study*. PhD thesis, Massachusetts Institute of Technology, Cambridge, MA, 2010.

[70] Stefano Freguia and Gary T Rochelle. Modeling of CO_2 capture by aqueous monoethanolamine. *AIChE Journal*, 49(7):1676–1686, 2003.

[71] David Tremblay, Suphat Wanatasiri, Yuhua Song, and Chau-Chyun Chen. *Benefits of Multi-Solvent NRTL Models in Aspen Plus: Best in Class Electrolyte Thermodynamics: An Industry White Paper*. AspenTech, 2012.

[72] Charles W Skarstrom. Method and Apparatus for Fractionating, 1960. US Patent 2,944,627.

[73] M.M. Hassan, D.M. Ruthven, and N.S. Raghavan. Air separation by pressure swing adsorption on a carbon molecular sieve. *Chemical Engineering Science*, 41(5):1333 – 1343, 1986.

[74] Frederick W Leavitt. Air separation pressure swing adsorption process, 1991. US Patent 5,074,892.

[75] S Sircar and T. C. Golden. Purification of hydrogen by pressure swing adsorption. *Separation Science and Technology*, 35(5):667–687, 2000.

[76] Jaeyoung Yang, Chang-Ha Lee, and Jay-Woo Chang. Separation of Hydrogen Mixtures by a Two-Bed Pressure Swing Adsorption Process Using Zeolite 5A. *Industrial Engineering Chemistry Research*, 36(7):2789–2798, 1997.

[77] A. Malek and S. Farooq. Hydrogen purification from refinery fuel gas by pressure swing adsorption. *AIChE Journal*, 44(9):1985–1992, 1998.

[78] J.W. Carter and M.L. Wyszynski. The pressure swing adsorption drying of compressed air. *Chemical Engineering Science*, 38(7):1093 – 1099, 1983.

[79] Hyungwoong Ahn and Chang-Ha Lee. Adsorption dynamics of water in layered bed for air-drying TSA process. *AIChE journal*, 49(6):1601–1609, 2003.

[80] Paul A Webley. Adsorption technology for CO_2 separation and capture: a perspective. *Adsorption*, 20(2-3):225–231, 2014.

[81] T Takeguchi, W Tanakulrungsank, and T Inui. Separation and/or concentration of CO_2 from CO_2/N_2 gaseous mixture by pressure swing adsorption using metal-incorporated microporous crystals with high surface area. *Gas Separation & Purification*, 7(1):3–9, 1993.

[82] Jérôme Merel, Marc Clausse, and Francis Meunier. Experimental investigation on co2 post-combustion capture by indirect thermal swing adsorption using 13x and 5a zeolites. *Industrial & Engineering Chemistry Research*, 47(1):209–215, 2008.

[83] Lu Wang, Zhen Liu, Ping Li, Jianguo Yu, and Alirio E Rodrigues. Experimental and modeling investigation on post-combustion carbon dioxide capture using zeolite 13x-apg by hybrid vtsa process. *Chemical Engineering Journal*, 197:151–161, 2012.

[84] Daeho Ko, Ranjani Siriwardane, and Lorenz T. Biegler. Optimization of a Pressure-Swing Adsorption Process Using Zeolite 13X for CO_2 Sequestration. *Industrial Engineering Chemistry Research*, 42(2):339–348, 2003.

[85] Penny Xiao, Jun Zhang, Paul Webley, Gang Li, Ranjeet Singh, and Richard Todd. Capture of co2 from flue gas streams with zeolite 13x by vacuum-pressure swing adsorption. *Adsorption*, 14(4-5):575–582, 2008.

[86] Reza Haghpanah, Aniruddha Majumder, Ricky Nilam, Arvind Rajendran, Shamsuzzaman Farooq, Iftekhar A Karimi, and Mohammad Amanullah. Multiobjective optimization of a four-step adsorption process for postcombustion CO_2 capture via finite volume simulation. *Industrial & Engineering Chemistry Research*, 52(11):4249–4265, 2013.

[87] Kenji Sumida, David L Rogow, Jarad A Mason, Thomas M McDonald, Eric D Bloch, Zoey R Herm, Tae-Hyun Bae, and Jeffrey R Long. Carbon dioxide capture in metal–organic frameworks. *Chemical reviews*, 112(2):724–781, 2011.

[88] Youn-Sang Bae and Randall Q Snurr. Development and evaluation of porous materials for carbon dioxide separation and capture. *Angewandte Chemie International Edition*, 50(49):11586–11596, 2011.

[89] Li-Chiang Lin, Adam H Berger, Richard L Martin, Jihan Kim, Joseph A Swisher, Kuldeep Jariwala, Chris H Rycroft, Abhoyjit S Bhown, Michael W

Deem, Maciej Haranczyk, et al. In silico screening of carbon-capture materials. *Nature Materials*, 11(7):633–641, 2012.

[90] MM Faruque Hasan, Eric L First, and Christodoulos A Floudas. Cost-effective CO_2 capture based on in silico screening of zeolites and process optimization. *Physical Chemistry Chemical Physics*, 15(40):17601–17618, 2013.

[91] Shreenath Krishnamurthy, Reza Haghpanah, Arvind Rajendran, and Shamsuzzaman Farooq. Simulation and Optimization of a Dual-Adsorbent, Two-Bed Vacuum Swing Adsorption Process for CO_2 Capture from Wet Flue Gas. *Industrial & Engineering Chemistry Research*, 53(37):14462–14473, 2014.

[92] AL Myers and John M Prausnitz. Thermodynamics of mixed-gas adsorption. *AIChE Journal*, 11(1):121–127, 1965.

[93] James A O'Brien and Alan L Myers. Rapid calculations of multicomponent adsorption equilibria from pure isotherm data. *Industrial & Engineering Chemistry Process Design and Development*, 24(4):1188–1191, 1985.

[94] James A O'Brien and Alan L Myers. A comprehensive technique for equilibrium calculations in adsorbed mixtures: the generalized FastIAS method. *Industrial & Engineering Chemistry Research*, 27(11):2085–2092, 1988.

[95] Luca Riboldi and Olav Bolland. Evaluating Pressure Swing Adsorption as a CO_2 separation technique in coal-fired power plants. *International Journal of Greenhouse Gas Control*, 39:1–16, 2015.

[96] Dong Xu, Penny Xiao, Jun Zhang, Gang Li, Gongkui Xiao, Paul A Webley, and Yuchun Zhai. Effects of water vapour on CO_2 capture with vacuum swing adsorption using activated carbon. *Chemical Engineering Journal*, 230:64–72, 2013.

[97] Reza Haghpanah, Arvind Rajendran, Shamsuzzaman Farooq, Iftekhar A Karimi, and Mohammad Amanullah. Discrete equilibrium data from dynamic

column breakthrough experiments. *Industrial & Engineering Chemistry Research*, 51(45):14834–14844, 2012.

[98] Reza Haghpanah, Ricky Nilam, Arvind Rajendran, Shamsuzzaman Farooq, and Iftekhar A Karimi. Cycle synthesis and optimization of a VSA process for postcombustion CO_2 capture. *AIChE Journal*, 59(12):4735–4748, 2013.

[99] R. Banerjee, K.G. Narayankhedkar, and S.P. Sukhatme. Exergy analysis of pressure swing adsorption processes for air separation. *Chemical Engineering Science*, 45(2):467 – 475, 1990.

[100] R. Banerjee, K.G. Narayankhedkar, and S.P. Sukhatme. Exergy analysis of kinetic pressure swing adsorption processes: comparison of different cycle configurations. *Chemical Engineering Science*, 47(5):1307 – 1311, 1992.

[101] Noam Lior and Hassan S Al-Sharqawi. Exergy analysis of flow dehumidification by solid desiccants. *Energy*, 30(6):915–931, 2005.

[102] WM Worek, W Zheng, and J-Y San. Thermodynamic properties of adsorbed water on silica gel: Exergy losses in adiabatic sorption processes. *Journal of Thermophysics and Heat Transfer*, 5(3):435–440, 1991.

[103] David T. Kearns and Paul A. Webley. Application of an adsorption non-flow exergy function to an exergy analysis of a pressure swing adsorption cycle. *Chemical Engineering Science*, 59(17):3537 – 3557, 2004.

[104] Josiah Willard Gibbs. *On the equilibrium of heterogeneous substances*. Connecticut Academy of Arts and Sciences, 1877.

[105] David Matheson Young and Albert Dary Crowell. *Physical Adsorption of Gases*. Butterworths, 1962.

[106] Wladyslaw Rudzinski and Douglas Hugh Everett. *Adsorption of gases on heterogeneous surfaces*. Academic Press, 1992.

[107] Gilbert Newton Lewis and Merle Randall. *Thermodynamics. Revised by Kenneth S. Pitzer and Leo Brewer.* McGraw-Hill Book Company, Inc., New York, 1961.

[108] Ralph T Yang. *Gas separation by adsorption processes.* Butterworth Publishers, Stoneham, MA, 1986.

[109] Michael J Moran. *Availability Analysis: A Guide to Efficient Energy Use.* Prentice-Hall, Inc., New Jersey, 1982.

[110] Adrian Bejan. *Advanced Engineering Thermodynamics, Third Edition.* John Wiley & Sons, Inc., Hoboken, New Jersey, 2006.

[111] David G. Goodwin, Harry K. Moffat, and Raymond L. Speth. Cantera: An object-oriented software toolkit for chemical kinetics, thermodynamics, and transport processes. http://www.cantera.org, 2015. Version 2.2.0.

[112] R Byron Bird, Warren E Stewart, and Edwin N Lightfoot. Transport phenomena. 2nd edition. *New York*, 2002.

[113] John Russell Heberle. *Coal Energy Conversion Integrated with Deep Saline Aquifer Carbon Storage via Combustion in Supercritical Water.* PhD thesis, Stanford University, Palo Alto, CA, 2012.

[114] Paul D. Mobley, Rebecca Z. Pass, and Chris F. Edwards. Exergy analysis of coal energy conversion with carbon sequestration via combustion in supercritical saline aquifer water. *ASME Conference Proceedings*, pages 1989–1997, 2011.

[115] Paul David Mobley. *Analysis of Zero Emission Power Generation from SCWO of Coal and Development of an Experimental Facility for Its Investigation.* PhD thesis, Stanford University, Palo Alto, CA, 2012.

[116] Kailai Thambimuthu, Mohammad Soltanieh, and Juan Carlos Abanades. Capture of CO_2. In *IPCC Special Report on Carbon Capture and Storage*, pages 105–178. Cambridge University Press, Cambridge, UK, 2005.

[117] MA Habib, HM Badr, SF Ahmed, R Ben-Mansour, K Mezghani, S Imashuku, Y Shao-Horn, ND Mancini, A Mitsos, P Kirchen, et al. A review of recent developments in carbon capture utilizing oxy-fuel combustion in conventional and ion transport membrane systems. *International Journal of Energy Research*, 35(9):741–764, 2011.

[118] Evgeny Yantovsky, Jan Górski, and Mykola Shokotov. *Zero emissions power cycles*. CRC Press, 2009.

[119] Philippe Mathieu and R Nihart. Zero-emission MATIANT cycle. *Journal of Engineering for Gas Turbines and Power*, 121(1):116–120, 1999.

[120] S. Houyou, P. Mathieu, and R. Nihart. Techno-economic comparison of different options of very low CO_2 emission technologies. In *Proceedings of the Fifth International Conference on Greenhouse Gas Control Technologies, Cairns, Australia*, 2000.

[121] W. Sanz, H. Jericha, B. Bauer, and E. Gottlich. Comparison of two promising oxy-fuel power cycles for CO_2 capture. *Transactions of the ASME: Journal of Engineering for Gas Turbine and Power*, 130, 2008.

[122] C. Gou, R. Cai, and H. Hong. An advanced oxy-fuel power cycle with high efficiency. *Proceedings of the Institution of Mechanical Engineers: Part A, Journal of Power and Energy*, 220:315–325, 2006.

[123] J. Martinez-Frias, S. M. Aceves, J. R. Smith, and H. Brandt. Thermodynamic analysis of zero-atmospheric emissions power plant. *Transactions of the ASME: Journal of Engineering for Gas Turbines and Power*, 126:2–8, 2004.

[124] J. Martinez-Frias, S. M. Aceves, J. R. Smith, and H. Brandt. A coal-fired power plant with zero-atmospheric emissions. *Transactions of the ASME: Journal of Engineering for Gas Turbines and Power*, 130, 2008.

[125] G Corchero, V P Timn, and J L Montas. A natural gas oxy-fuel semiclosed combined cycle for zero CO_2 emissions: a thermodynamic optimization. *Proceedings of the Institution of Mechanical Engineers, Part A: Journal of Power and Energy*, 225(4):377–388, 2011.

[126] E. Iantovski and P. Mathieu. Highly efficient zero emission CO_2-based power plant. *Energy Conversion Management*, 38:S141–S146, 1997.

[127] H. Jericha and M. Fesharaki. The Graz Cycle: 1500C max temperature potential H_2-O_2 fired CO_2 capture with CH_4-O_2 firing. *Proceedings of the ASME: Cogen-Turbo Power Conference*, 1995.

[128] H. Jericha, E. Gottlich, W. Sanz, and F. Heitmeir. Design optimization of the Graz Cycle prototype plant. *Proceedings of the ASME Turbo Expo*, 2003.

[129] Jefferson W. Tester and others. Supercritical Water Oxidation Technology. In *Emerging Technologies in Hazardous Waste Management III*, chapter 4, pages 35–76. American Chemical Society, 1993.

[130] Sally Benson and Peter Cook. Underground Geological Storage. In *IPCC Special Report on Carbon Capture and Storage*, pages 195–276. Cambridge University Press, Cambridge, UK, 2005.

[131] M. Paulus and S. Penoncello. Correlation for the carbon dioxide and water mixture based on the Lemmon-Jacobsen mixture model and the Peng-Robinson equation of state. *International Journal of Thermophysics*, 27:1373–1386, 2006.

[132] W. Wagner and A. Pruss. The IAPWS formulation 1995 for the thermodynamic properties of ordinary water substance for general and scientific use. *J. Phys. Chem. Ref. Data*, 31:387–535, 1996.

[133] R. Span and W. Wagner. A new equation of state for carbon dioxide covering the fluid region from the triple-point temperature to 1100 K at pressures up to 800 MPa. *J. Phys. Chem. Ref. Data*, 25:1509–1596, 1996.

[134] D. Peng and D. Robinson. A New Two-Constant Equation of State. *Ind. Eng. Chem., Fundam.*, 15:59–64, 1976.

[135] J.O. Valderrama. The state of the cubic equation of state. *Ind. Eng. Chem. Res.*, 42:1603–1618, 2003.

[136] H.G. Rackett. Equation of state for saturated liquids. *Journal of Chemical and Engineering Data*, 15:514–517, 1970.

[137] S. Posch and M. Haider. Optimization of CO_2 compression and purification units (CO_2CPU) for CCS power plants. *Fuel*, 101:254–263, 2012.

[138] Kwee-Yan Teh. *Thermodynamics of Efficient, Simple-Cycle Combustion Engines*. PhD thesis, Stanford University, Palo Alto, CA, 2007.

[139] MSA Baksh, ES Kikkinides, and RT Yang. Lithium type X zeolite as a superior sorbent for air separation. *Separation Science and Technology*, 27(3):277–294, 1992.